

Performance Evaluation of HMA Consisting of Modified Asphalt Binder

**Research Report 0-4824-2
Project Number 0-4824**

Conducted for

**Texas Department of Transportation
P.O. Box 5080
Austin, Texas 78763**

February 2007

**Center for Transportation Infrastructure Systems
The University of Texas at El Paso
El Paso, Texas 79968
(915) 747-6925**

TECHNICAL REPORT STANDARD TITLE PAGE

1. Report No. FHWA/TX-07/0-4824-2	2. Government Accession No.	3. Recipient's Catalog No.	
4. Title and Subtitle Performance Evaluation of HMA Consisting of Modified Asphalt Binder		5. Report Date February 2007	
		6. Performing Organization Code	
7. Author(s) Rajpal Sugandh, MS Manuel Zea, BS Vivek Tandon, PhD, PE Andre Smit, PhD Jorge Prozzi, PhD		8. Performing Organization Report No. 0-4824-2	
		9. Performing Organization Name and Address Center for Transportation Infrastructure Systems The University of Texas at El Paso El Paso, Texas 79968-0516	
12. Sponsoring Agency Name and Address Texas Department of Transportation Research and Technology Implementation Office P.O. Box 5080 Austin, Texas 78763		10. Work Unit No.	11. Contract or Grant No. 0-4824
		13. Type of Report and Period Covered Technical Report: September 03 thru July 06	
15. Supplementary Notes Research performed in cooperation with the Texas Department of Transportation and the Federal Highway Administration. <i>Project title: Guidelines for Selecting Asphalt Mixtures and Evaluation of Polymer-Modified Mixes</i>		14. Sponsoring Agency Code	
		16. Abstract To achieve Strategic Highway Research Program (SHRP) specified PG grades, refineries make use of modifiers to enhance the properties of base asphalt. Even though modified binders may meet PG specifications, some perform better than others. This can be attributed to binder/hot mix asphalt (HMA) tests inability in consistently identifying the problems with the binders especially if the modifier is added to the binder. Therefore, it is necessary to identify a binder/HMA test that can consistently predict performance. The research performed for SHRP has significantly increased the understanding of HMA mix behavior among national and international highway-related agencies, which has resulted in an increase in the number of mixes available for placement. The increase in mix types makes it difficult for designers to select the appropriate mix for a given application. Therefore, it is necessary to have a HMA selection guideline. To achieve the objectives of this study, a survey was conducted to identify commonly placed mix and modifier types and logic followed in selection of mixes. Based on survey results, three mixes (Type D, CMHB-C, and PFC) were selected. In addition, the four modifier types: SBS, SBR, TR, and Elvaloy were selected and evaluated. The evaluation results and recommendations are included in this report.	
17. Key Words Modifier, Asphalt binder, HWTD, Flow time, Flow number, Dynamic modulus, Static creep, and Flexural fatigue.		18. Distribution Statement No restrictions. This document is available to the public through the National Technical Information Service, Springfield, Virginia 22161, www.ntis.gov	
19. Security Classif. (of this report) Unclassified	20. Security Classif. (of this page) Unclassified	21. No. of Pages 120	22. Price

Performance Evaluation of HMA Consisting of Modified Asphalt Binder

By

**Rajpal Sugandh, MS
Manuel Zea, BS
Vivek Tandon, PhD, PE
Andre Smit, PhD
Jorge Prozzi, PhD**

**Report Number 0-4824-2
Project Number 0-4824**

**Project Title: Guidelines for Selecting Asphalt
Mixtures and Evaluation of
Polymer-Modified Mixes**

Performed in cooperation with the

**Texas Department of Transportation
and the Federal Highway Administration**

**The Center for Transportation Infrastructure Systems
The University of Texas at El Paso
El Paso, Texas 79968-0516
February 2007**

Disclaimer:

The contents of this report reflect the view of the authors, who are responsible for the facts and the accuracy of the data presented herein. The contents do not necessarily reflect the official views or policies of the Texas Department of Transportation or the Federal Highway Administration. This report does not constitute a standard, specification, or regulation.

**NOT INTENDED FOR CONSTRUCTION, BIDDING, OR
PERMIT PURPOSES**

Rajpal Sugandh, MS
Manuel Zea, BS
Vivek Tandon, PhD, PE (88219)
Andre Smit, PhD
Jorge Prozzi, PhD
Andre Smit, PhD

ACKNOWLEDGEMENTS

The authors are grateful for the assistance and input from a number of TxDOT personnel. The authors wish to acknowledge in particular Dr. Magdy Mikhail, Project Director, and Mr. Elias Rmeili, Project Coordinator, for facilitating the collaboration with TxDOT Districts, and for their valuable guidance and input. In addition, the authors would like to acknowledge Mr. Vishal Gossain, Mr. Issac Puentes, Edgar Gurrero, Ms. Jessica Retana, and Mr. Raymond Guerra for specimen preparation and testing.

This page replaces an intentionally blank page in the original.

-- CTR Library Digitization Team

ABSTRACT

To achieve Strategic Highway Research Program (SHRP) specified PG grades, refineries make use of modifiers to enhance the properties of base asphalt. Even though modified binders may meet PG specifications, some perform better than others. This can be attributed to binder/hot mix asphalt (HMA) tests inability in consistently identifying the problems with the binders especially if the modifier is added to the binder. Therefore, it is necessary to identify a binder/HMA test that can consistently predict performance.

The research performed for SHRP has significantly increased the understanding of HMA mix behavior among national and international highway-related agencies, which has resulted in an increase in the number of mixes available for placement. The increase in mix types makes it difficult for designers to select the appropriate mix for a given application. Therefore, it is necessary to have a HMA selection guideline.

To achieve the objectives of this study, a survey was conducted to identify commonly placed mix and modifier types and logic followed in selection of mixes. Based on survey results, three mixes (Type D, CMHB-C, and PFC) were selected. In addition, the four modifier types: SBS, SBR, TR, and Elvaloy were selected and evaluated.

The evaluation results suggest that the no matter whether the mixes were modified with SBS, SBR or Elvaloy, all outperform the unmodified mixes but none of the products significantly outperform the others. Although base binders have similar PG grades, their performance can be significantly different. Therefore, it is important to closely monitor the changes in crude source or binder batch. In terms of rutting, all of the performance tests with the exception of dynamic modulus can identify the presence of modifier although they ranked the different binder types differently. In terms of fatigue/stiffness, the only flexural beam fatigue test was able to identify the presence of modifier consistently. In comparing the two mix types, the CMHB-C has better rut resistance, especially in the presence of lower grade binder, in comparison to Type D. On the other hand, Type D has significantly higher fatigue resistance in comparison to CMHB-C.

This page replaces an intentionally blank page in the original.

-- CTR Library Digitization Team

TABLE OF CONTENTS

ACKNOWLEDGEMENTS	II
ABSTRACT	IV
TABLE OF CONTENTS	VI
LIST OF FIGURES	VIII
LIST OF TABLES	X
LIST OF TABLES	X
CHAPTER 1 INTRODUCTION.....	1
1.1 INTRODUCTION.....	1
1.2 RESEARCH OBJECTIVE	2
1.3 ORGANIZATION.....	3
CHAPTER 2 PERFORMANCE TESTS FOR HMA MIXES.....	5
2.1 HAMBURG WHEEL TRACKING DEVICE (TEX-242-F).....	6
2.1.1 <i>Test Procedure and Calculations for HWTB Tests</i>	6
2.2 STATIC CREEP TEST (TEX-231-F)	8
2.2.1 <i>Test Procedure and Calculations for Static Creep Tests</i>	8
2.3 DYNAMIC MODULUS TEST	9
2.3.1 <i>Dynamic Modulus E^* Prediction Models</i>	11
2.3.1.1 Witzak Model	11
2.3.1.2 Witzak and Fonseca's Model.....	11
2.3.1.3 Andrei, Witzak and Mirza's Revised Model	12
2.3.2 <i>Test Procedure and Calculations for Dynamic Modulus Test</i>	13
2.4 FLOW NUMBER TEST.....	15
2.4.1 <i>Test Procedure and Calculations for Flow Number Test</i>	18
2.5 FLOW TIME TEST	21
2.5.1 <i>Test Procedure and Calculations for Flow Time Test</i>	21
2.6 INDIRECT TENSILE (IDT) STRENGTH TEST	23
2.6.1 <i>Test Procedure and Calculations for Indirect Tensile Test</i>	23
2.7 FLEXURAL BEAM FATIGUE TEST.....	25
2.7.1 <i>Test Procedure and Calculations for Flexural Beam Fatigue Test</i>	27
2.8 ULTRASONIC TESTING.....	28
2.8.1 <i>Test Procedure and Calculations for Ultrasonic Test</i>	28
CHAPTER 3 EXPERIMENT DESIGN AND SPECIMEN PREPARATION FOR PERFORMANCE EVALUATION.....	31
3.1 SELECTION OF MIXES	31
3.2 MIX DESIGN AND BINDER TYPES	36
3.3 SPECIMEN PREPARATION.....	39
3.4 TEST MATRIX.....	40
CHAPTER 4 DATA ANALYSIS AND TEST RESULTS	43
4.1 HAMBURG WHEEL TEST DEVICE RESULTS	43
4.2 DYNAMIC MODULUS TEST RESULTS	47
4.2.1 <i>Master Curves</i>	52
4.2.2 <i>Prediction of Master Curve Using Models</i>	58
4.3 FLOW NUMBER AND FLOW TIME TEST RESULTS	62

4.4	INDIRECT TENSILE STRENGTH TEST RESULTS.....	66
4.5	STATIC CREEP TEST RESULTS.....	73
4.6	SEISMIC MODULUS.....	77
4.7	FLEXURAL FATIGUE BEAM TEST RESULTS.....	80
4.7.1	<i>Input in the Mechanistic-Empirical Pavement Design Guide</i>	84
CHAPTER 5	STATISTICAL ANALYSES AND COMPARISON OF	
	PERFORMANCE TEST RESULTS.....	91
5.1	STATISTICAL ANALYSES.....	91
5.2	COMPARISON OF PERFORMANCE TEST RESULTS.....	97
5.2.1	<i>Rutting Potential of HMA</i>	97
5.2.2	<i>Stiffness of HMA</i>	99
CHAPTER 6	CLOSURE.....	101
6.1	SUMMARY.....	101
6.2	CONCLUSIONS.....	102
6.3	RECOMMENDATIONS.....	103
REFERENCES.....		105

LIST OF FIGURES

Figure 2.1 Hamburg Wheel Tracking Device Test Set Up	7
Figure 2.2 A Typical HWTD Test Result.....	7
Figure 2.3 Loading Pattern for Static Creep Testing.....	9
Figure 2.4 Typical Vertical Strain versus Time Plot for Static Creep Test.....	9
Figure 2.5 Variations in Stress and Strain with Time for Different Materials	10
Figure 2.6 A Schematic of Dynamic Modulus Test Setup	14
Figure 2.7 Typical Dynamic Modulus versus Frequency Relationship at Different Temperatures.....	16
Figure 2.8 Typical Log Shift Factor versus Temperature Plot.....	16
Figure 2.9 Shifted Dynamic Modulus versus Frequency Relationship	17
Figure 2.10 Typical Master Curve	17
Figure 2.11 Load Application and Expected Response from Flow Number Test..	19
Figure 2.12 Flow Number Test Results	20
Figure 2.13 Flow Time Test Results.....	22
Figure 2.14 Typical Data Recorded During the IDT Strength Test.....	24
Figure 2.15 Indirect Tensile Strength Test Results (Load versus Deformation)...	25
Figure 2.16 Fatigue Beam Testing Apparatus	27
Figure 2.17 Sinusoidal Load Waveform	28
Figure 2.18 Ultrasonic Test Device for HMA Specimens	30
Figure 3.1 HMA Use in the Districts.....	32
Figure 3.2 HMA Structural Problems Experienced	32
Figure 3.3 HMA Construction Problems Experienced	34
Figure 3.4 HMA Mixes Resistance to Rutting.....	34
Figure 3.5 HMA Mixes Resistance to Fatigue.....	35
Figure 3.6 Modifiers Typically Used in HMA Mixes	35
Figure 4.1 HWTD Specimen Setup	43
Figure 4.2 HWTD Rut Depth for Type D Mix Design at the Center of Specimen	45
Figure 4.3 HWTD Rut Depth for CMHB-C Mix Design at the Center of Specimen	46
Figure 4.4 Comparison Between CMHB-C and Type D Mixes Rut Depth Obtained from HWTD	47
Figure 4.5 Comparison of Dynamic Modulus Values of CMHB-C and Type D Mixes.....	52
Figure 4.6 Measured Dynamic Modulus and Frequency Plot for CMHB-C Mix Consisting of W 64 Asphalt Binder.....	54
Figure 4.7 Log Shift Factor versus Temperature Plot for CMHB-C Mix Consisting of W 64 Asphalt Binder.....	54
Figure 4.8 Shifted Dynamic Modulus versus Frequency Relationship for CMHB-C Mix Consisting of W 64 Asphalt Binder.....	55
Figure 4.9 Developed Master Curve Using Sigmoidal Function for CMHB-C Mix Consisting of W 64 Asphalt Binder.....	55
Figure 4.10 Comparison Between PG 76 Grade Asphalt Binder and	

Type D Mixes	56
Figure 4.11 Comparison Between PG 76 Grade Asphalt Binder and CMHB-C Mixes	56
Figure 4.12 Comparison Between PG 64 Grade Asphalt Binder and Type D Mixes	57
Figure 4.13 Comparison Between PG 64 Grade Asphalt Binder and CMHB-C Mixes	57
Figure 4.14 Comparison Between all Asphalt Binders and Type D Mixes	59
Figure 4.15 Comparison Between all Asphalt Binders and CMHB-C Mixes	59
Figure 4.16 Comparison Between all Asphalt Binders and PFC Mixes	60
Figure 4.17 Dynamic Modulus Comparisons for CMHB-C Consisting of W 76 SBS & TR	61
Figure 4.18 Dynamic Modulus Comparisons for Type D Consisting of W 76 SBS & TR	61
Figure 4.19 Flow Number Test Results for Mixes Consisting of Valero Asphalt	63
Figure 4.20 Flow Number Test Results for Mixes Consisting of Wright Asphalt.....	63
Figure 4.21 Flow Number Test Results for Mixes Consisting of Ultrapave Asphalt.....	64
Figure 4.22 Flow Time Test Results for Mixes Consisting of Wright Asphalt.....	64
Figure 4.23 Flow Number Test Results for Two Mix Types.....	69
Figure 4.24 Flow Time Test Results for Two Mix Types	69
Figure 4.25 Energy till Failure Test Results for Type D and CMHB-C Mixes.....	71
Figure 4.26 Tensile Strength Test Results for Type D and CMHB-C Mixes.....	72
Figure 4.27 Fracture Energy Test Results for Type D and CMHB-C Mixes	72
Figure 4.28 Static Creep Test Results for Type D Mix Consisting of W 64 Asphalt Type	74
Figure 4.29 Total Strain Comparison for Type D and CMHB-C Mixes	76
Figure 4.30 Permanent Strain Comparison for Type D and CMHB-C Mixes	76
Figure 4.31 Creep Stiffness Comparison for Type D and CMHB-C Mixes.....	77
Figure 4.32 Influence of Coring on Seismic Modulus.....	79
Figure 4.33 Seismic Modulus Comparison between Type D and CMHB-C Mixes.....	80
Figure 4.34 A Typical Flexural Stiffness-Cycle Curve Obtained from Fatigue Test.....	81
Figure 4.35 Results of the Fatigue Test for the Type D Mixes	85
Figure 4.36 Results of the Fatigue Test for the CMHB-C Mixes	85
Figure 4.37 Influence of Binder Type on Fatigue Resistance	86
Figure 4.38 Influence of Mix Type on Fatigue Resistance	87
Figure 5.1 Statistics of the Regression Analysis for CMHB-C Mixes	95
Figure 5.2 Statistics of the Regression Analysis for Type D Mixes	96

LIST OF TABLES

Table 2.1 TxDOT Specifications for Hamburg Wheel Tracking Device.....	8
Table 3.1 Job Mix Formula for Type D, PFC and CMHB-C Mix Designs.....	37
Table 3.2 Rheological Properties of Asphalt Binders.....	38
Table 3.3 Mixing and Compaction Temperatures for Individual Binder Types ...	39
Table 3.4 Test Matrix.....	41
Table 4.1 Binder Abbreviations Used in This Study.....	45
Table 4.2 Rut Depth at the End of the Testing.....	46
Table 4.3 Average Dynamic Modulus, Standard Deviation, and Coefficient of Variation of Type D Mixes	49
Table 4.4 Average Dynamic Modulus, Standard Deviation, and Coefficient of Variation of CMHB-C Mixes.....	50
Table 4.5 Average Dynamic Modulus, Standard Deviation, and Coefficient of Variation of PFC Mixes.....	51
Table 4.6 A and VTS Parameters for Dynamic Modulus Prediction	60
Table 4.7 Flow Number and Flow Time Test Results	65
Table 4.8 Flow Number Model Data	67
Table 4.9 Flow Number Model Data	68
Table 4.10 Indirect Tensile Strength Test Results for CMHB-C	70
Table 4.11 Indirect Tensile Strength Test Results for Type D.....	70
Table 4.12 Static Creep Test Results for CMHB-C	74
Table 4.13 Static Creep Test Results for Type D	75
Table 4.14 Seismic Modulus Test Results.....	78
Table 4.15 Results of the Fatigue Test for Type D Mixes.....	82
Table 4.16 Results of the Fatigue Test for CMHB-C Mixes.....	83
Table 4.17 Fatigue Parameters for CMHB-C Mixes	88
Table 4.18 Fatigue Parameters for Type D Mixes.....	89
Table 5.1 Flow Number ANOVA.....	92
Table 5.2 Flow Time ANOVA.....	92
Table 5.3 Dynamic Modulus ANOVA for Type D and CMHB-C Mixes.....	94
Table 5.4 Dynamic Modulus ANOVA for Three Mix Types	94
Table 5.5 Seismic Modulus ANOVA	95
Table 5.6 Rutting Potential Ranking of CMHB-C Mixes.....	98
Table 5.7 Rutting Potential Ranking of Type D Mixes.....	98
Table 5.8 Stiffness Ranking of CMHB-C Mixes	100
Table 5.9 Stiffness Ranking of Type D Mixes.....	100

This page replaces an intentionally blank page in the original.

-- CTR Library Digitization Team

CHAPTER 1 INTRODUCTION

1.1 INTRODUCTION

In recent decades, the Strategic Highway Research Program (SHRP) suggested new performance based specifications for asphalt binders to be used in the hot mix asphalt concrete. These new specifications, known as Performance Grade (PG) specifications, suggest performing tests at the service temperature rather than at a set temperature based on previous specifications. To meet these new PG-specifications, manufacturers either altered manufacturing practices (such as air blown asphalt) or added modifiers such as polymers (King et al., 1999). In general, the addition of modifiers improved the performance of hot mix asphalt (HMA) while the air blown asphalt or acid modifications decreased the durability of the mixes (King et al., 1999).

Typically, the new performance tests do not differentiate between polymer modified asphalts and acid modified asphalts (Anderson et. al., 2002). To ensure that manufacturers provided modified asphalt binder, state highway agencies began to specify type and percentage of modifier. Occasionally, the percent and type of modifier specified is strictly governed by anecdotal information rather than actual performance evaluations. In recent years, the elastic recovery test (ASTM D 6084 and Tex-539-C) has been proposed as the test that can differentiate between asphalt binder consisting of modifier and acid modified asphalt binders. However, based on discussions with asphalt producers, it was determined that the asphalt modified with Styrene Butadiene Rubber (SBR) does not pass the elastic recovery test but performs well in the field. The test evaluates the elasticity of the modified asphalt and may not be suitable for asphalt modified with non-elastomer type polymers. In addition, the test does not provide the fundamental property of asphalt binder.

Recently, the repeated creep test was proposed by the Federal Highway Administration (FHWA) that measures the fundamental properties of asphalt binders and can be used to identify the presence of modifiers (Bahia et. al., 2001). Therefore, the first objective of this study was to evaluate the suitability of the repeated creep tests to identify the presence of modifier in addition to the elastic recovery tests.

To implement the AASHTO 2002 Pavement Design Guide, the Texas Department of Transportation (TxDOT) needs to evaluate mixes using newly proposed mixture performance tests (dynamic modulus, flow time, and flow number tests). Since manufacturers typically use modified binders to meet the PG grade, evaluation of the mixes consisting of modified binder using new tests is necessary. Therefore, the second objective of this study was to identify the

influence of modifiers on the performance of HMA and provide HMA parameters needed for designing pavements using AASHTO's 2002 Pavement Design Guide.

The research performed for SHRP has significantly increased the understanding of HMA mix behavior among national and international highway-related agencies, which has resulted in an increase in the number of mixes available for placement. The increase in mix types makes it difficult for designers to select the appropriate mix for a given application.

A report published by the National Asphalt Pavement Association (NAPA) provides designers with tools for selecting appropriate mix types while considering factors such as traffic, environment, subsurface pavement structure, existing pavement condition, preparation, and economics (NAPA Information Series 128). Since no guidelines are available for the Texas mixes, TxDOT is concerned about the performance and proper application of their asphalt mixes. For example, in 1995 TxDOT evaluated all Coarse Matrix High Binder (CMHB) projects placed by the Department. At the time, 77 CMHB projects were reviewed. Districts were interviewed and projects were visually assessed. Results showed that CMHB was rut resistant and that it reduced segregation problems. Flushing was found to be a problem due to excessive binder content as a result of erroneous mix designs and inadequate construction quality control. Use of CMHB by the districts increased because conventional type hot mix did not appear to serve (to the same degree) the increased truck traffic without excessive rutting and degradation. It was further noted that the mix was not suitable for curb and gutter applications and that it should never be used to directly overlay a flexible base. Therefore, the third objective of this study was to develop a guideline/expert system to aid in the selection of suitable mixes. A final objective was to develop workshop material and conduct workshops to familiarize TxDOT staff with the guidelines/expert system.

1.2 RESEARCH OBJECTIVE

The main objectives of this research are:

- Evaluation of the suitability of the binder tests (including elastic recovery test) to identify the presence of inodifier.
- Identification of the influence of modifiers on performance of HMA using proposed simple performance tests in addition to the fatigue and Hamburg Wheel Tracking Device (HWTD) test and provide HMA parameters needed for designing pavements using the AASHTO 2002 Pavement Design Guide.
- Development of a guideline/expert system to aid in the selection of suitable mixes.
- Development of material to conduct workshops to train District personnel in the use of guidelines for selecting asphalt mixtures.

To perform this study, three mix designs used by TxDOT – Type-D, Coarse Matrix High Binder (CMHB-C), and Porous Friction Course (PFC) – were selected. The Type-D and PFC mixes were obtained from the Austin District and the CMHB-C was obtained from the Bryan District. All of the chosen mixes have shown to be successful in the field and have recently been placed using modifiers. The modifiers assessed in this study include Styrene-Butadiene-Styrene (SBS), Styrene-Butadiene-Rubber (SBR), Tire Rubber (TR), and Elvaloy.

The results of binder evaluation were reported by Hrdlicka et al. (2007) and the guidelines/expert system development and workshop materials were developed by Smit et al. (2007). Therefore, the focus of this report is to present HMA performance evaluation results and data needed for the AASHTO 2002 Pavement Design Guide.

1.3 ORGANIZATION

The introduction, research objectives and report organization are included in this chapter. Chapter 2 discusses the background information on types of modifiers and test procedures. Chapter 3 discusses the mix and binder selection, mix design and test matrix evaluated in this research. Included in Chapter 4 are the test results and analysis of the collected data. Statistical analyses and comparative performance analyses is included in Chapter 5. Conclusions and recommendations for future research are presented in Chapter 6.

CHAPTER 2 PERFORMANCE TESTS FOR HMA MIXES

Although SHRP evaluated various performance tests, a specific test for evaluating the performance of HMA has not been recommended. The only performance test recommended was the AASHTO T-283 test to evaluate moisture sensitivity of HMA. Currently, TxDOT specifies the HWTD test (Tex-242-F) or static creep test (Tex-231-F) to evaluate performance of HMA. However, the HWTD test only identifies the rut potential of HMA, and static creep tests have lower repeatability (Swami et al., 2006). With the current trend toward mechanistic pavement design and the need for more reliable design procedures, accurate characterization of the HMA properties is vital.

Witczak et al. (2002) evaluated various performance tests and proposed what is commonly known as “Simple Performance Tests (SPT)” for National Cooperative Highway Research Program (NCHRP) Project 9-19. These tests include dynamic modulus to predict the permanent deformation and fatigue cracking, and axial repeated (flow number) and axial creep (flow time) tests to predict the permanent deformation. The dynamic modulus test is also recommended in the “Guide for Mechanistic-Empirical Design of New and Rehabilitated Pavement Structures.” In addition, Nazarian et al. (2003) demonstrated that the dynamic modulus tests and seismic tests can be combined to obtain a master curve to be used as a field acceptance criterion.

The Strategic Highway Research Program (SHRP) and Roque et al. (2006) advocated an indirect tensile (IDT) strength test to measure the creep-compliance and strength of HMA (AASHTO TP9-94). The test is performed to assess the low-temperature cracking potential of HMA.

An AASHTO test method for determining the fatigue life of compacted HMA is the flexural beam fatigue test (AASHTO T321-03), which was recommended by Tayebehi et al. (1994), Tangella et al. (1990), and Monismith et al. (1985). The test involves subjecting an HMA beam specimen to repeated flexural bending loads until failure in order to estimate fatigue life of the specimen.

Based on the literature review, the dynamic modulus, flow number, and flow time tests were selected to evaluate their capabilities in identifying the presence of modifiers in HMA. The HWTD and static creep tests were selected because they are included in the TxDOT specifications. The flexural fatigue test was selected to identify whether the stiffer modified binders are increasing the brittleness of HMA, thus reducing the fatigue life of HMA. In addition, seismic modulus test was also performed because it is a nondestructive test. The background information on each test procedure and expected results are reported in the following sections.

2.1 Hamburg Wheel Tracking Device (Tex-242-F)

The Hamburg Wheel Tracking Device (HWTD) has been used in Germany as a specification tool since the mid 1970s. Since Hamburg is the major seaport for Germany, the roads are subjected to a large number of heavily loaded, slow moving trucks. The Road Authority uses the Wheel Tracking Device test as a specification requirement for their most severely stressed pavements. This device has been adopted by several state highway agencies including TxDOT.

The HWTD (Figure 2.1) measures the combined effects of rutting and moisture damage by rolling a steel wheel across the surface of an asphalt concrete test specimen that is immersed in hot water. Each steel wheel makes up to 20,000 passes or until 20mm of deformation is reached. The results that are customarily reported include the depth of deformation versus the number of wheel passes. The test setup is designed for testing slab specimens. However, with the increasing use of the gyratory compactor, TxDOT (Izzo and Tahmoressi, 1999) has adopted a test protocol that uses cylindrical specimens compacted in the Superpave Gyratory Compactor (SGC).

The only disadvantage of this test is that it does not provide a fundamental property that can be used for modeling purposes. Recommended values for specific climates and traffic levels are also not available (Solaimanian et al., 2004). However, the test is easy to perform and is part of the TxDOT acceptance criterion (Items 341, 344 and 346).

2.1.1 Test Procedure and Calculations for HWTD Tests

To perform tests, four specimens are compacted to a density of $93 \pm 1\%$ using a SGC. The compacted specimens, which are 6 in. (150 ± 2 mm) in diameter and 2.5 in. (62 ± 2 mm) in height, are cooled to room temperature for a period of 24 hours. The four specimens are then divided into two groups. Approximately $5/8$ in. (16 mm) of the edge of each specimen is then trimmed with a masonry saw. The specimens are placed in an acrylic mold and then placed in a mounting tray. The thickness of the acrylic mold is 2.4 in. (60 mm). The specimens in the mold are labeled with the percent air voids, mix type and height.

Information regarding the specimens and water temperature is entered into the computer. The mounting trays are then fastened to the empty water bath. The water bath is filled with water and heated to 122°F (50°C). The test specimens are allowed to saturate in the water bath for an additional 60 minutes once the 122°F (50°C) water temperature is reached. This waiting time is also referred to as start delay time. Once the test starts, the specimens are maintained in the heated water bath for 307 minutes. The test is automatically stopped when either the required number of passes or the maximum allowable rutting depth of 0.5 in. (12.5 mm) is reached. The number of passes to failure or the final rut depth is recorded at the end of the test. A typical test result, shown in Figure 2.2,

indicates that the mix meets the TxDOT criterion of less than 0.5 in. (12.5 mm) deformation at the end of the 20,000 cycles.

Depending on the binder grade, an acceptable mix should meet the requirement suggested in Table 2.1. The maximum allowable deformation is 0.5 in. (12.5 mm) for all binder grades at different number of passes. According to the TxDOT specification, the maximum rut depth anywhere in the wheel path should be measured. In this study, tests were performed to 20,000 cycles regardless of the binder grade.

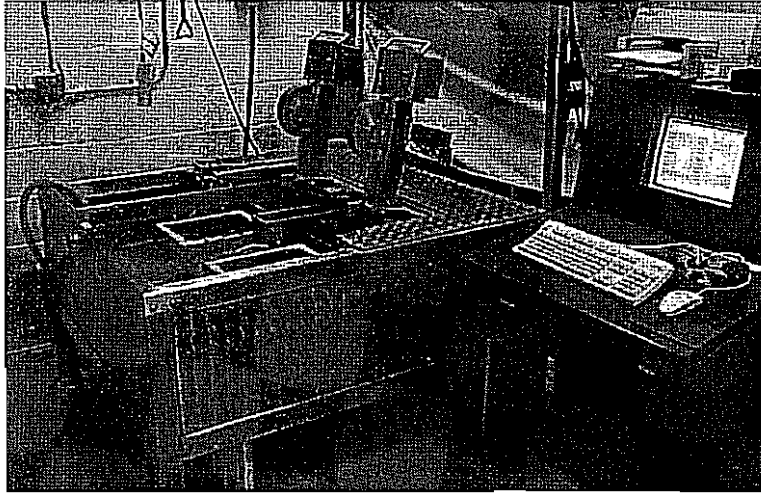


Figure 2.1 Hamburg Wheel Tracking Device Test Set Up

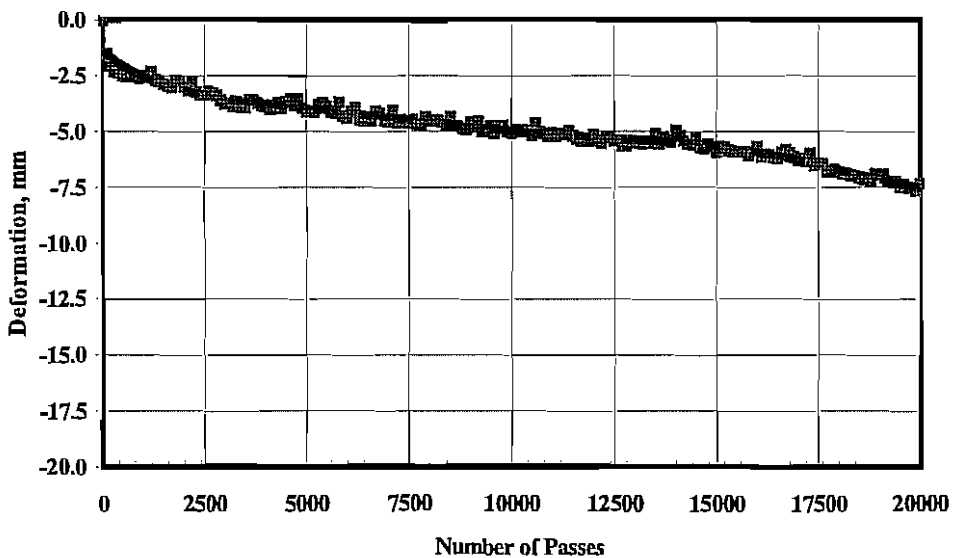


Figure 2.2 A Typical HWT Test Result

Table 2.1 TxDOT Specifications for Hamburg Wheel Tracking Device

High Temperature PG Grade	Number of Passes¹ for Max. Deformation of 12.5 mm
64	10,000
70	15,000
76	20,000

¹ May be decreased or waived when shown on plans

2.2 Static Creep Test (Tex-231-F)

The Static Creep test method is used to determine the resistance to permanent deformation of HMA at temperatures and loads similar to those experienced in the field. Measured creep properties include the total strain, permanent strain, recovered strain and slope of the steady-state portion of the creep curve. According to TxDOT, the main disadvantage of this test is that the results do not seem to be repeatable. The main advantage of this test is that it can be performed within a day and test results reasonably predict the field performance.

2.2.1 Test Procedure and Calculations for Static Creep Tests

Specimens are compacted to a density of $97 \pm 1\%$ using a Texas Gyrotory Compactor (TGC). The compacted specimens, which are nominally 4 in. (100 ± 2 mm) in diameter and 2 in. (50 ± 1 mm) in height, are cooled to room temperature for a period of 24 hours. Three cycles of a 125-lb (556-N) square wave preload in one-minute intervals are applied, followed by a one-minute rest period for each cycle at 104°F (40°C). This allows for the loading platens to achieve a more uniform contact with the specimen. After applying the three seating loading cycles; a 125-lb (556-N) load is applied to the specimen for one hour. At the end of one hour, the load is removed to allow the specimen to rebound for 10 minutes. A typical load versus time diagram is shown in Figure 2.3. During the entire loading and unloading time, the load applied and the resulting vertical deformations from linear variable differential transformers (LVDTs) are monitored and recorded. The parameters evaluated for the analysis are denoted in the Figure 2.4. Creep properties of a specimen, such as stiffness, permanent strain and slope of the steady-state portion of creep curve, can also be determined from the plot.

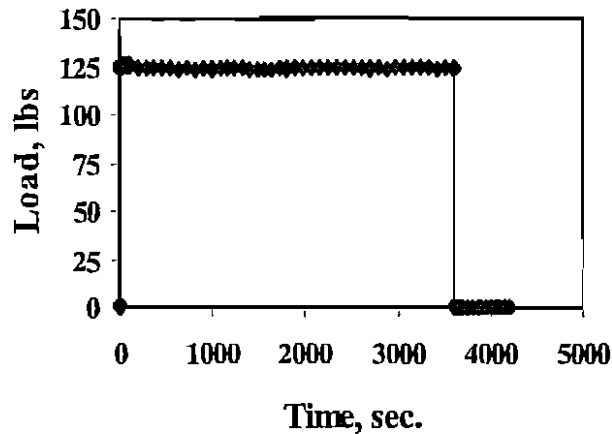


Figure 2.3 Loading Pattern for Static Creep Testing

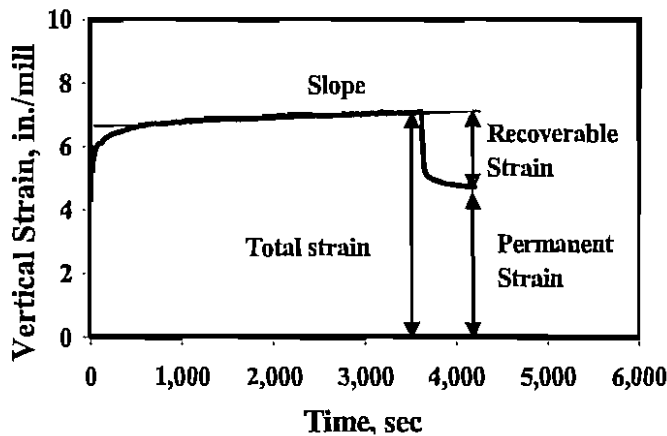


Figure 2.4 Typical Vertical Strain versus Time Plot for Static Creep Test

2.3 Dynamic Modulus Test

To mechanistically model the true behavior of a material, its fundamental properties should be measured. The response of a viscoelastic material such as HMA under a sinusoidal load is sinusoidal, but the response will be out-of-phase with respect to the applied load as shown in Figure 2.5. A phase angle (ϕ) of zero is indicative of a pure elastic material; while $\phi = 90^\circ$ is associated with a pure viscous (Newtonian) material. A phase angle between 0° and 90° corresponds to a viscoelastic material.

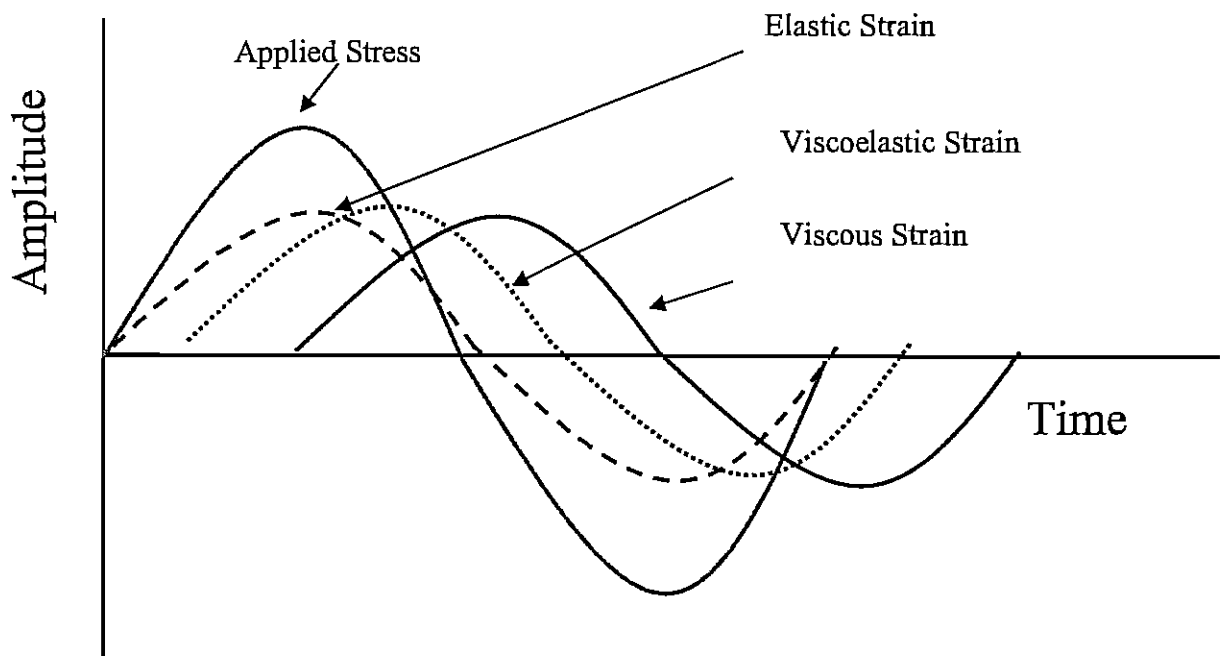


Figure 2.5 Variations in Stress and Strain with Time for Different Materials

For sinusoidal load, the applied stress and observed strain can be denoted by the following equations:

$$\sigma = \sigma_0 \sin \omega t \quad (2.1)$$

and

$$\varepsilon = \varepsilon_0 \sin (\omega t - \varphi) \quad (2.2)$$

Where:

σ = stress at time t

σ_0 = maximum applied stress

ω = angular velocity

φ = phase shift between stress and strain

ε = strain at time t

ε_0 = maximum observed strain

The complex modulus of the material, which is the ratio of the applied stress and the measured strain, can be defined as:

$$E^* = E_0 e^{j\varphi} \quad (2.3)$$

Where:

E_0 is the ratio of σ_0 and ε_0 , j is the identity number and E^* is the complex modulus of the material. The absolute value of $|E^*|$ is termed as dynamic modulus.

One of the advantages of using the dynamic modulus is that the shear modulus, $|G^*|$, can be easily estimated from $|E^*|$ knowing or estimating a Poisson's ratio. Since the new asphalt binder specifications are based on the measured shear

modulus, relationships between the shear moduli of asphalt binder and mixes can also be developed. In addition, the creep-compliance or stress relaxation properties can be fundamentally obtained using $|E^*|$ (Pagen, 1963). The permanent deformation and low temperature cracking models usually utilize $|E^*|$. Above all, the dynamic modulus measurements are used in the newly-proposed mechanistic pavement design guide.

2.3.1 Dynamic Modulus $|E^|$ Prediction Models*

Over the last 50 years, numerous prediction models or related equations have been developed. The $|E^*|$ predicted models and equations were developed on the basis of the conventional multivariate linear regression or non-linear regression, laboratory analysis, test data, and the established or anticipated basic engineering behavior and/or properties of the HMA and its components. The prediction models have the capability to predict the dynamic modulus of dense-graded HMA mixtures over a range of temperatures, rates of loading, and aging conditions from information that is readily available from conventional binder tests and the volumetric properties of the HMA mixtures.

In this study, only the last two versions of the Witczak model are used to compare with the calculated $|E^*|$ values. Although the Hirsch Model was proposed by the researchers, it was not used in this study because of non-availability of G^* data for the whole temperature range.

2.3.1.1 Witczak Model

The first Witczak model was developed more than 25 years ago by Witczak and colleagues at the University of Maryland. Improvements were made to early models; in 1990 Witczak and Fonseca developed a model considered to be superior to the previous versions because this latest version had the ability to evaluate the dynamic modulus taking into consideration a wide variety of asphalt mixtures. In addition, the 1990 version considered some degree of short term and long term aging. In 1999, Andrei, Witczak and Mirza calibrated the previous model using a broader database that included the use of modified asphalts.

2.3.1.2 Witczak and Fonseca's Model

Witczak and Fonseca realized that the previous models $|E^*|$ models had several limitations, the most important being:

- The database on Dynamic Modulus testing was only on lab prepared specimens.
- The models had been based on penetration at 77°F or viscosity at 70°F of the original binder, rather than aged binder, so those models could not be used to predict $|E^*|$ of long-term field aged mixtures.
- The models were calibrated from data obtained between temperature ranges of 41 to 104°F (5 to 40°C). The master curve of such a limited temperature falls into the linear sloped portion of the sigmoidal master curve. Therefore, extrapolation of any parameter outside the range of

variables used to develop the model would lead to erroneous predictions, especially at extreme temperatures beyond those used in the testing.

To correct these limitations, Witczak and Fonseca focused on the following improvements (changes):

- The new model should use actual binder viscosity as predictor variable for binder stiffness.
- The new model form should be selected so it would predict accurately for very cold or hot temperatures.
- The classic 3 factorial temperature-frequency analysis proposed by ASTM should be expanded to 5 temperatures and 6 frequencies.

Taking these parameters into consideration Witczak and Fonseca developed a model using 1430 data points and 149 mixes. The prediction model is as follows:

$$\log E = -0.261 + 0.008225 \cdot \rho_{200} - 0.0000101 \cdot (\rho_{200})^2 + 0.00196 \cdot \rho_4 - 0.03157 \cdot V_a - 0.415 \cdot \frac{V_{b_{eff}}}{(V_{b_{eff}} + V_a)} + \frac{1.87 + 0.002808 \cdot \rho_4 + 0.0000404 \cdot \rho_{38} - 0.0001786 \cdot (\rho_{38})^2 + 0.0164 \cdot \rho_{34}}{1 + e^{(-0.716 \cdot \log(f) - 0.7425 \cdot \log(\eta))}} \quad (2.4)$$

Where:

E = dynamic modulus, 10^5 psi

η = binder viscosity, 10^6 Poise

f = Load frequency in Hz

V_a = air void content, %

$V_{b_{eff}}$ = effective bitumen content, % by volume

ρ_{34} = cumulative % retained on 19 mm sieve

ρ_{38} = cumulative % retained on 9.5 mm sieve

ρ_4 = cumulative % retained on 4.76 mm sieve

ρ_{200} = % passing 0.075 mm sieve

2.3.1.3 Andrei, Witczak and Mirza's Revised Model

The Witczak and Fonseca model had the limitation that the database from which it was created used only traditional binders. The existing database was expanded to include modified binders. The new database included dynamic modulus test results for 56 additional HMA mixtures (including 34 mixtures with modified binders) that provided 1320 new data points for analysis. Andrei et al. (1999) analyzed the expanded database having 2750 data points obtained from 205 HMA mixtures, and came up with a revised E^* predictive model using the similar sigmoidal form as developed earlier by Fonseca and Witczak. To the pavement

community, this model is presently known as the “Witczak E* Predictive Equation” and is as follows:

$$\log E = -1.249937 + 0.029232 \cdot \rho_{200} - 0.001767 \cdot (\rho_{200})^2 - 0.002841 \cdot \rho_4 - 0.058097 \cdot Va - 0.802208 \cdot \frac{Vb_{eff}}{(Vb_{eff} + Va)} + \frac{3.871977 + 0.0021 \cdot \rho_4 + 0.003958 \cdot \rho_{38} - 0.000017 \cdot (\rho_{38})^2 + 0.00547 \cdot \rho_{34}}{1 + e^{(-0.603313 - 0.31335 \cdot \log(f) - 0.393532 \cdot \log(\eta))}} \quad (2.5)$$

It is important to mention that this predicted model is the one currently included in the new Mechanistic-Empirical Design Guide.

2.3.2 Test Procedure and Calculations for Dynamic Modulus Test

The dynamic modulus test procedure is described in the test protocols submitted to the NCHRP under Project 9-19, *Superpave Support and Performance Models Management* (Witczak et al., 2002). Specimens are manufactured by coring and sawing 4 in. (100 mm) diameter by 6 in. (150 mm) high test specimens from the middle portions of 6 in. (150 mm) by 6.5 in. (165 mm) high SGC compacted specimens. The air void content of the cored and sawed specimens should be 93 ± 1%.

The measurement setup for dynamic modulus (DM) must be rigid enough to withstand the applied cyclic loads. A hydraulic dynamic servo-valve closed-loop system manufactured by the MTS Corporation was used in this study. The schematic of the loading subsystem is shown in Figure 2.6. The specimen is placed on the bottom end platen, which is tightly attached to a steel base plate through a stainless steel cylinder. To minimize the vibration of the specimen, all components should be precisely machined, and custom matched.

Two LVDTs are used to measure the deformation of the specimen. The positions of the LVDTs are shown in Figure 2.6. Two targets are fixed on one side of the specimen with a gauge length of 4 in. (102 mm) and two other targets are fixed exactly on the opposite side of the specimen. The strain experienced by the specimen is the average of the deformations on the two opposite sides of the specimen divided by the gauge length.

To measure the dynamic modulus, the test procedure and data reduction process proposed in Project 9-19, *Superpave Support and Performance Models Management* were adopted. Since that test procedure recommended that the strain within the specimen should be maintained within a range of 50 µε to 150 µε, the applied load is adjusted for every frequency and temperature to achieve the appropriate strain level. A seating load is applied at each loading sequence in a manner that the minimum loads were never less than 5% of the maximum load.

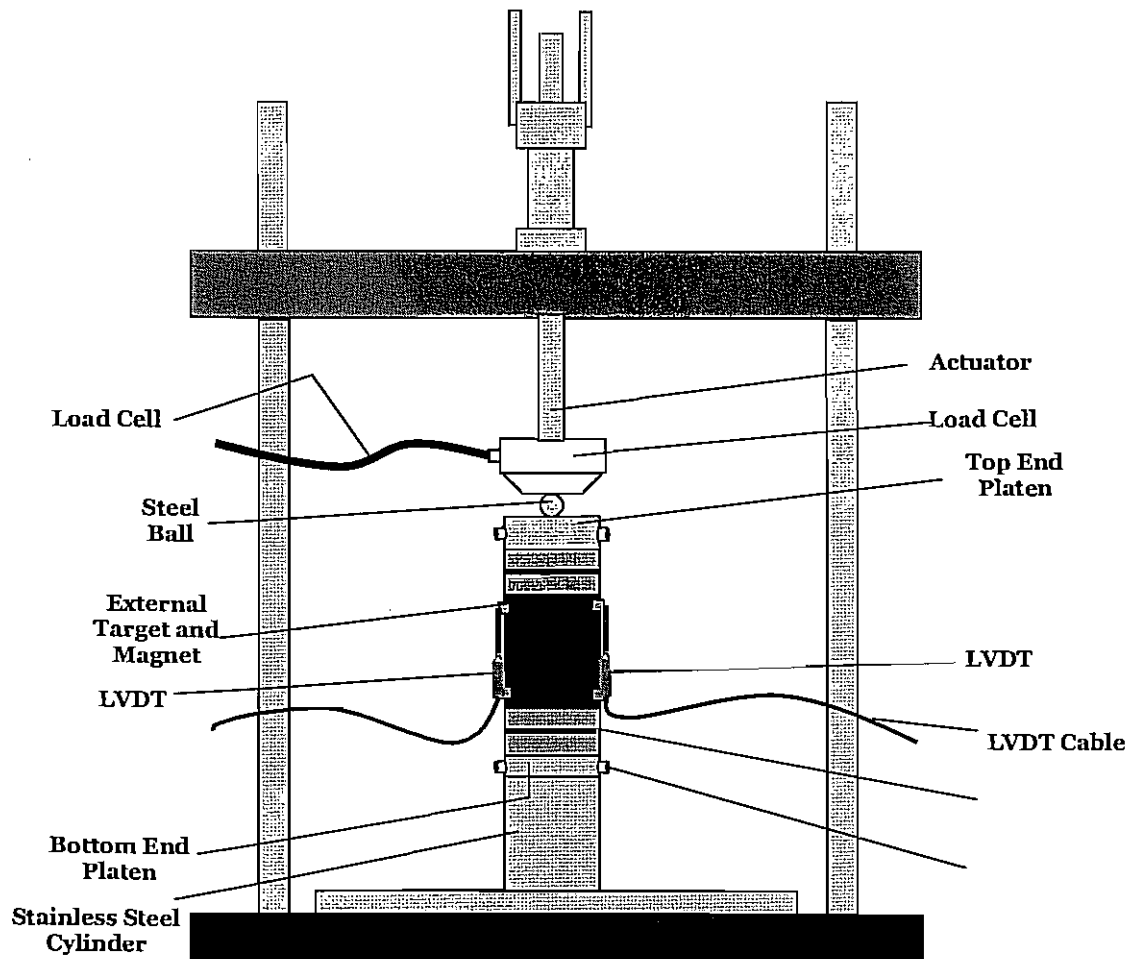


Figure 2.6 A Schematic of Dynamic Modulus Test Setup

Each specimen is tested at five temperatures: 14, 40, 73, 100 and 130°F (-10, 4, 23, 38 and 54°C). To perform the test at each temperature, the specimen is initially subjected to 200 conditioning cycles at 20 Hz. After the initial conditioning, the specimen is subjected to 50 loading cycles at 10 Hz and 5 Hz. In the end, the specimen is subjected to seven loading cycles at frequencies of 10, 5, 2 and 1 Hz. This sequence of testing results in a total of 50 dynamic modulus tests on each specimen. To minimize the potential internal damage to the specimen, tests are performed from the lower to the higher temperatures and from the higher to lower frequencies. After each test, the data is analyzed to ensure that the strains are between 50 µε and 150 µε and that the displacements of the opposite sides of the specimen are within 15% of one another. If the difference exceeds 15%, the specimen is discarded and a new specimen is tested. To estimate the dynamic modulus, the average amplitude of the load and the strain over the last six loading cycles are recorded. The dynamic modulus is estimated using the ratio of peak stress and peak strain.

A typical plot of measured dynamic modulus at each frequency and at different temperatures is shown in Figure 2.7. Assuming that the time-temperature superposition principle is valid, the moduli from each temperature are shifted horizontally to produce a master curve at a reference temperature. Typical shift factor plot is shown in Figure 2.8. The shifted master curve at 23°C (73°F) is shown in Figure 2.9. As expected, the dynamic moduli for the higher temperatures (54°C and 38°C) have to be shifted to the left while the moduli for the lower temperatures (4°C and -10°C) have to be shifted to the right to generate the master curve. The curve fitting to the master curve (Figure 2.10) is done by using a method developed by Pellinen and Witczak (2002). That method consists of fitting a sigmoidal curve described in Equation 2.8 to the measured dynamic modulus test data using nonlinear least-squares regression techniques.

$$\text{Log} (E^*) = \delta + \frac{\alpha}{1 + e^{[\beta + \gamma \log(\frac{1}{Hz})]}} \quad (2.8)$$

2.4 Flow Number Test

The flow number test is a variation of the repeated load permanent deformation test that has been used to measure the rutting potential of asphalt concrete mixtures (Roberts et al., 1996). Haversine axial compressive load pulses similar to resilient modulus are applied to the specimen. The permanent axial deformation at the end of the rest period is monitored during repeated loading and converted to strain. Witczak et al. (2002) introduced the concept of flow number, which is defined as the number of load pulses when the minimum rate of change in permanent strain occurs during the repeated load test. It is determined by differentiating the permanent strain versus number of load cycles curve. The flow time test is quite appealing as a simple performance test because it is possible to use relatively simple equipment.

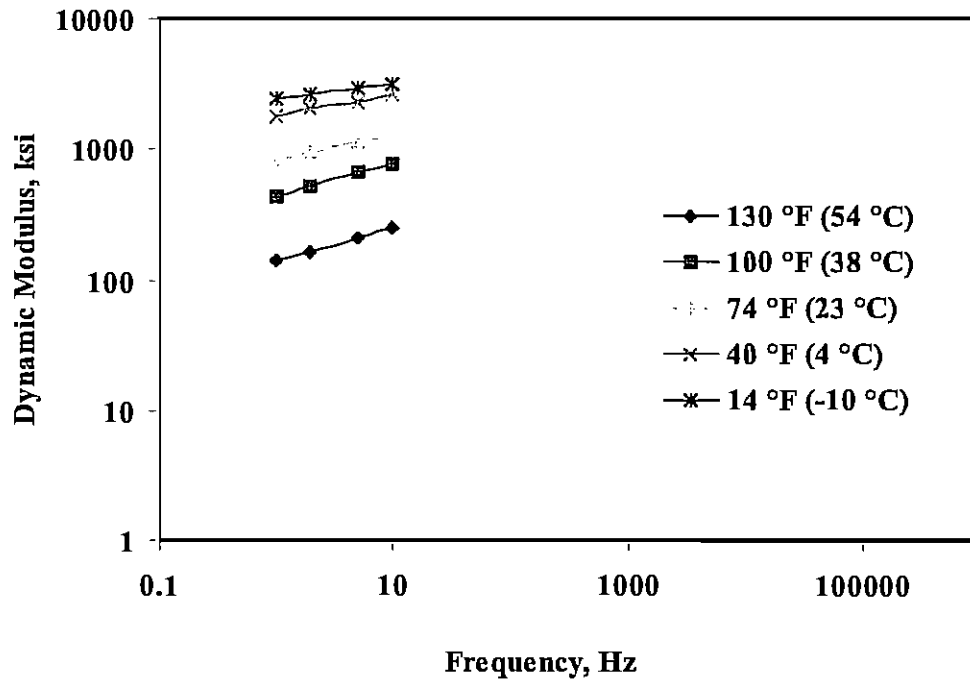


Figure 2.7 Typical Dynamic Modulus versus Frequency Relationship at Different Temperatures

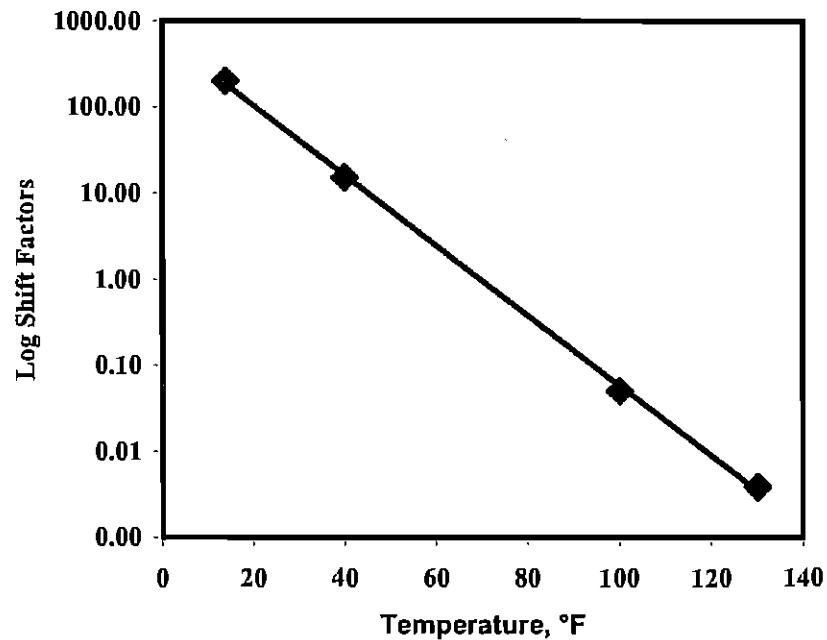


Figure 2.8 Typical Log Shift Factor versus Temperature Plot

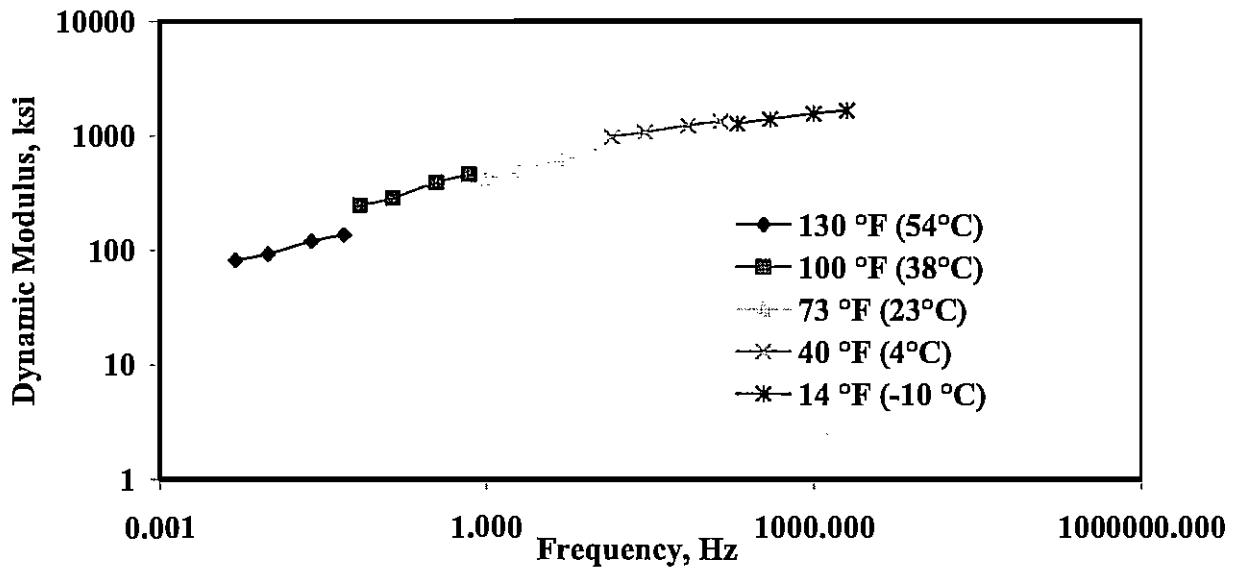


Figure 2.9 Shifted Dynamic Modulus versus Frequency Relationship

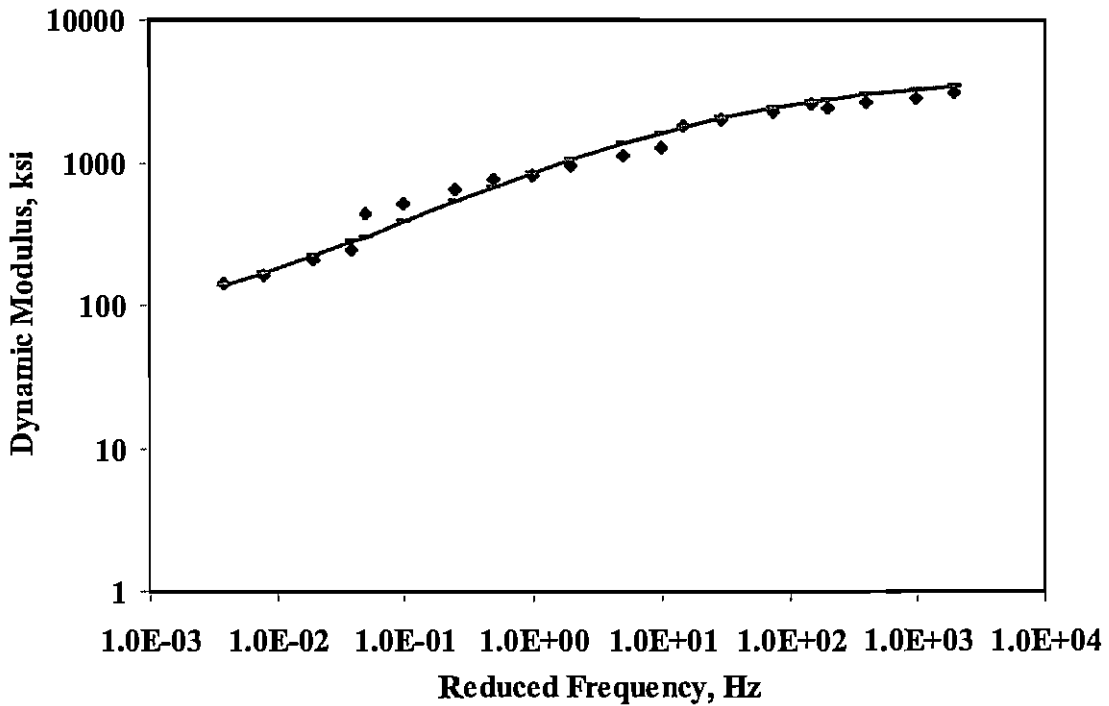


Figure 2.10 Typical Master Curve

2.4.1 Test Procedure and Calculations for Flow Number Test

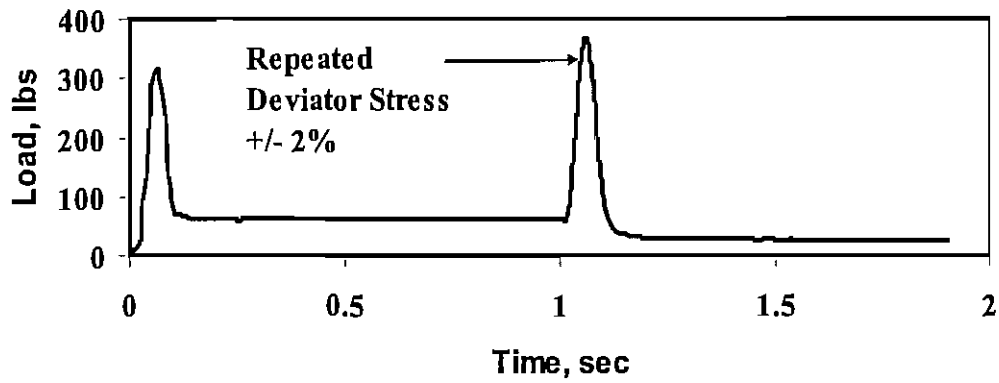
The specimen preparation process and test setup are similar to the dynamic modulus test with one exception. The deformation of specimen is monitored with the actuator LVDT rather than LVDTs mounted on the specimen. The flow number test is performed by the application of haversine axial compressive load pulses rather than sinusoidal load pulses to a specimen with a diameter of 4 in. and height of 6 in. as shown in Figure 2.11a. The duration of the load pulse is 0.1 seconds, followed by a rest period of 0.9 seconds. The test duration is about 3 hours for 10,000 loading cycles. The permanent axial deformation measured at the end of the rest period is monitored during the repeated loading (Figure 2.11b) and converted to strain. The recommended test protocol consists of testing the asphalt mix at one effective pavement temperature T_{eff} and one design stress level. The effective pavement temperature T_{eff} covers approximately the temperature range of 77°F (25°C) to 140°F (60°C). The design stress levels cover the range between 10 psi (69 kPa) and 30 psi (207 kPa) for the unconfined tests. Typical confinement levels range between 5 psi (35 kPa) and 30 psi (207 kPa).

In NCHRP Project 9-19, the SPT tests results were correlated with the actual field distress for three test sites (MnRoad, WestTrack and the ALF). The flow number and flow time tests were performed at axial stresses of 10 psi and 30 psi and 100°F and 140°F. They found that the flow number and flow time results at a stress of 30 psi conducted at 140°F (54°C) correlated well with the rutting resistance of the mixtures used in the experimental sections at MnRoad, WestTrack and the ALF. Therefore, a test temperature of 140°F (54°C) and a stress level of 30 psi (210 kPa) were selected for this study.

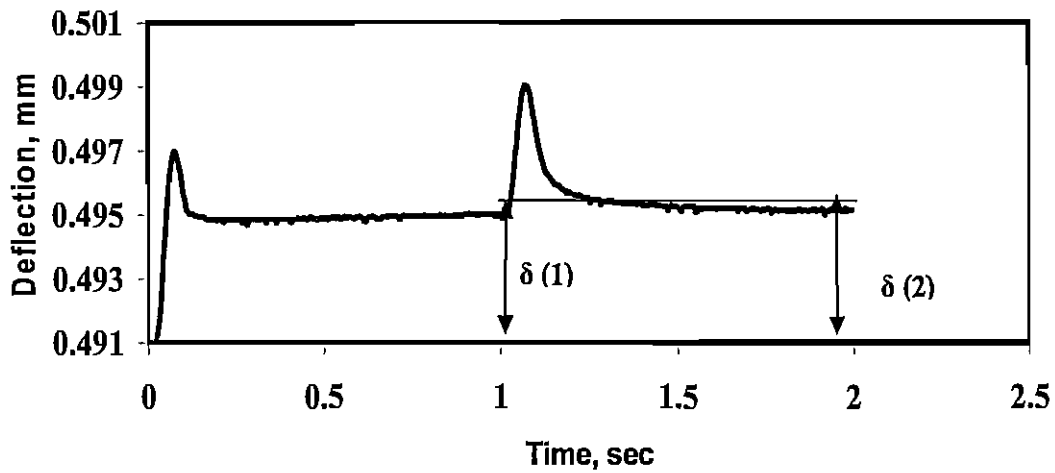
The results of the permanent deformation test in terms of the cumulative permanent strain versus the number of loading cycles on a log-log scale are presented in Figure 2.12a. The intercept a represents the permanent strain for the first cycle, whereas the slope b represents the rate of change in loading cycles. These two are derived from the linear portion of the cumulative plastic strain-repetitions relationship. The equation used to analyze these test results is

$$\epsilon_p = aN^b \quad (2.9)$$

Another graph is drawn between the rate of change of axial strain and the loading cycle as shown in Figure 13b. The flow number is defined as the number of load cycles corresponding to the minimum rate of change in the permanent axial strain. In this study, the response presented in Figure 2.12b was used to determine the number of load cycles to failure as well.

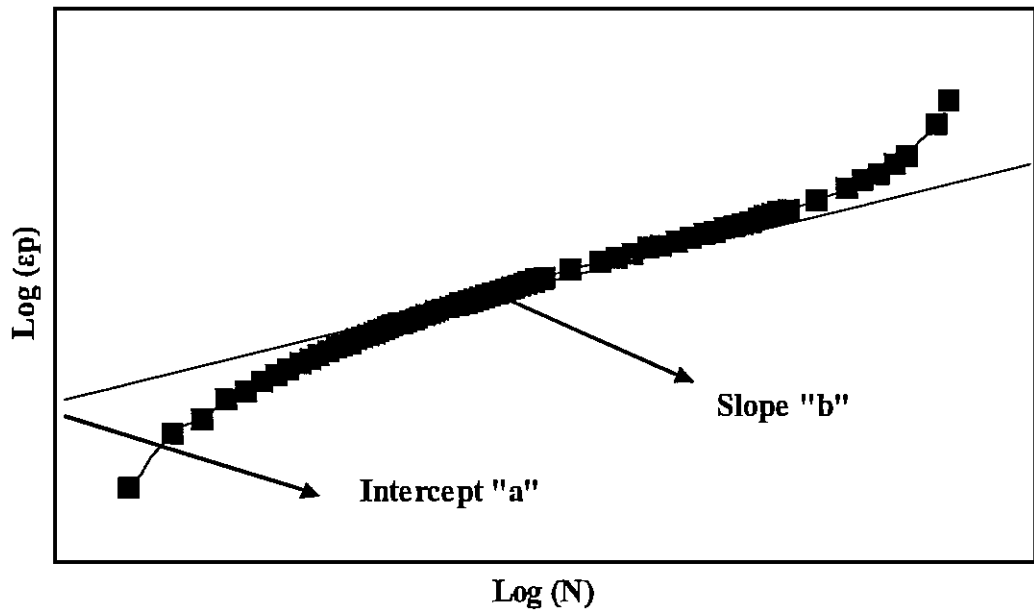


(a) Load versus Time Plot

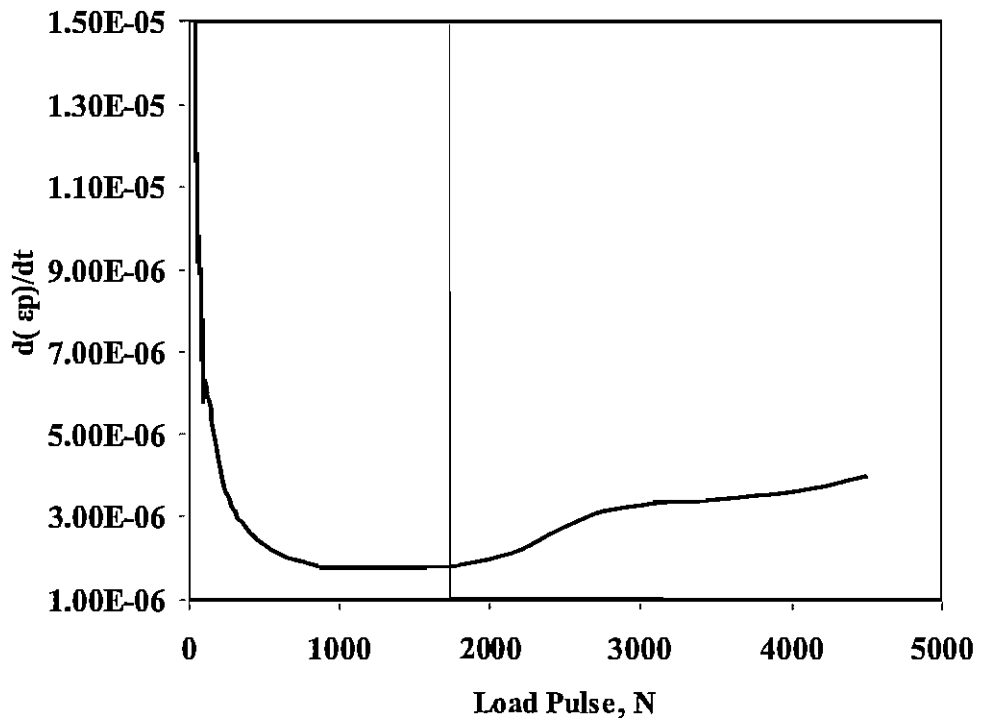


(b) Deflection versus Time Plot

Figure 2.11 Load Application and Expected Response from Flow Number Test



a) Regression Constants 'a' and 'b'



b) Rate of Change of Permanent Axial Strain versus Load Pulse

Figure 2.12 Flow Number Test Results

2.5 Flow Time Test

The modulus of a material is an important property that relates stress to strain and is used to predict pavement distresses. For viscoelastic materials, however, it is more advantageous to use the term “compliance” or $D(t)$. Compliance is the reciprocal of the modulus. The main advantage of its use in the viscoplastic theory is that the compliance allows for the separation of the time-independent and time-dependent components of the strain. In a static compressive creep test, a total strain-time relationship for a mixture is established in the laboratory under unconfined or confined conditions. The static creep test, using either one load-unload cycle or incremental load-unload cycles, provides sufficient information to determine the instantaneous elastic (i.e., recoverable) and plastic (i.e., irrecoverable) components of the material response (which are time independent), as well as the viscoelastic and viscoplastic components (which are time dependent).

The flow time test is a variation of the static creep test commonly performed by TxDOT to assess the rutting potential of HMA. In this test, a static load is applied to the specimen, and the resulting strains are recorded as a function of time. The variation introduced in the NCHRP study is the concept of flow time, which is defined as the time when the minimum rate of change in strain occurs during the creep test. The flow time is determined by differentiating the strain versus time curve. The flow time test is quite appealing as a simple performance test because the equipment is simple and the training required for its implementation is minimal. One major difference between the NCHRP and TxDOT procedures is the specimen size (4 in. by 6 in. cylinder) which may be one factor that reduces the variability of the test results as compared to the TxDOT process.

2.5.1 Test Procedure and Calculations for Flow Time Test

The specimen preparation process and test setup are similar to the flow number test setup with one exception. Tests are performed at a temperature of 140 °F (54°C) and a stress level of 30 psi (210 kPa) similar to the flow number tests. However, the stress level of 30 psi is maintained for three hours rather than applying the dynamic haversine axial compressive cyclic loads.

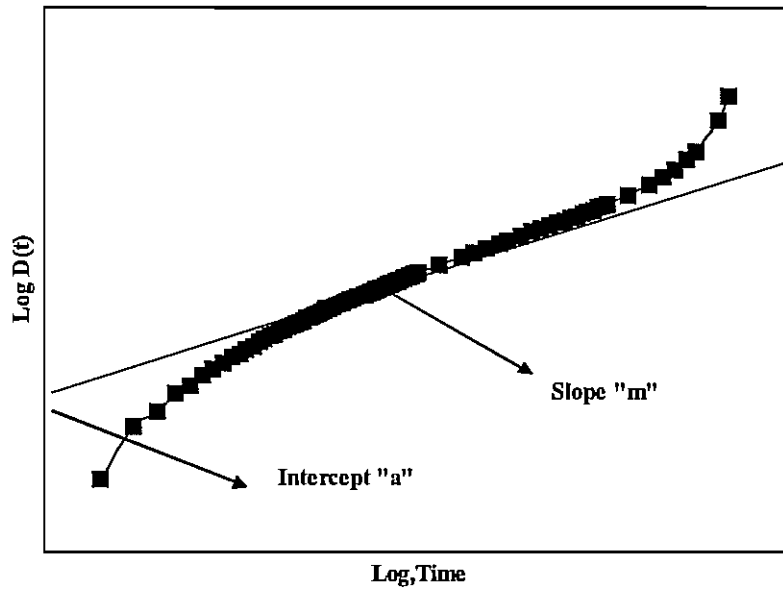
Figure 2.13a shows a typical relationship between the calculated total compliance and loading time. The point at which a large increase in compliance occurs at a constant volume is defined as the flow time, which has been found to be a significant parameter in evaluating the rutting resistance of an HMA mixture. In general, power models are used to model the secondary (i.e., linear) phase of the creep compliance curve, as illustrated in Figure 2.13b. A common model is in the form of

$$D'(t) = D(t) - D_o = at^m \quad (2.10)$$

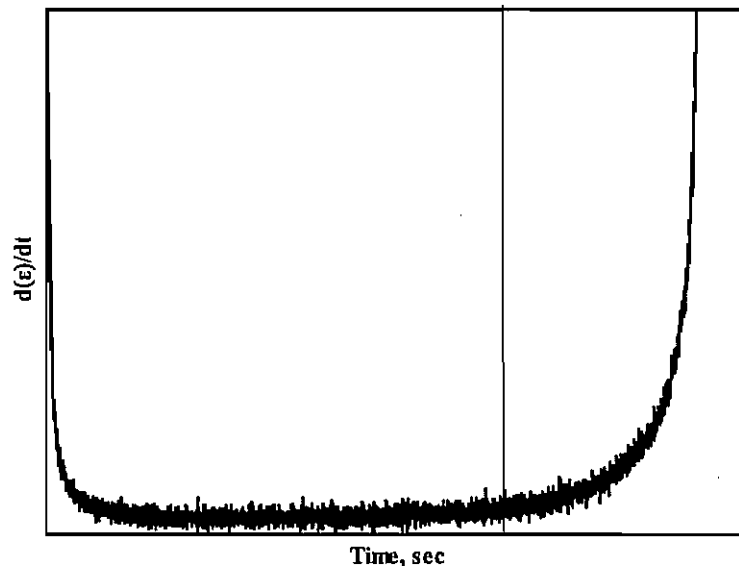
Where:

$D'(t)$ = viscoelastic compliance component at time t ,

$D(t)$ = total compliance at time t ,
 D_0 = instantaneous compliance,
 t = loading time, and
 a, m = material regression coefficients.



a) Regression Constant "a" and "m"



b) Rate of Change in Compliance versus Loading Time

Figure 2.13 Flow Time Test Results

The regression coefficients a and m are generally referred to as the compliance parameters. In general, the larger the value of a , the larger the compliance value, $D(t)$, the lower the modulus, and the larger the permanent deformation will be.

For a constant a , an increase in the slope parameter m means a higher rate of permanent deformation.

The flow time also is viewed as the minimum point in the relationship of the rate of change of compliance to loading time, as shown in Figure 2.13b. The flow time is therefore defined as the time at which the shear deformation under constant volume begins. In this study, the response presented in Figure 2.13b was used to assess the failure of the mixes as well.

2.6 Indirect Tensile (IDT) Strength Test

According to Witczak et al. (2002), the indirect tensile test (IDT) has been extensively used in the structural design of flexible pavements since the 1960s and, to a lesser extent, in HMA mixture design. The IDT is the test recommended for mixture characterization in the Long-Term Pavement Performance (LTPP) Program, and to support the structural design in the 1986 and 1993 AASHTO design guides. The IDT is one of the most popular tests used for the characterization of HMA mixtures, primarily because cores from thin lifts can be tested directly in the laboratory. Although the reliability of the IDT to detect and predict moisture damage is questionable, no other test has been found to provide consistent results at a higher reliability. In addition, SHRP recommended the use of the indirect tensile creep test method to characterize the HMA mixtures for thermal-cracking predictions.

The IDT method is used to develop the tensile stresses along the diametral axis of a test specimen. The test is conducted by applying a compressive load to a cylindrical specimen through two diametrically opposed, arc shaped rigid platens. Based on the theory of elasticity, the strain can be expressed in three dimensions. Ideally, the 3-D analysis can be reduced to a 2-D analysis for special element-size and loading conditions. For the case of a circular disk, the 2-D analysis can be categorized as plane stress.

2.6.1 Test Procedure and Calculations for Indirect Tensile Test

The IDT is specified in test method Tex-226-F "Indirect Tensile Strength Test". The specimens are compacted to a density of $93 \pm 1\%$ using a TGC. The compacted specimens that are 4 in. in diameter and 2 in. thick are loaded diametrically at a rate of 2 in./min. along and parallel to their vertical diametric planes. The loading configuration described develops a relatively uniform state of tensile stresses perpendicular to the load direction, which results in splitting of the specimen. In this study, tests were performed at 40°F (5°C) to estimate the low temperature properties of the mixes. Although it was decided to perform tests at 14°F, the load cell limits required that tests be performed at a higher temperature. During the test, load and vertical displacement are recorded as shown in Figure 2.14.

The recorded load at failure, P_f , is used to calculate the indirect tensile strength of the specimen using Equation (2.11):

$$\sigma_f = \frac{2P_f}{\pi dt} \quad (2.11)$$

Where:

σ_f = stress at failure, which is equivalent to the indirect tensile strength,

P_f = recorded load at failure,

d = specimen diameter, and

t = specimen thickness.

Other parameters that can be obtained from the IDT strength test include the fracture energy to failure (area under the load-vertical deformation curve until maximum load) and total fracture energy (area under the load-vertical deformation curve) (Witczak et al., 2002). A typical plot of two fracture energies is included in Figure 2.15.

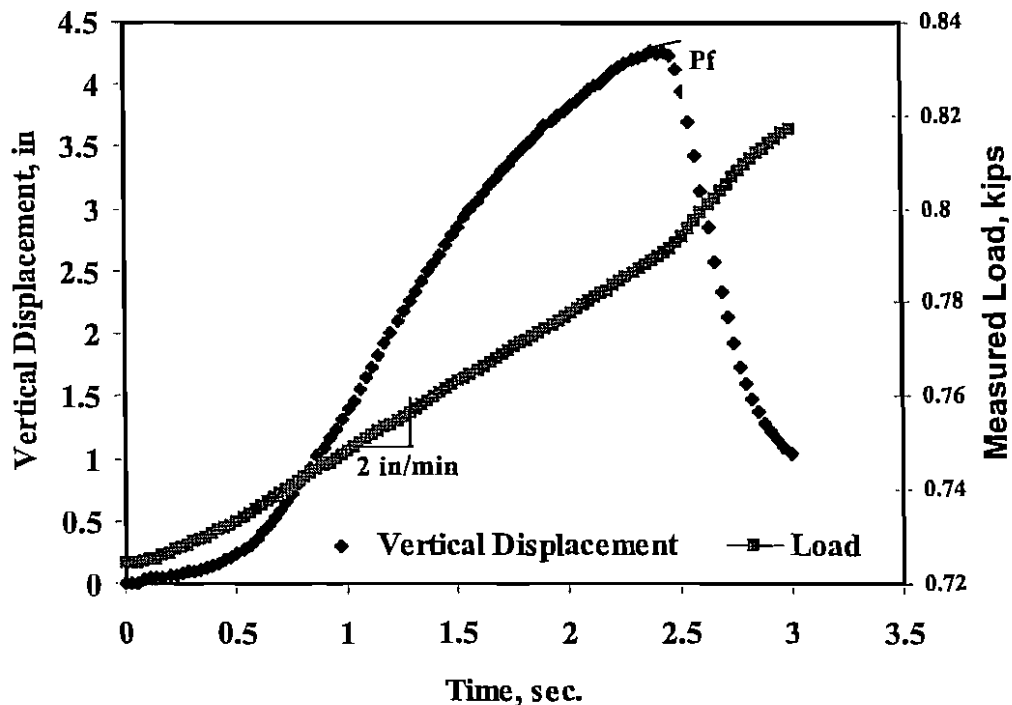


Figure 2.14 Typical Data Recorded During the IDT Strength Test

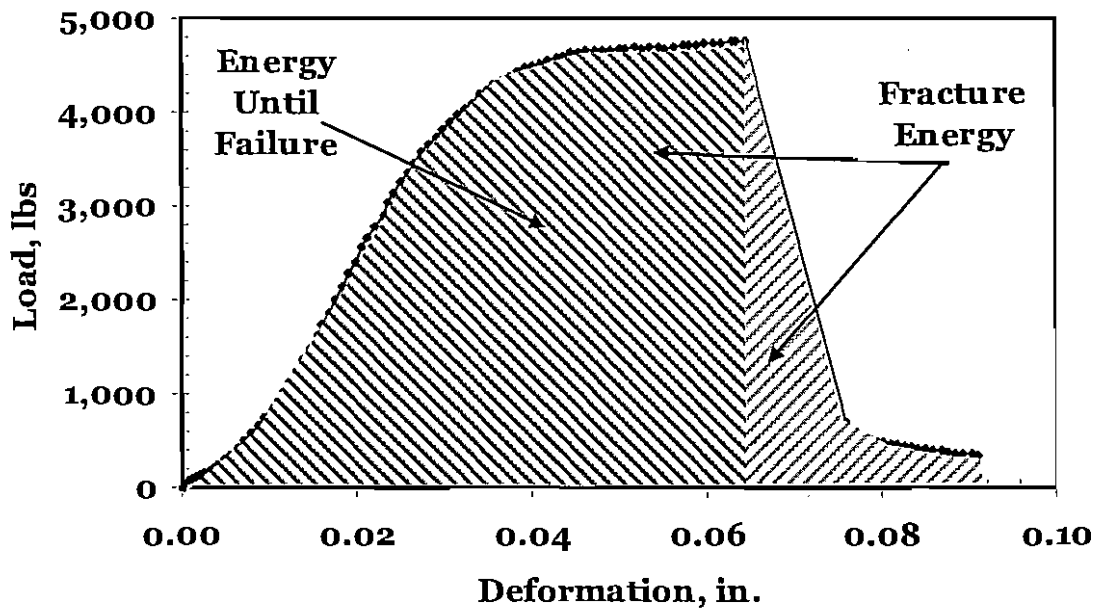


Figure 2.15 Indirect Tensile Strength Test Results (Load versus Deformation)

2.7 Flexural Beam Fatigue Test

Load-associated fatigue cracking is one of the major distress types occurring in flexible pavement systems (Monismith et al., 1985; Tangella et al., 1990; Tayebali et al., 1994). The action of repeated loading caused by traffic induces tensile and shear stresses in the bound layers, which will eventually lead to a loss in the structural integrity of a stabilized layer. Fatigue cracks initiate at points where critical tensile strains and stresses occur. Additionally, the critical strain is also a function of the stiffness of the mix. Since the stiffness of an asphalt mix in a pavement varies with depth, these changes will eventually affect the location of the critical strain that causes fatigue damage. Once the damage initiates at the critical location, the action of traffic eventually causes these cracks to propagate through the entire bound layer.

As pavement technology has progressed over the last 3 to 4 decades, it has been generally assumed that fatigue cracking normally initiates at the bottom of the asphalt layer and propagates to the surface (bottom-up cracking). This is due to the bending action of the pavement layer that results in flexural stresses developing at the bottom of the bound layer. However, numerous recent worldwide studies have clearly demonstrated that fatigue cracking may also be initiated from the top and propagated down (top-down cracking). This type of fatigue is not as well defined from a mechanistic viewpoint as the more classical "bottom-up" fatigue. In general, it is hypothesized that critical tensile and/or shear stresses develop at the surface and cause extremely large contact pressures

at the tire edge-pavement interface. This scenario, coupled with highly-aged (stiff) thin surface layers that have become oxidized, is felt to be responsible for the surface cracking. To characterize fatigue in asphalt layers, numerous models can be found in the existing literature. The most common model used to predict the number of load repetitions to fatigue cracking is a function of the tensile strain and mix stiffness (modulus).

The fatigue resistance of an asphalt mix is its ability to withstand repeated bending without fracture. Fatigue fracture is the result of repeated tensile stresses and strains caused by traffic loading and thermal stresses in the pavement. For typical heavy duty pavements, fatigue cracking results from repeated tensile stresses or strains at the underside of the asphalt layers having a maximum value less than the tensile strength of the material. The maximum principal tensile strain is considered the primary determinant of fatigue cracking. Laboratory tests such as AASHTO T321-03 (AASHTO, 2004) are available to subject an asphalt beam to repeated loading while measuring the flexural stiffness of the beam to simulate the field loading conditions of an asphalt pavement. One application of loading and unloading is termed as a cycle. Monismith developed Equation 2.12 based on the same concept to predict the fatigue life of a specific mix based on the strain levels used for testing and initial mix stiffness (Monismith et al., 1985).

$$N_f = a \left(\frac{1}{\epsilon_0} \right)^b \left(\frac{1}{S_0} \right)^c \quad (2.12)$$

Where:

N_f = fatigue life (number of cycles to reach 50% of initial stiffness),

ϵ_0 = tensile strain,

S_0 = initial mix stiffness,

a, b and c = experimentally determined parameters

In the laboratory, two types of controlled loading are generally applied for fatigue characterization: constant stress and constant strain. In constant stress testing, the applied stress during the fatigue testing remains constant. As the repetitive load causes damage in the test specimen, the strain increases resulting in a lower stiffness with time. In the case of the constant strain test, the strain remains constant with the number of repetitions. Because of the damage due to repetitive loading, the stress must be reduced resulting in a reduced stiffness as a function of repetitions. The constant stress type of loading is considered applicable to thicker pavement layers usually more than 8 in., while constant strain of loading is considered applicable to thinner pavements usually less than 4 in. (SHRP-A-404). For AC thicknesses between these extremes, fatigue behavior is governed by a mixed mode of loading, mathematically expressed as some model yielding intermediate fatigue prediction to the constant strain and stress conditions.

2.7.1 Test Procedure and Calculations for Flexural Beam Fatigue Test

The AAHTO T321-03 (AASHTO, 2004) standard provides procedures for determining the fatigue life and fatigue energy of HMA beam specimens subjected to repeated flexural bending until failure. The fatigue life and failure energy determined by this standard can be used to estimate the fatigue life of HMA pavement layers under repeated traffic loading. The four point bending beam test procedure (at constant strain) entails applying repeated loading and unloading to a beam specimen until the flexural stiffness of the specimen reduces to a predetermined value (usually 50% of original stiffness). One such application of loading and unloading is termed as a load cycle. The load is so applied that the specimen experiences constant strain amplitude during each loading cycle. Repeated sinusoidal loading at a frequency range of 5 to 10 Hz is usually applied subjecting specimens to four-point bending with free rotation and horizontal translation at all load and reaction points with the flexural stiffness estimated after every 10 cycles.

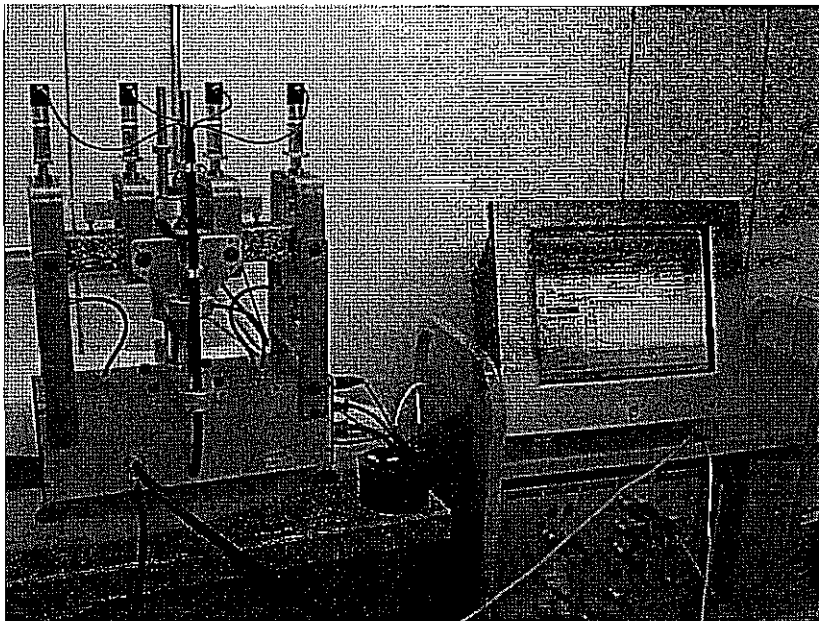


Figure 2.16 Fatigue Beam Testing Apparatus

The constant strain level can be fixed from 250 to 750 microstrains as specified by AASHTO T321. Based on screening tests, strain levels from 250 to 500 microstrains were considered appropriate for mixes with unmodified binders, and between 500 and 750 $\mu\epsilon/\epsilon$ (microstrains) were considered appropriate for modified binders. These strain levels were selected so that the duration of the test is appropriate (it neither fails in less than 100,000 cycles as specified by AASHTO nor continues for more than one week). The loading frequency was fixed at 10 Hz

and the temperature chamber maintained at 68°F (20°C). The loading waveform was selected as sinusoidal as shown in Figure 2.17.

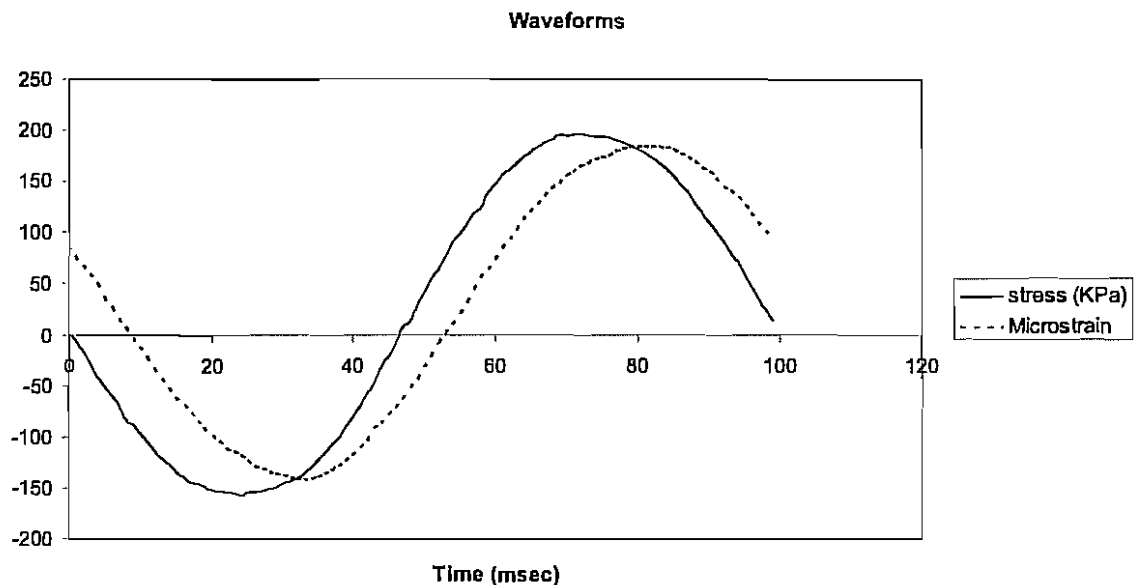


Figure 2.17 Sinusoidal Load Waveform

2.8 Ultrasonic Testing

The ultrasonic device is a portable seismic device that measures travel time of seismic wave pulses through a material. The seismic waves are generated by a built-in pulse generator, which transforms an electrical pulse to a mechanical vibration through a transducer. The seismic wave arrival time is recorded by a receiver, which is connected to an internal clock. The internal clock has the capability of automatically measuring and displaying the travel time of the waves. The travel time and the density of the specimen are used to determine the moduli of the HMA specimens. The main advantage of this test is that it is nondestructive. In addition, the tests can be performed on both laboratory-prepared specimens and field cores. Another advantage is that the modulus measured can be combined with dynamic modulus curve to develop field acceptance criterion.

2.8.1 Test Procedure and Calculations for Ultrasonic Test

The specimens prepared for the tests described above can be used to perform ultrasonic tests (Nazarian et al., 2003). The ultrasonic laboratory setup used in this study is shown in Figure 2.18. The elastic modulus of a specimen is measured using an ultrasonic device containing a pulse generator and a timing circuit, coupled with piezoelectric transmitting and receiving transducers. The

dominant frequency of the energy imparted to the specimen is 54 kHz. The timing circuit digitally displays the time needed for a wave to travel through a specimen. To ensure full contact between the transducers and a specimen, special removable epoxy couplant caps are used on both transducers. To secure the specimen between the transducers, a loading plate is placed on top of the specimen, and a spring-supporting system is placed underneath the transmitting transducer. The receiving transducer, which senses the propagating waves, is connected to an internal clock. The clock automatically displays the travel time, t_v that can be used to calculate the constrained modulus, M_v , as:

$$M_v = \rho V_p^2 = \rho \left(\frac{L}{t_v} \right)^2 \quad (2.13)$$

Where:

ρ = density

V_p = compression wave velocity

L = average length of the specimen

This equation may be simplified to:

$$M_v = \frac{4mL}{\pi d^2 t_v^2} \quad (2.14)$$

Where:

m = mass of the specimen

d = average diameter of the specimen.

Young's Modulus, E_v , may be determined from:

$$E_v = M_v \left[\frac{(1-2\nu)(1+\nu)}{(1-\nu)} \right] \quad (2.15)$$

The Poisson's ratio, ν , can be assumed based on experience.



Figure 2.18 Ultrasonic Test Device for HMA Specimens

CHAPTER 3 EXPERIMENT DESIGN AND SPECIMEN PREPARATION FOR PERFORMANCE EVALUATION

To evaluate the influence of modified binder on performance, three mix types and seven binders were selected and tested. The reasons for the selection of mixes, mix design, asphalt binder properties and relevant information are presented in this chapter.

3.1 Selection of Mixes

To achieve the objectives of this study, a survey of TxDOT districts was performed. The purpose of the survey was to gather information required for the selection of HMA and polymer modified binders. In addition, the survey aimed to identify and bring together current practices and opinions to aid in the development of guidelines for the selection of HMA and modified binders in Texas. The survey was sent to TxDOT district offices as well as area offices. A total of 27 survey responses were received.

The survey asked specific questions relating to different aspects of asphalt mixture design, cost and performance. The use of polymer-modified binders was also addressed. It should be mentioned that the survey at best reflects a general trend. Responders did not answer each and every question posed. There were many gaps in the responses; hence, the "general consensus" parameter as plotted is low overall for most of the questions posed. The ranking of the elements of each question posed should therefore be considered relatively. Since results of the survey were communicated to TxDOT via a Technical Memorandum (Smit et al., 2004), only the information relevant to this report is provided here.

The response to the question of mix types used in the various districts is included in Figure 3.1. The majority of the districts use the regular dense type mixes. Typically, Type A and Type B mixes are used for base layers while Type C and D are used in surface layers. The Stone Matrix Asphalt (SMA), Superpave and CMHB mixes are also popular. Three of the survey responders cited other mixes used in their districts including asphalt roof tab (10%) (Dallas) and asphalt stabilized base (Beaumont). The point was made that CMHB-F and Crumb Rubber Modified asphalt concrete (CRM-HMAC) are similar mixes. The responder from the Paris District noted that most hot mix used in that district contains bottom asb instead of field sand.

The response to the question of HMA problems experienced with the cited mixes in terms of rutting, fatigue and cracking is included in Figure 3.2.

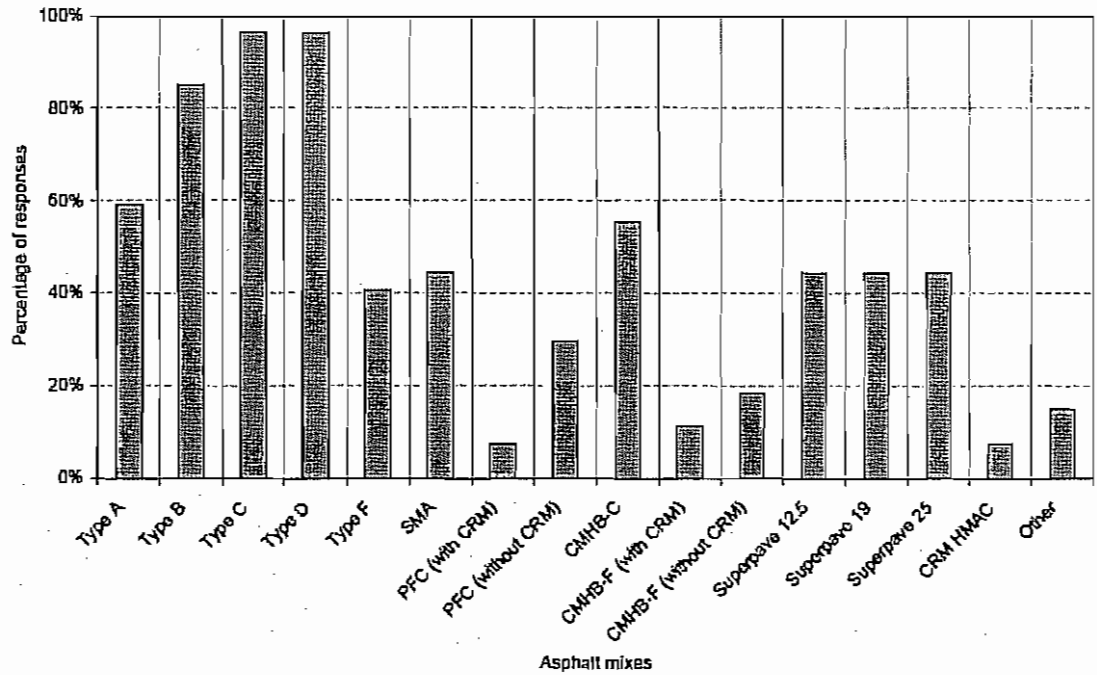


Figure 3.1 HMA Use in the Districts

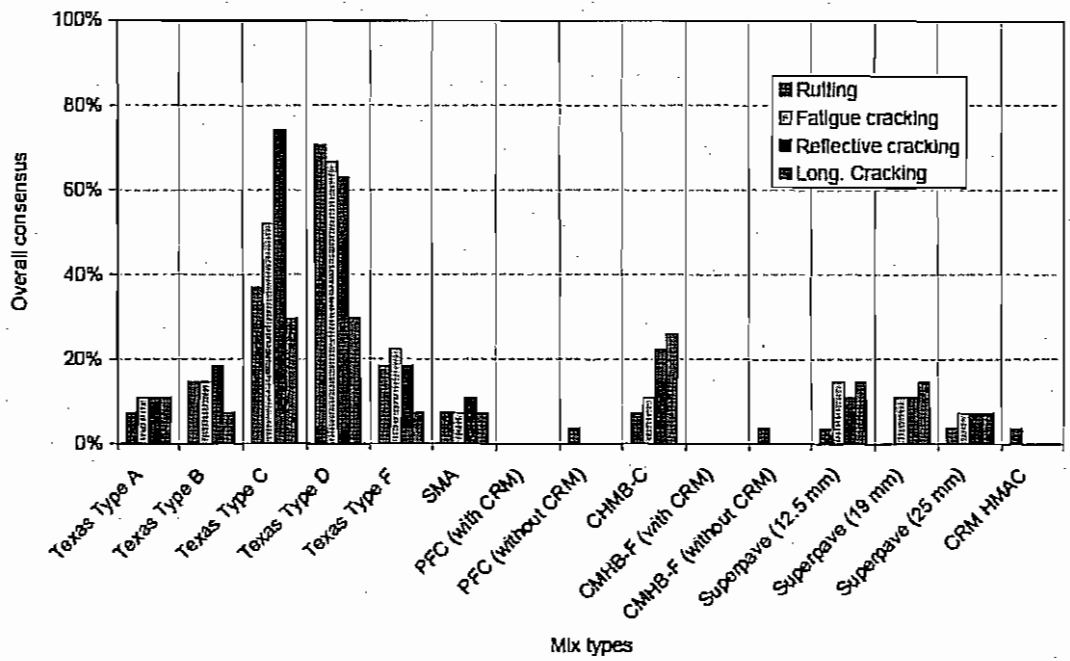


Figure 3.2 HMA Structural Problems Experienced

Figure 3.3 shows problems experienced in terms of flushing, segregation, raveling and stripping. A cause for concern should be the high consensus regarding rutting, fatigue and reflective cracking of Type D mixes in Texas as well as the high consensus regarding reflective cracking and fatigue of Type C mixes. The fatigue and cracking problems with these mixes are known given that their design is more focused on alleviating rutting, resulting in the use of lower binder contents and stiffer binders. Segregation appears to be a problem for all mixes and is probably due to placement procedure rather than production and hauling of the mixes. Stripping of Type D mixes is emphasized.

The districts were also asked to rank their experience regarding the performance of mixes used in Texas with respect to rutting, fatigue, reflective and longitudinal cracking as well as noise, skid and splash. Figure 3.4 shows the responses with respect to resistance to rutting. Overall, it appears that rutting is not a problem for the mixes cited. Mixes with stiffer (PG 76) binders have superior rutting performance. Poor rutting performance is noted for Type D mixes with PG 64 binders. Poor rutting performance is also reported for Type F mixes. As expected, superior rutting resistance is shown for SMA mixes. Figure 3.5 shows the consensus regarding the fatigue resistance of the mixes. While the general consensus is that fatigue resistance of mixes appears to be adequate, the percentage of positive responses concerning poor fatigue resistance is relatively high for the regular dense type mixes regardless of binder stiffness.

Figure 3.6 shows which modifiers have been used with the listed mixes in Texas. The most commonly used modifier is SBS followed by SBR Latex and then Tire Rubber. Elvaloy is considered, particularly for the dense graded mixes. Only Beaumont reported the use of EVA with Type C mixes. Modifiers are generally not used in the Paris District. The Childress District requires SBS in all mixes. They point out that they tried Elvaloy a couple of years ago, but that it didn't perform well. The Atlanta District reported experiencing compatibility issues with latex during the 1990s. The El Paso District only recently began to require an additive in the asphalt. Previously, El Paso was the only district in the state using a PG 76-16 produced without an additive on all mixes and construction projects. The Tyler District normally specifies SBR or SBS for mixes with PG 70-22 binder only. Atlanta will select a modified binder if there is a possibility that siliceous gravel will be used in the mix.

Based on the survey results, it can be concluded that the TxDOT districts have more experience with traditional types of mixes, and newer mixes are gaining in popularity. Since the main objective of the study was to identify the influence of modifiers on performance, the survey results suggest using surface mixes because modifiers are typically not used in the base layers. For surface layers, Type C and Type D are most commonly used followed by CMHB mixes. The researchers decided to select a Type D mix. Because CMHB-F is similar to CRM-HMAC (having been evaluated under TxDOT Research Project 0-4821), another mix was selected as a CMHB-C mix. The third mix type, PFC, was selected because it has only recently been placed on Texas highways and the performance is not yet

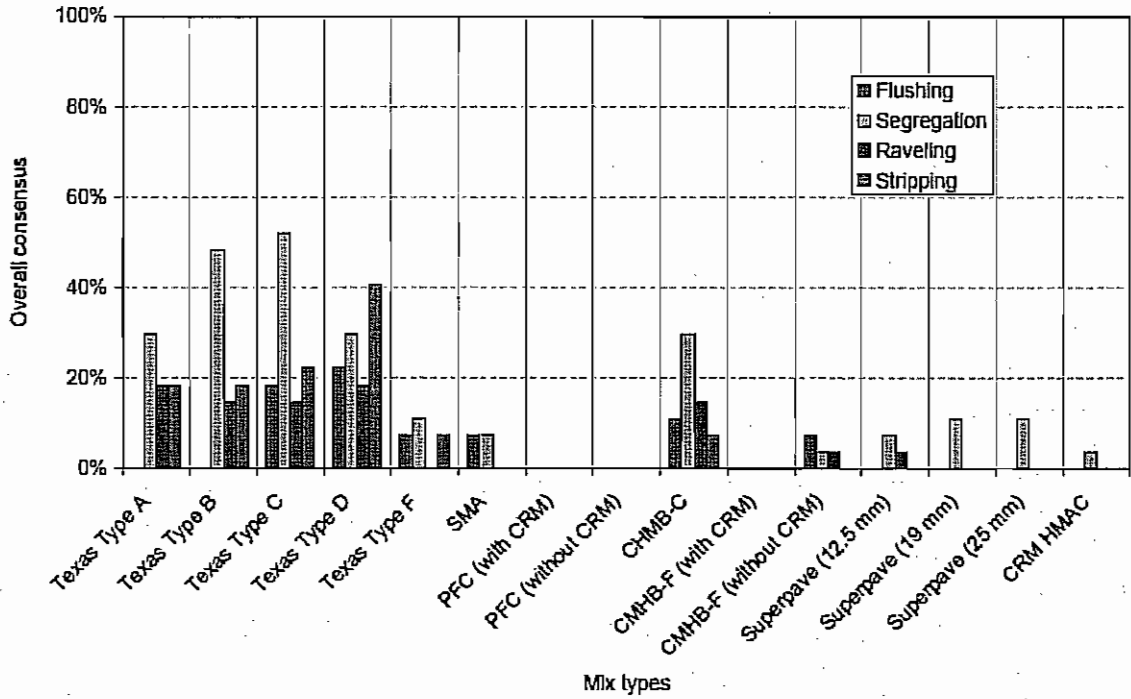


Figure 3.3 HMA Construction Problems Experienced

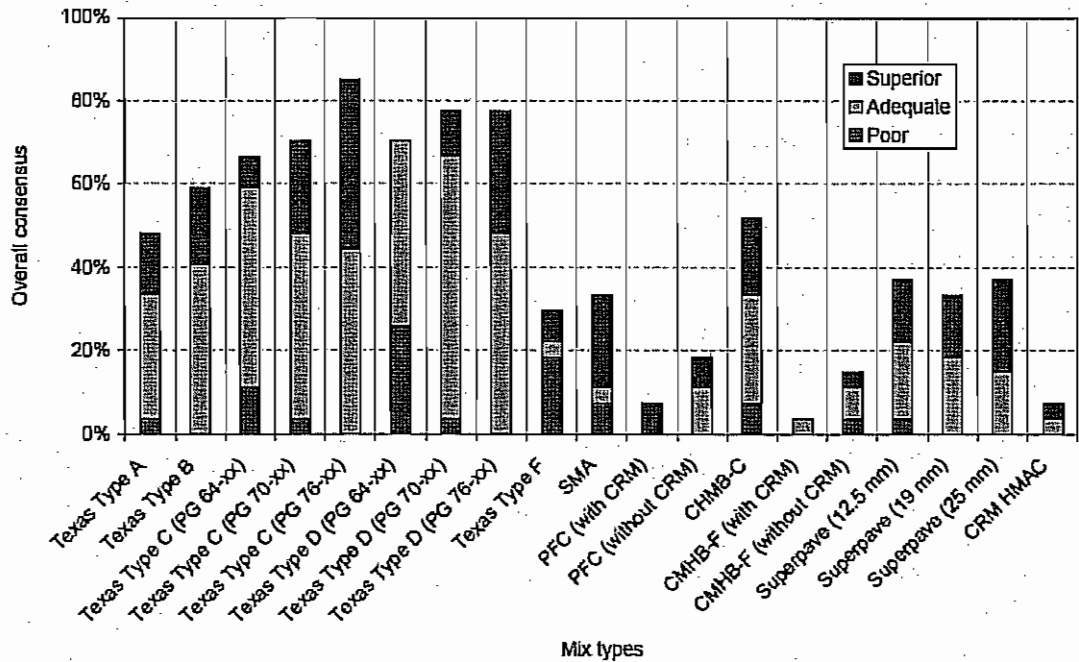


Figure 3.4 HMA Mixes Resistance to Rutting

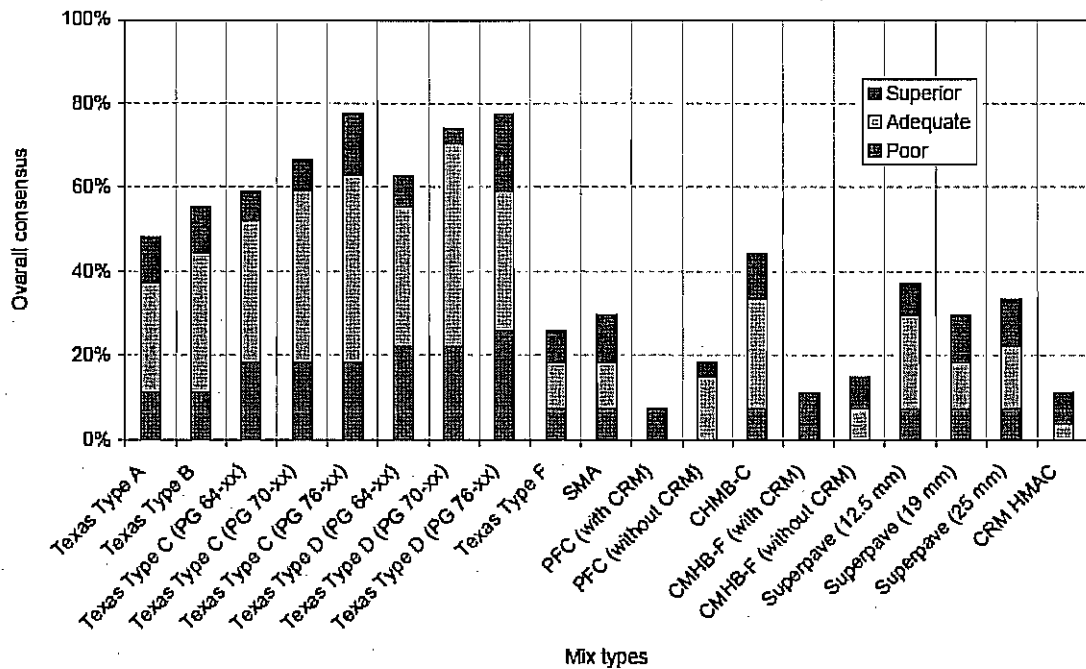


Figure 3.5 HMA Mixes Resistance to Fatigue

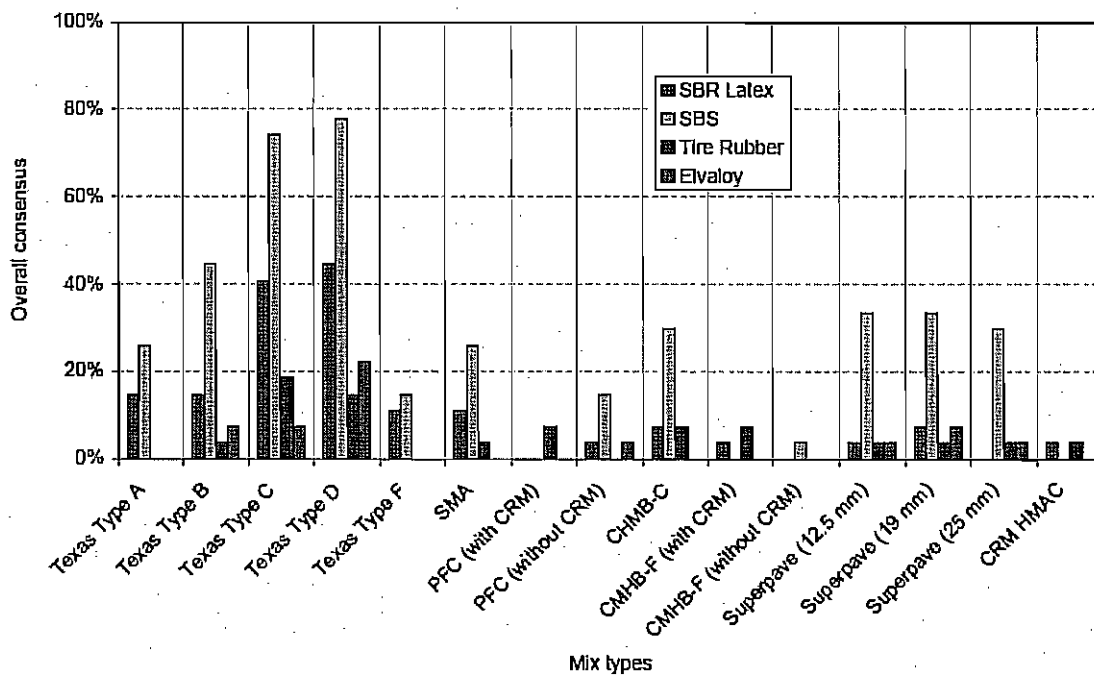


Figure 3.6 Modifiers Typically Used in HMA Mixes

known. In addition, the use of PFC is increasing due to reduction in splash and traffic noise. The survey also identified four modifiers that have been commonly used within TxDOT; therefore, it was decided to evaluate all of the modifiers (SBS, SBR latex, Elvaloy and Tire Rubber) in this study.

3.2 Mix Design and Binder Types

The Type D mix was obtained from the Austin District, while CMHB-C mix was obtained from the San Antonio District. In addition, a Permeable Friction Course (PFC) mix from the Austin District was also evaluated. Historically, the selected Type D and CMHB-C mixes have performed well over the years. Although the historic performance of PFC mix is unknown, the binder and aggregates are obtained from the same source, except the gradation and binder contents have been changed to meet TxDOT specifications.

To ensure that the mix design evaluated in the laboratory is similar to the placed mixes, the Job Mix Formulas (JMF) of recently placed mixes were provided by TxDOT and are summarized in Table 3.1. The binder content of CMHB-C is slightly higher than Type D mix while the aggregate gradation of two mixes is significantly different. CMHB-C is a gap graded mix design containing a large quantity of coarse aggregate with asphalt binder-filler mastic. CMHB-C mixtures have been known to be more resistant to moisture and rutting in the field. Type D mix consists of a maximum aggregate size of 1/2 in. and is most commonly used in the overlay layer placement (TxAPA, 2005). The PFC mix consists of 6.0% binder content and has less than 10% passing No. 4 sieve, suggesting that the mix is open graded. The PFC mix is designed for 17% air voids and is typically placed around 20% to 22% air voids.

The properties of four modifier types used in this study are summarized in Table 3.2. To ensure that the influence of the modifier was evaluated, base (unmodified) binder was obtained from the manufacturers, as well. In addition, an attempt was made to obtain binder (both modified and unmodified) that had been or would be placed on highways. The reason for this step was to make sure that incompatible asphalt binders were not obtained. Since one of the objectives was to develop a database for the new design guide, it was also decided to obtain asphalt binder that has been recently placed on the highways.

The asphalt binders obtained from Wright and Ultrapave provided Superpave gradation and are included in Table 3.2. The asphalt binders obtained from Valero Armor did not provide the PG grade; therefore, the limited available test results are also included in Table 3.2. The results indicate that, in general, the asphalt binders meet PG specifications.

Although different binders were evaluated in this study, the binder contents of mixes were not changed from the original JMF. It is quite possible that the change in binder types can alter the optimum binder content; however, the change in binder content can influence the performance of mix types. Therefore,

it was decided to keep the binder content constant. Another thing to keep in mind is that the modifiers typically improved the higher temperature grade while maintained the lower temperature grade of -22.

Table 3.1 Job Mix Formula for Type D, PFC and CMHB-C Mix Designs

Mix Design			
Binder Grade	PG 64-22, PG67-22, PG70-22, PG76-22		
Mix Type	Type D	PFC	CMHB-C
Binder Content, %	4.5	6.0	4.9
Sieve Size	Percent Passing		
3/4	100.0	100.0	100.0
1/2	100.0	90.0	100.0
3/8	97.0	47.5	61.0
No. 4	65.0	10.5	34.8
No. 10	35.5	5.5	20.4
No. 40	17.1	4.0	11.6
No. 80	6.6	3.5	8.8
No. 200	2.6	2.5	7.0
Maximum Specific Gravity	2.550	2.366	2.423
Aggregate Bulk Specific Gravity	2.655	2.579	2.591
Air Voids	4.0	18.0	4.0
VMA	14.3	28.0	17.6
VFA	71.9	35.8	77.3
V _{eff} %	3.6	5.3	3.7

Table 3.2 Rheological Properties of Asphalt Binders

Asphalt Producer	Wright Asphalt			Ultrapave		Valero Armor	
PG grade	64-22	70-22	76-22	67-22	76-22	64-22	76-22
Modifier	0%	3.0% SBS	SBS+TR	0%	3.5% SBR	0%	3.5% Elvaloy
Rotational Viscosity, @ 135°C	0.53	1.4	2.133	0.587	1.367	1.025	5.122
Softening Point, F	0.23	137	153	N/T	N/T*	N/T	N/T
Penetration @25 °C	61	56	52	N/T	N/T	N/T	N/T
G*/sinδ @ 10rad/sec, kPa	1.75	1.517	1.329	2.5	3.02	3.72	1.45
Phase Angle @ 10rad/sec	84.6	74.2	69.1	81.1	70.7	81.7	72.2
Specific Gravity @ 60°F	1.04	1.038	1.039	N/T	N/T	N/T	N/T
Elastic Recovery @ 10°C	N/A	52.5	62.5	N/T	N/T	N/T	54.7
RTFO Aging	N/T						
G*/sinδ @ 10rad/sec, kPa	4.47	3.388	2.958	6.35	10.6	7.57	3.34
Phase Angle @ 10rad/sec	79.8	69.8	66.8	85.2	85.4	85.3	67.2
Change in mass	0.02	0.019	0.02	N/T	N/T	N/T	N/T
PAV Aging	N/T						
G*/sinδ @ 10rad/sec, kPa	1978.9	2184.8	2374.8	3086	2585	N/T	N/T
S, -12 °C @ 60sec	147.2	1.335	107.4	122	114	N/T	N/T
m, -12 °C @ 60sec	0.3137	0.3283	0.3135	0.325	0.317	N/T	N/T

* Not Tested

3.3 Specimen Preparation

The specimens for the dynamic modulus, flow time and flow number tests were prepared in accordance with the Superpave mix design. Mixing and compaction temperatures were identified by performing viscosity tests specified by the SHRP using Brookfield Viscometer. The estimated mixing and compaction temperatures for individual binder types are summarized in Table 3.3. After mixing with a mechanical mixer, the loose materials were subjected to short-term aging in a forced-draft oven at a constant temperature for 2 hours as recommended by TxDOT. During the short-term aging period, the loose mix was stirred every hour to ensure uniform aging. The loose mix was compacted into 6-in. diameter by 7-in. high specimens using the SGC. The compacted specimens were cooled to room temperature for a period of 24 hours, and then cored and saw cut to a diameter of 4 in. and a height of 6 in. The air void content of each specimen was measured using the CoreLok device to ensure a density of $93 \pm 0.5\%$.

The specimens for the HWTD tests were prepared using the Tex-242-F method with an SGC. The specimens for IDT tests and Static Creep tests were prepared following Tex-226-F and Tex-231-F methods using TGC, respectively.

Table 3.3 Mixing and Compaction Temperatures for Individual Binder Types

Binder	Mixing Temperature (°F)	Compaction Temperature (°F)
Wright Asphalt 64-22	300-310	275-285
Wright Asphalt 70-22 3.5% SBS	330-340	300-310
Wright Asphalt 76-22 SBS & TR	330-340	300-310
Valero Armor 64-22	300-310	275-285
Valero Armor 76-22 3.5% Elvaloy	325-335	300-310
Ultrapave 67-22	310-320	290-300
Ultrapave 76-22 3.5% SBR	325-335	300-310

The specimens for the flexural fatigue tests were prepared by aging the loose mix for 4 hours at 275°F (135°C) to simulate the aging process that occurs during the time it takes to transport the mix from the plant to the pavement. The aged mix

is typically poured into the mold, and then the mold is placed in the Asphalt Vibratory Compactor (AVC) and compacted. The AVC was designed to compact rectangular and cylindrical specimens of HMA. The AVC compacts samples at the same amplitude, frequency and relative weight that a contractor applies with a vibratory compactor on the roadway (AVC Manual, 2003). After the samples are compacted, they are extracted with the help of an air cylinder. After compaction, the slabs are left overnight and then tested for their bulk density. The slabs are then sawed to derive two beams 15 in. (380 mm) long (l) by 2 in. (50 mm) high (h) by 2.5 in. (63 mm) wide (b) out of each slab. The slabs are cut in such a way that each beam side is sawed. The beams are then conditioned for seven days in a temperature control chamber at 68°F (20°C).

3.4 Test Matrix

The tests performed on various mixes and binders are shown in Table 3.4. All of the identified tests were performed for Type D and CMHB-C mixes. However, all of the tests were not performed on PFC mixes. For instance, HWTD tests were not performed on PFC because PFC will fail regardless of the binder type due to the fact that the PFC aggregate skeleton is not strong enough to withstand HWTD loads. In addition, the PFC tests were performed only using Wright Asphalt binder because this was the only binder that had been used in the field. In addition, the focus of this study was to document performance of commonly used mixes; thus, PFC mixes were prepared and tested only using Wright Asphalt. An attempt was made to prepare and test at least three for each combination shown in the table. However, occasionally three specimens were not tested because of the shortage of binder types and have been documented in the appropriate sections of the following chapter. Since seismic testing is nondestructive, the specimens prepared for flow time and flow number tests were evaluated before being subjected to loading. Therefore, no new specimens were prepared for seismic testing.

Table 3.4 Test Matrix

Binder Type	Mix Type	Performance Test							
		Dynamic Modulus	Flow Time	Flow Number	Fatigue Test	Static Creep	HWTD	IDT	Seismic
Wright Asphalt 64-22	Type D	✓	✓	✓	✓	✓	✓	✓	✓
	CMHB-C	✓	✓	✓	✓	✓	✓	✓	✓
	PFC	✓	✓	✓					✓
Wright Asphalt 70-22 3.5% SBS	Type D	✓	✓	✓	✓	✓	✓	✓	✓
	CMHB-C	✓	✓	✓	✓	✓	✓	✓	✓
	PFC	✓	✓	✓					
Wright Asphalt 76-22 SBS & TR	Type D	✓	✓	✓	✓	✓	✓	✓	✓
	CMHB-C	✓	✓	✓	✓	✓	✓	✓	✓
	PFC	✓	✓	✓					
Valero Armor 64-22	Type D	✓	✓	✓	✓	✓	✓	✓	✓
	CMHB-C	✓	✓	✓	✓	✓	✓	✓	✓
Valero Armor 76-22 3.5% Elvaloy	Type D	✓	✓	✓	✓	✓	✓	✓	✓
	CMHB-C	✓	✓	✓	✓	✓	✓	✓	✓
Utrapave 67-22	Type D	✓	✓	✓	✓	✓	✓	✓	✓
	CMHB-C	✓	✓	✓	✓	✓	✓	✓	✓
Utrapave 76-22 3.5% SBR	Type D	✓	✓	✓	✓	✓	✓	✓	✓
	CMHB-C	✓	✓	✓	✓	✓	✓	✓	✓

This page replaces an intentionally blank page in the original.

-- CTR Library Digitization Team

CHAPTER 4 DATA ANALYSIS AND TEST RESULTS

4.1 HAMBURG WHEEL TEST DEVICE RESULTS

To perform HWTD tests, four specimens are compacted to a density of $93 \pm 1\%$ using a SGC. According to TxDOT procedure (Tex 242-F), the maximum rut depth anywhere in the wheel path should be measured (Figure 4.1). For this study, permanent deformations were recorded at two other locations as well. The first location was the center of each specimen, and is designated as center of specimen in Figure 4.1. For this location, the deformation from the center of each specimen was averaged for each wheel and is reported as the deformation observed at the center of specimen. The advantage of measuring the deformation at this location is that only two specimens can be tested to assess the field performance of a HMAC rather than four specimens. The second location was selected to be at the interface of the two specimens (as shown in Figure 4.1) and is reported as deformation observed at the center of the slab. Thus, the deformation was recorded at three locations: center of specimen, center of the slab and maximum rut depth along wheel path, as shown in Figure 4.1.

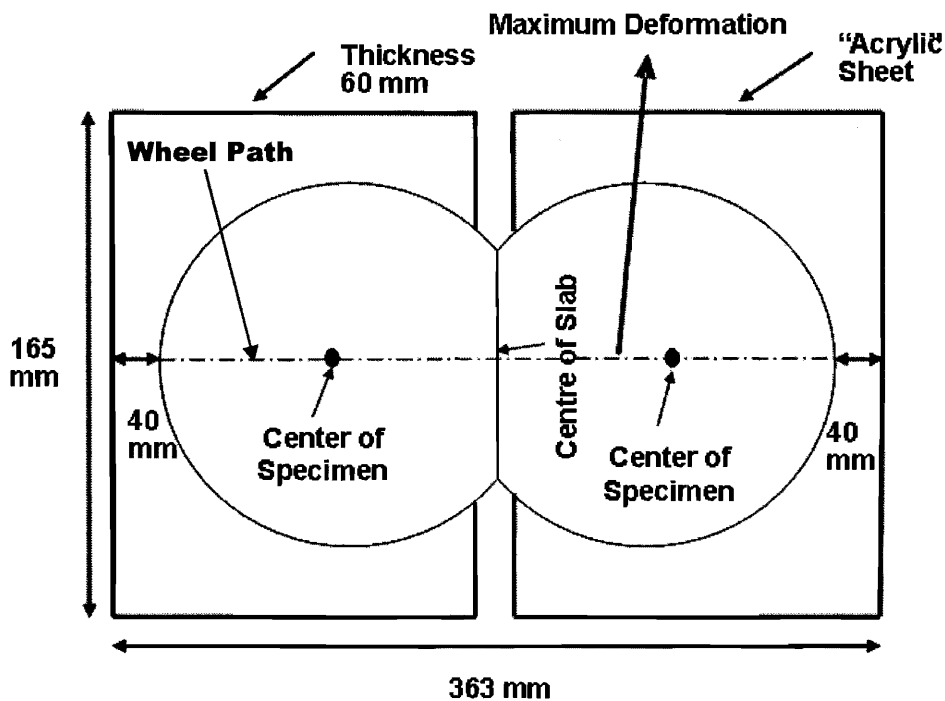


Figure 4.1 HWTD Specimen Setup

The study conducted by Hrdlicka et al. (2007) identified that raw data can be represented with a 3rd degree polynomial fit, which gave a reasonable trend of the observed deformations in the specimens. It was also decided to abbreviate the binder types, and the acronyms used are included in Table 4.1. These two steps minimized the clutter in the presentation of data. A typical test results for the Type D and CMHB-C mix designs at the center of specimens are reported in Figures 4.2 and 4.3. The test results suggest that the modified binders performed better in comparison to base binders for the two mix types.

The estimated rut depth at the end of 20,000 cycles or when the device stopped after excessive deformation for all three locations is summarized in Table 4.2. The HWTD tests on PFC specimens were not performed because the purpose of the PFC layer is to drain water and TxDOT does not specify HWTD testing for PFC mixes.

For Type D mix, only two binders exceeded the set maximum 0.5 in. (12.5 mm) deformation limitation of TxDOT specifications (maximum deformation): Ultrapave 67-22 and Valero Armor 64-22. However, both binders need only to remain under 12.5mm deformation until 10,000 cycles because they have temperature grade of 64 (Table 2.1). Exposing these virgin binders to 20,000 cycles provided a better understanding of their overall performance. In comparing Ultra Pave 67-22 to Valero Armor 64-22 at 10,000 cycles, the two seem almost identical in their performance (both deforming around 4 mm). By allowing the two binders to endure 20,000 cycles, it was seen that Valero Armor is actually a better binder because it only reaches a deformation of 6 mm compared to the 15 mm of deformation experienced by Ultra Pave. This observation could not have been made if the binders had been tested to only the 10,000 cycles specified by TxDOT for PG 64 binder. The prompt failure after 10,000 cycles seen in the virgin Valero Armor binder can be attributed to moisture susceptibility of the binder (Sagi, 2004).

HWTD test results for CMHB-C mix design specimens show similar trends to that of the Type D mix design, with only Valero Armor 64-22 exceeding the 0.5 in. (12.5 mm) deformation limit.

The base binder that performed the best overall was Wright Asphalt, followed by Ultra Pave and Valero Armor. When modified, all three binders improved significantly, reducing the deformation to 5-mm or less.

The amount of deformation across the specimen is higher in the center of the slab when compared to the average between the centers of the two specimens. Therefore, when using the center of specimen as an indicator of performance, the requirement for the maximum allowable deformation should be stricter since less deformation occurs.

Table 4.1 Binder Abbreviations Used in This Study

Binder Type	Abbreviation
Wright Asphalt PG 64-22	W 64
Wright Asphalt PG 70-22 3.5% SBS	W 70 SBS
Wright Asphalt PG 76-22 SBS & TR	W 76 SBS & TR
Ultrapave PG 67-22	U 67
Ultrapave PG 76-22 3.5% SBR	U 76 SBR
Valero Armor PG 64-22	V 64
Valero Armor PG 76-22 3.5% Elvaloy	V 76 E

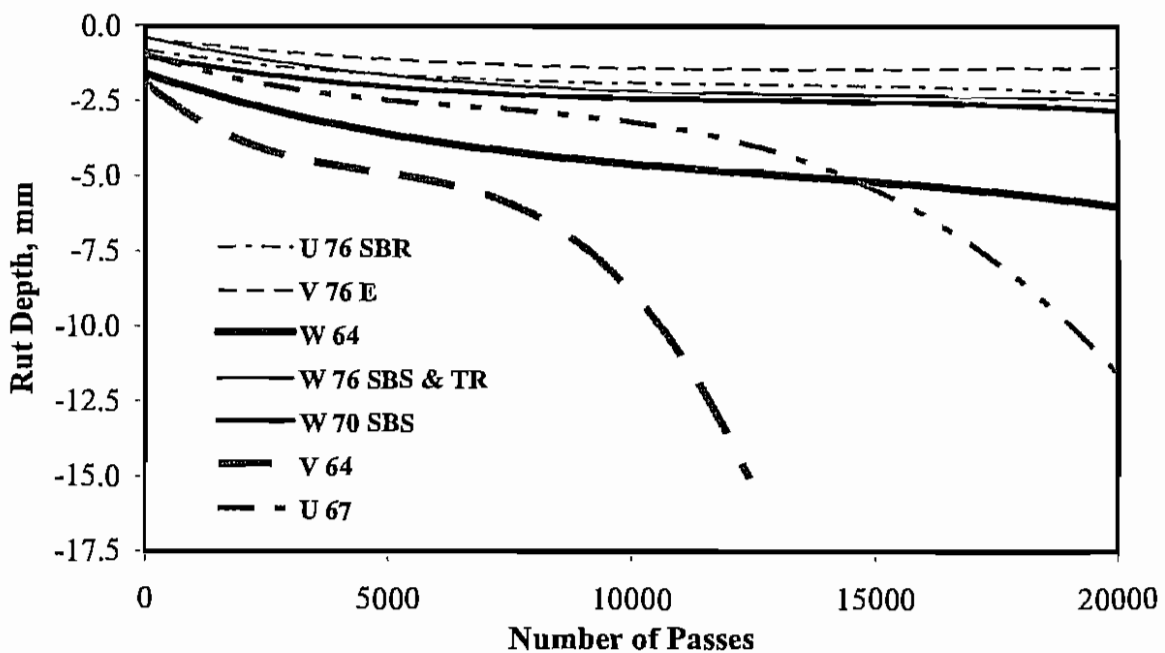


Figure 4.2 HWTD Rut Depth for Type D Mix Design at the Center of Specimen

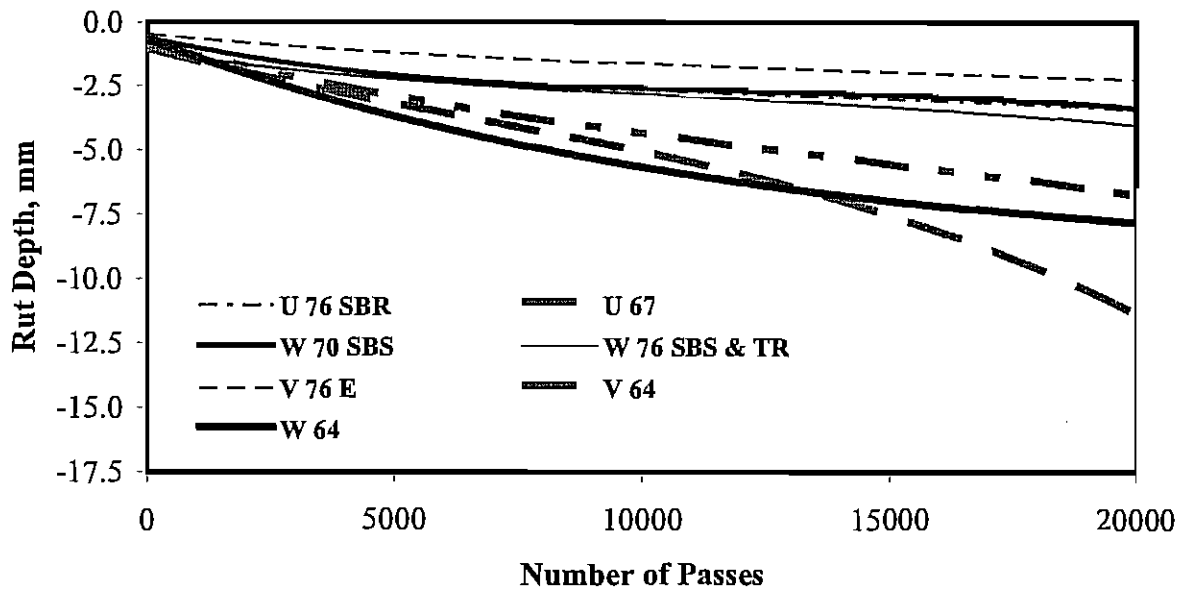


Figure 4.3 HWTD Rut Depth for CMHB-C Mix Design at the Center of Specimen

Table 4.2 Rut Depth at the End of the Testing

Asphalt Type	Center of Specimen Deformation, mm		Maximum Deformation, mm		Center of Slab Deformation, mm	
	Type D	CMHB-C	Type D	CMHB-C	Type D	CMHB-C
W 64	4.0	8.0	4.4	6.1	4.0	6.1
W 70 SBS	2.9	3.4	2.8	4.9	2.7	4.6
W76 SBS & TR	2.7	4.1	3.0	5.4	2.6	4.2
V 64	14.2	9.3	17.0	12.7	16.4	12.0
V 76 E	2.3	2.6	2.3	3.4	1.6	2.0
U 67	9.2	7.2	14.4	11.1	13.3	7.6
U 76 SBR	2.5	3.5	3.2	3.9	2.8	3.0

Deformation values of CMHB-C mix design are slightly less or similar to those of Type D mix in most cases except for Wright Asphalt 64, where CMHB-C deformation is twice that observed with Type D. In the cases where the deformation exceeded 5mm, the CMHB-C mix design withstood deformation better than the Type D mix design (Figure 4.4). A line fit to the data suggests that CMHB-C deformation is 50% less than that observed with Type D mixes (Figure 4.4), indicating that CMHB-C is a more resilient mix compared to the Type D mix. This result was expected as CMHB-C mix is designed for heavier loading conditions.

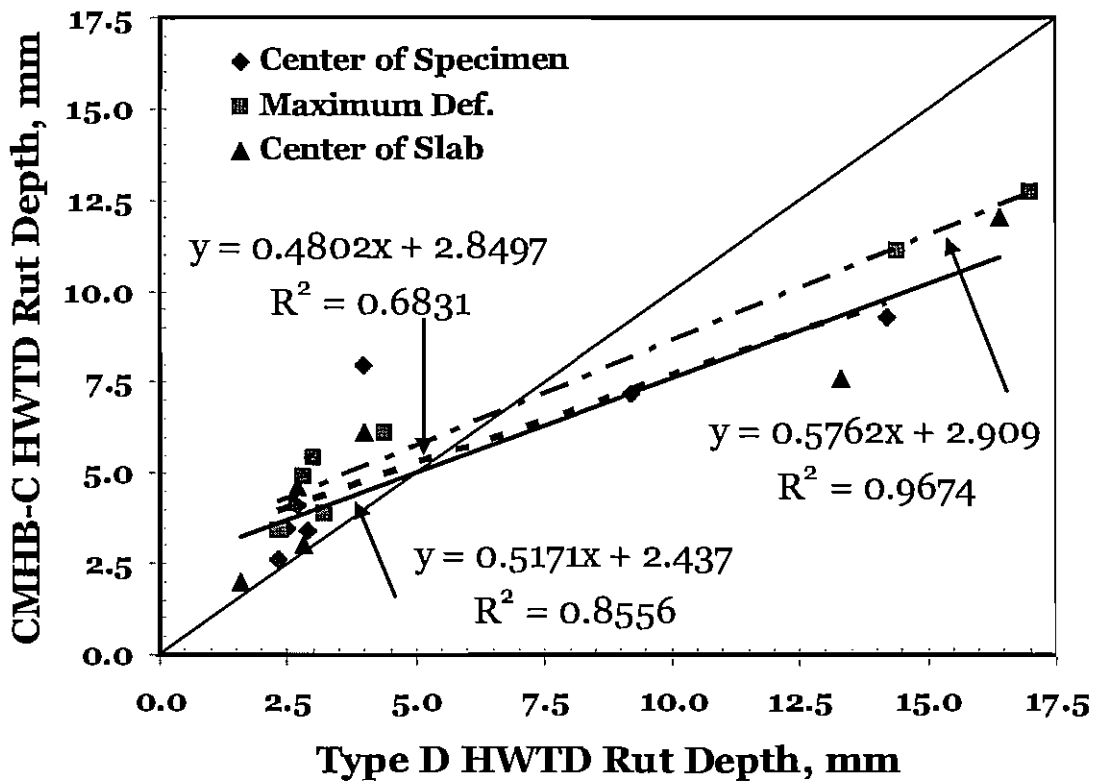


Figure 4.4 Comparison Between CMHB-C and Type D Mixes Rut Depth Obtained from HWTD

4.2 Dynamic Modulus Test Results

After dynamic modulus estimation of each specimen, the results from three specimens were averaged for the same test conditions (i.e., for each temperature and test frequency). The average value, the standard deviation (SD) and the coefficient of variation (COV) were calculated for each mix type for each test condition, and the results for three mixes are shown in Tables 4.3 through 4.5. A

higher dynamic modulus value was obtained at lower temperatures and higher frequencies (load applied for shorter duration). The measured dynamic modulus value varied from roughly 4,000 ksi to 40 ksi depending on the mix type and test conditions. The data also shows that the SD values varied from 1 ksi to 340 ksi, while COV varied from almost 0% to 43% depending on test conditions and mix types indicating that the test setup may not be repeatable, particularly at 130°F (at this temperature COV increased significantly). The tests on CMHB-C mixes for Valero Asphalt 64-22 were not performed due to binder shortage. In addition, the PFC tests were only performed on the Wright Asphalt because other binder types have not typically been in PFC mix production.

In terms of Type D mixes, the measured dynamic modulus values dropped by almost 95% (from 3000 to 150 ksi) when modulus values were compared at the highest temperature with the lowest test temperature at the lowest frequencies regardless of asphalt binder type. These results indicate that the binder type plays a significant role. The COV values were less than 15% (even less than 5% in some cases) until test temperature of 100°F, indicating that the test is repeatable to this temperature. However, the COV values jumped to almost 25% indicating that at 130°F there may be some damage to the specimen because the same specimen tested at lower temperatures had only 5% COV. The test results also suggest that the SD values were higher at lower temperatures and vice versa. The SD values dropped by almost 95% (from 270 ksi to 8 ksi) when SD values were compared at the highest and lowest temperatures.

In terms of CMHB-C mixes, the measured dynamic modulus values again dropped by more than 95% (from 3000 to 100 ksi) when a comparison was made of modulus values at the highest temperature with the lowest test temperature at the lowest frequencies regardless of asphalt binder type. The COV values were less than 10% (even less than 5% in some cases) to a test temperature of 100°F, indicating that there is some damage to the specimen. The test results also suggest that the SD values were higher at lower temperatures and vice versa. The drop in SD values was similar to that of Type D mixes.

In terms of PFC mixes, the measured dynamic modulus values again dropped by more than 95% (from 1300 to 50 ksi) when a comparison was made of modulus values at the highest temperature with the lowest test temperature at the lowest frequencies regardless of asphalt binder type. The COV values were highest for PFC mixes in comparison to other mix types, in some cases by as much as 43%, which indicates that the test is not repeatable for PFC mix types. The test results also suggest that the SD values were higher at lower temperatures and vice versa. The drop in SD values was similar to that of Type D mixes.

Table 4.3 Average Dynamic Modulus, Standard Deviation, and Coefficient of Variation of Type D Mixes

Binder Type	Statistical Parameter	E* Dynamic Modulus, ksi																			
		Temperature, °F																			
		14				40				73				100				130			
		Frequency, Hz				Frequency, Hz				Frequency, Hz				Frequency, Hz				Frequency, Hz			
10	5	2	1	10	5	2	1	10	5	2	1	10	5	2	1	10	5	2	1		
W 64	Average	3392	3139	2833	2571	2425	2178	1884	1662	1261	1092	872	745	484	407	317	263	250	209	172	143
	SDV	137.3	132.3	149.5	149.0	134.9	113.5	102.1	79.9	105.2	98.2	90.6	85.6	50.7	48.2	38.1	36.7	61.3	51.2	37.9	35.2
	COV,%	4.0	4.2	5.3	5.8	5.6	5.2	5.4	4.8	8.3	9.0	10.4	11.5	10.5	11.8	12.0	13.9	24.5	24.5	22.0	24.6
W 70 SBS	Average	3746	3394	3018	2690	2581	2298	1975	1723	1333	1173	947	815	549	465	363	318	276	250	208	192
	SDV	200.7	168.7	142.0	116.9	146.9	113.5	96.9	80.6	54.0	45.8	54.6	57.1	54.2	54.3	42.0	42.0	24.7	24.8	21.0	18.0
	COV,%	5.4	5.0	4.7	4.3	5.7	4.9	4.9	4.7	4.1	3.9	5.8	7.0	9.9	11.7	11.6	13.2	9.0	9.9	10.1	9.4
W 76 SBS & TR	Average	2955	2653	2293	2002	1891	1630	1355	1158	924	794	626	543	401	349	277	243	213	194	167	156
	S.D.	175.5	134.6	126.5	90.6	67.5	36.4	39.1	21.7	18.1	22.9	21.8	26.2	43.0	39.7	32.3	28.8	19.2	18.2	12.9	11.4
	COV,%	5.9	5.1	5.5	4.5	3.6	2.2	2.9	1.9	2.0	2.9	3.5	4.8	10.7	11.4	11.7	11.9	9.0	9.4	7.7	7.3
U 67	Average	3394	3058	2709	2434	2407	2167	1842	1631	1420	1232	988	862	672	577	459	399	283	246	205	185
	SDV	417.2	336.8	303.5	245.7	384.0	322.2	254.5	209.1	160.2	128.6	95.5	77.3	71.0	52.4	38.3	27.9	13.6	16.2	14.1	12.7
	COV,%	12.3	11.0	11.2	10.1	16.0	14.9	13.8	12.8	11.3	10.4	9.7	9.0	10.6	9.1	8.4	7.0	4.8	6.6	6.9	6.9
U 76 SBR	Average	3480	3129	2735	2401	2219	1933	1614	1376	1123	966	758	650	449	390	312	273	231	206	174	163
	SDV	337.1	256.6	181.8	143.5	152.7	112.6	83.7	56.3	94.1	77.4	57.8	45.4	17.2	18.0	11.7	9.0	7.3	6.4	8.6	5.2
	COV,%	9.7	8.2	6.6	6.0	6.9	5.8	5.2	4.1	8.4	8.0	7.6	7.0	3.8	4.6	3.8	3.3	3.2	3.1	4.9	3.2
V 64	Average	3083	2793	2463	2204	2003	1742	1456	1257	965	835	655	564	435	371	296	259	204	182	160	149
	SDV	637.3	533.6	455.5	390.9	339.1	311.6	261.9	228.6	114.9	97.6	82.3	71.6	40.1	37.5	28.0	21.7	17.6	15.9	12.6	12.8
	COV,%	20.7	19.1	18.5	17.7	16.9	17.9	18.0	18.2	11.9	11.7	12.6	12.7	9.2	10.1	9.5	8.4	8.7	8.8	7.9	8.6
V 76 E	Average	3174	2867	2488	2196	2076	1849	1568	1385	1087	942	753	659	505	441	351	312	252	227	196	183
	SDV	269.2	211.3	190.2	222.5	202.9	196.4	180.2	165.4	68.0	58.0	47.2	38.2	26.2	24.8	20.6	20.1	17.2	14.5	9.3	7.8
	COV,%	8.5	7.4	7.6	10.1	9.8	10.6	11.5	11.9	6.3	6.2	6.3	5.8	5.2	5.6	5.9	6.5	6.8	6.4	4.7	4.3

Table 4.4 Average Dynamic Modulus, Standard Deviation, and Coefficient of Variation of CMHB-C Mixes

Binder Type	Statistical Parameter	E* Dynamic Modulus, ksi																			
		Temperature, °F																			
		14				40				73				100				130			
		Frequency, Hz				Frequency, Hz				Frequency, Hz				Frequency, Hz				Frequency, Hz			
10	5	2	1	10	5	2	1	10	5	2	1	10	5	2	1	10	5	2	1		
W 64	Average	3199	2936	2623	2324	2118	1869	1563	1339	970	797	605	477	410	380	301	223	135	119	107	92
	SDV	186.3	49.6	11.9	103.1	70.1	19.4	0.2	16.6	31.3	30.1	26.9	26.2	6.1	5.9	6.3	2.8	34.4	29.6	33.0	29.3
	COV,%	5.8	1.7	0.5	4.4	3.3	1.0	0.0	1.2	3.2	3.8	4.5	5.5	1.5	1.6	2.1	1.2	25.5	24.8	30.8	31.9
W 70 SBS	Average	3097	2795	2477	2218	2154	1932	1628	1413	994	838	639	522	396	324	265	221	197	174	145	136
	SDV	128.0	66.5	81.4	76.5	83.5	69.3	53.2	46.2	25.8	15.8	14.2	2.8	15.6	13.4	9.5	6.2	4.5	5.6	5.5	5.7
	COV,%	4.1	2.4	3.3	3.4	3.9	3.6	3.3	3.3	2.6	1.9	2.2	0.5	3.9	4.1	3.6	2.8	2.3	3.2	3.8	4.2
W 76 SBS & TR	Average	2556	2357	2099	1887	1669	1479	1235	1064	728	621	484	399	319	266	222	185	165	149	139	119
	S.D.	116.2	125.3	141.4	124.3	24.9	11.4	8.3	12.0	32.9	29.6	23.8	14.6	14.9	8.0	10.2	7.2	3.9	4.6	3.1	2.4
	COV,%	4.5	5.3	6.7	6.6	1.5	0.8	0.7	1.1	4.5	4.8	4.9	3.7	4.7	3.0	4.6	3.9	2.4	3.1	2.2	2.0
U 67	Average	2630	2369	2072	1818	1679	1472	1185	1000	750	609	461	378	346	273	213	187	158	142	125	113
	SDV	17.5	26.4	41.9	35.5	41.2	48.6	50.8	49.6	45.3	40.0	22.8	18.7	21.1	18.3	19.1	18.9	15.4	10.7	1.4	2.7
	COV,%	0.7	1.1	2.0	2.0	2.5	3.3	4.3	5.0	6.0	6.6	5.0	4.9	6.1	6.7	9.0	10.1	9.7	7.5	1.1	2.4
U 76 SBR	Average	3030	2753	2491	2280	2005	1810	1550	1369	1050	905	621	589	538	453	347	297	222	192	146	129
	SDV	272.2	154.1	131.5	94.7	155.6	142.8	133.9	126.7	2.7	8.6	107.1	8.3	13.2	14.2	19.4	18.9	32.7	25.0	16.4	13.9
	COV,%	9.0	5.6	5.3	4.2	7.8	7.9	8.6	9.3	0.3	0.9	17.2	1.4	2.4	3.1	5.6	6.4	14.8	13.0	11.3	10.8
V 76 E	Average	2192	1956	1639	1433	1469	1284	1049	888	608	490	366	307	289	234	184	164	148	132	122	109
	SDV	187.7	184.6	205.9	181.6	35.5	29.0	25.3	21.6	20.4	13.9	10.7	7.6	0.4	0.6	1.8	1.8	0.8	2.3	6.7	2.2
	COV,%	8.6	9.4	12.6	12.7	2.4	2.3	2.4	2.4	3.3	2.8	2.9	2.5	0.1	0.3	1.0	1.1	0.6	1.8	5.5	2.0

Table 4.5 Average Dynamic Modulus, Standard Deviation, and Coefficient of Variation of PFC Mixes

Binder Type	Statistical Parameter	E* Dynamic Modulus, ksi																			
		Temperature, °F																			
		14				40				73				100				130			
		Frequency, Hz				Frequency, Hz				Frequency, Hz				Frequency, Hz				Frequency, Hz			
10	5	2	1	10	5	2	1	10	5	2	1	10	5	2	1	10	5	2	1		
W 64	Average	1205	1063	920	768	714	622	500	428	307	260	204	169	123	101	79	67	51	44	35	31
	SDV	32.1	26.3	46.9	22.3	11.4	13.9	10.6	12.2	15.1	8.0	4.4	3.0	1.5	2.4	3.5	4.5	7.2	6.2	3.0	3.3
	COV,%	2.7	2.5	5.1	2.9	1.6	2.2	2.1	2.9	4.9	3.1	2.2	1.7	1.2	2.4	4.5	6.7	14.1	14.0	8.6	10.7
W 70 SBS	Average	1178	1079	960	858	798	707	547	482	439	378	291	236	167	151	121	98	82	71	64	51
	SDV	209.6	192.9	177.7	156.9	171.3	149.3	134.8	66.6	86.1	71.4	61.9	60.9	47.3	42.2	34.5	30.4	27.9	30.6	22.8	16.3
	COV,%	17.8	17.9	18.5	18.3	21.5	21.1	24.7	13.8	19.6	18.9	21.3	25.8	28.3	27.9	28.5	30.9	34.2	42.9	35.4	31.8
W 76 SBS & TR	Average	1324	1178	1021	901	863	769	643	549	431	372	293	245	169	150	129	102	87	79	79	57
	S.D.	305.0	272.7	253.7	206.7	169.2	175.6	159.3	143.4	93.8	74.4	62.1	50.9	37.9	38.6	39.0	33.1	24.0	22.9	19.6	10.0
	COV,%	23.0	23.2	24.8	22.9	19.6	22.8	24.8	26.1	21.8	20.0	21.2	20.7	22.5	25.7	30.2	32.5	27.5	29.0	24.9	17.6

Comparing data from the two mix types (CMHB-C and Type D), the measured dynamic values are plotted in Figure 4.5. The data suggest that the CMHB-C mixes exhibited lower stiffness compared to Type D mixes and a trend line fitted through the data suggests that the CMHB-C mixes have 15% lower dynamic modulus compared to Type D mixes. The test results show an opposite trend to that of field performance, where CMHB-C mixes perform better in comparison to Type D mixes.

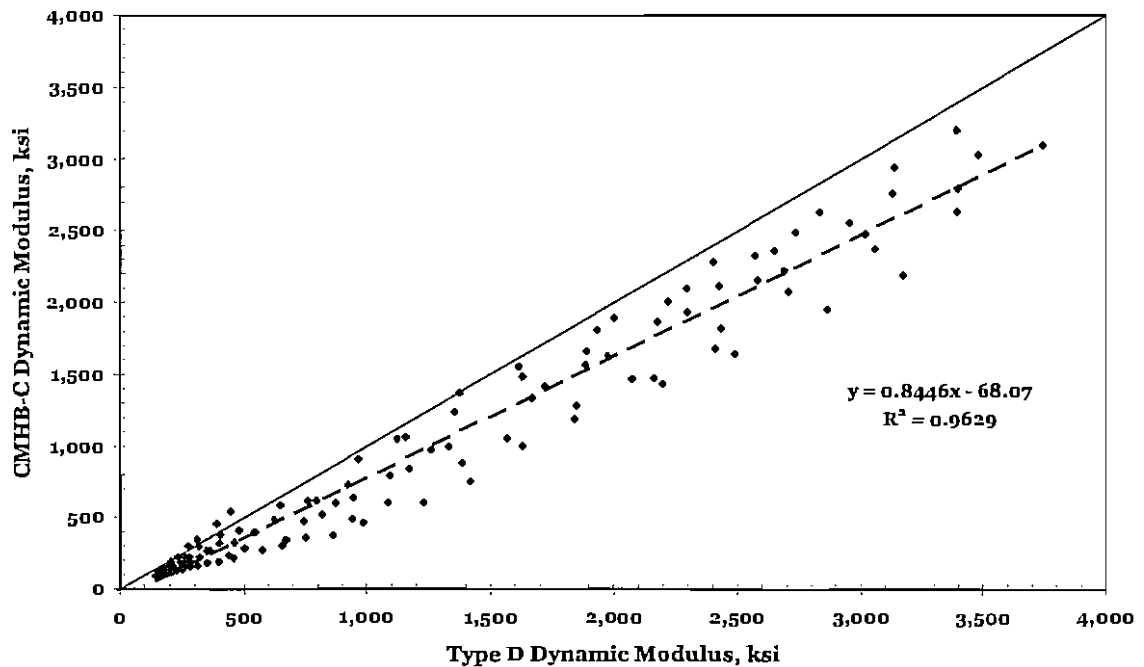


Figure 4.5 Comparison of Dynamic Modulus Values of CMHB-C and Type D Mixes

4.2.1 Master Curves

To identify the influence of binder and mix types and to utilize the dynamic modulus in the Mechanistic Pavement Design Guide, Witczak et al. (2002) proposed using the master curve. As mentioned in the previous chapter, the dynamic modulus values at various temperatures are shifted to one reference temperature using the time temperature superposition principle; a sigmoidal function proposed by Pellinen and Witczak et al. (2002) is then used to fit the data (Chapter Two).

The process of developing a master curve is shown in Figures 4.6 through 4.9. A plot of measured dynamic modulus at each frequency and test temperature for

Wright Asphalt 76-22 is shown in Figure 4.6. The moduli from each temperature are shifted horizontally to produce a master curve at a reference temperature.

The magnitude of shift depends on test temperature and mix type. The shift factor plot for Wright Asphalt 76-22 is shown in Figure 4.7 and the shifted master curve at 73°F (23°C) is shown in Figure 4.8. As expected, the dynamic moduli for the higher temperatures (130°F and 100°F) have to be shifted to the left while the moduli for the lower temperatures (14°F and 40°F) have to be shifted to the right to generate the plot. A curve fitting to the data is performed and the identified sigmoidal parameters are then used to generate a master curve as shown in Figure 4.9. Typically the R^2 obtained was more than 0.97, indicating that the data fits the sigmoidal function well. The master curves for three mix types and seven binder types were generated at a reference temperature of 73°F.

The master curves generated for asphalt binder grade PG 76 are shown in Figures 4.10 and 4.11. The data suggest that the influence of binder type varies for different mix types. For instance, the dynamic modulus values obtained for Valero asphalt (V 76 E) were lowest for CMHB-C mix, while for Wright Asphalt (W 76 SBS & TR) the values were lowest for Type D mix. The data also show that the Ultrapave asphalt was the most susceptible to temperature because it exhibited highest modulus values at higher frequency and lowest modulus values at lower frequency in comparison to other binder types.

Another important factor to note is that the obtained dynamic modulus values are similar at lower and higher frequencies but are different at the intermediate frequencies. This influence was more pronounced for CHMB-C mixes. For instance, at 10 Hz the dynamic modulus value of 1,000 ksi was observed while only 600 ksi was observed for Ultrapave (U 76 SBR) and Valero (V 76 E), respectively. This suggests that the master curve should be further evaluated at the frequency ranges of 0.1 to 10 Hz to identify influence of asphalt types. The data presented in Figures 4.10 and 4.11 indicate that overall, U 76 SBR seems to be preferable to the other two asphalt types.

The data for PG 64 asphalt type is presented in Figures 4.12 and 4.13. The figures show different trends than those observed with PG 76 grade asphalt binder. For Type D mix, Ultrapave asphalt (U 67) seems to be less susceptible to temperature than Wright or Valero asphalts (W 64 and V 64). In addition, the most significant difference was observed at 0.2 Hz, with U 67 performing best, a trend similar to that observed with modified asphalt binder (U 76 SBR). The dynamic modulus value at 10 Hz suggests that W 64 binder is better than V 64 asphalt, which is similar to that identified using HWTD test results. For CMHB-C mix type, the Wright Asphalt (W 64) exhibited higher modulus values at higher frequency compared to Ultrapave (U 67), but the trend reversed at lower frequency.

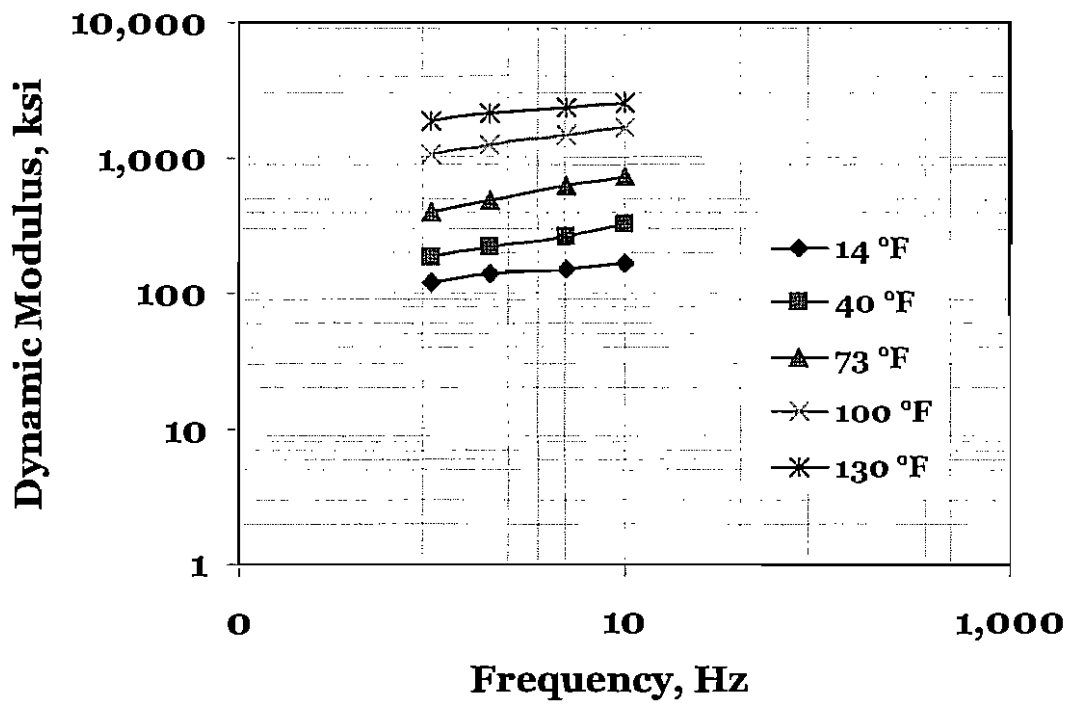


Figure 4.6 Measured Dynamic Modulus and Frequency Plot for CMHB-C Mix Consisting of W 64 Asphalt Binder

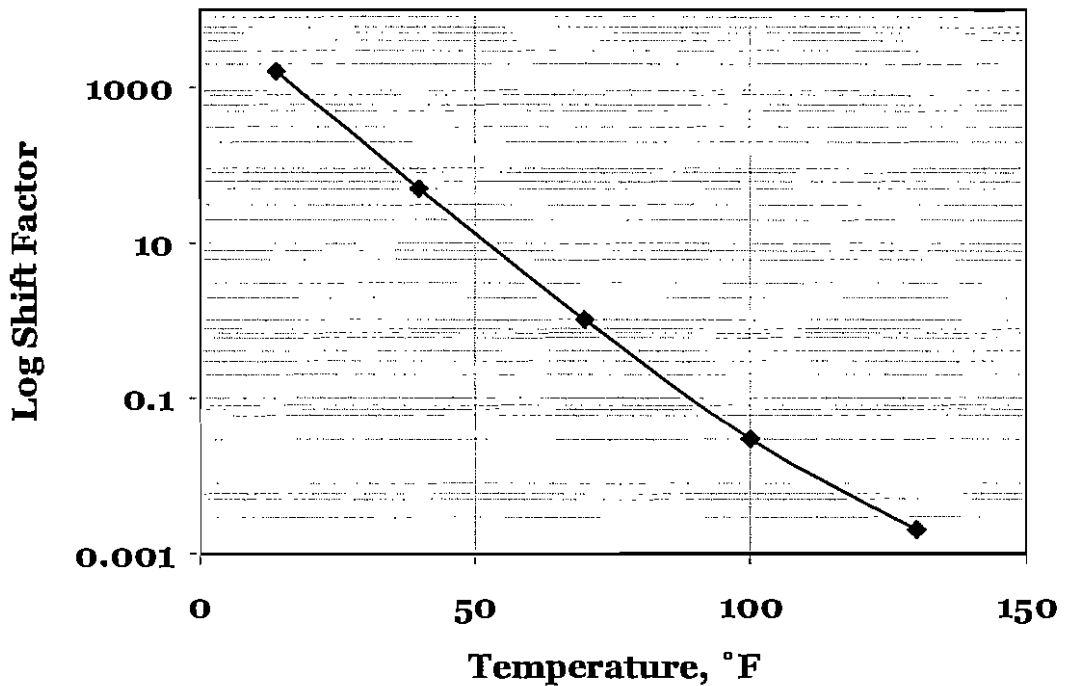


Figure 4.7 Log Shift Factor versus Temperature Plot for CMHB-C Mix Consisting of W 64 Asphalt Binder

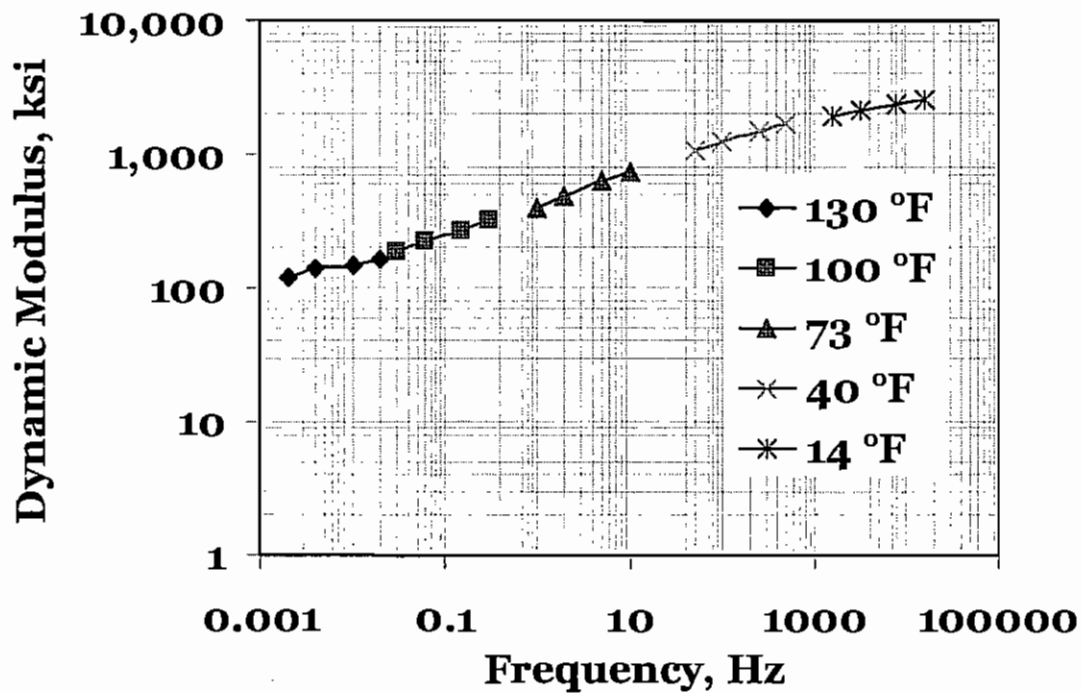


Figure 4.8 Shifted Dynamic Modulus versus Frequency Relationship for CMHB-C Mix Consisting of W 64 Asphalt Binder

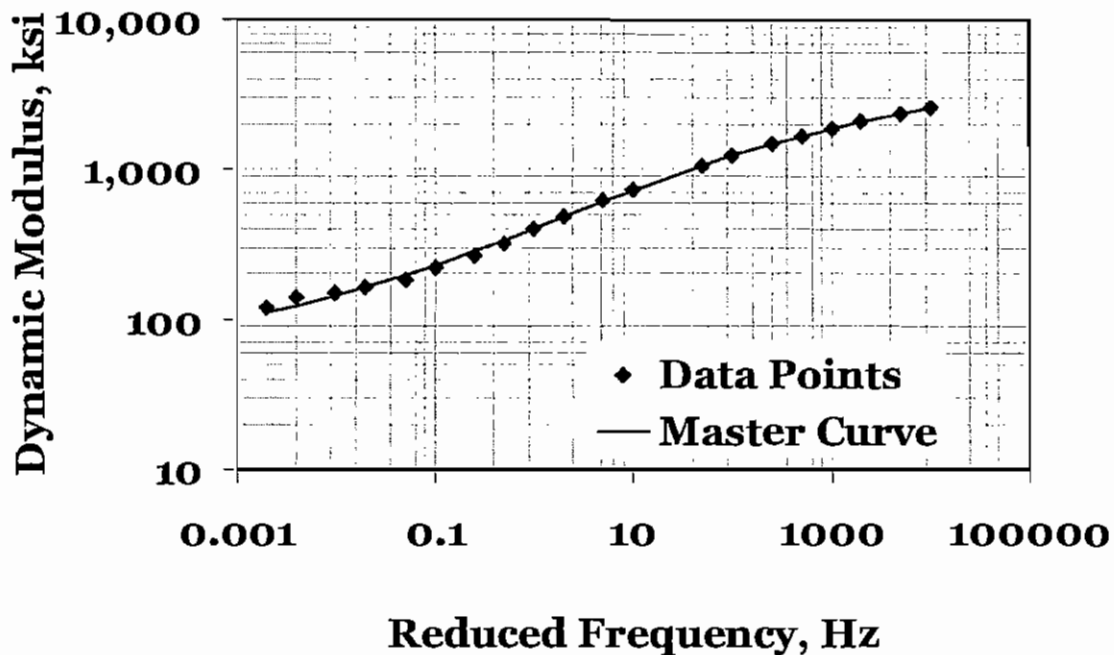


Figure 4.9 Developed Master Curve Using Sigmoidal Function for CMHB-C Mix Consisting of W 64 Asphalt Binder

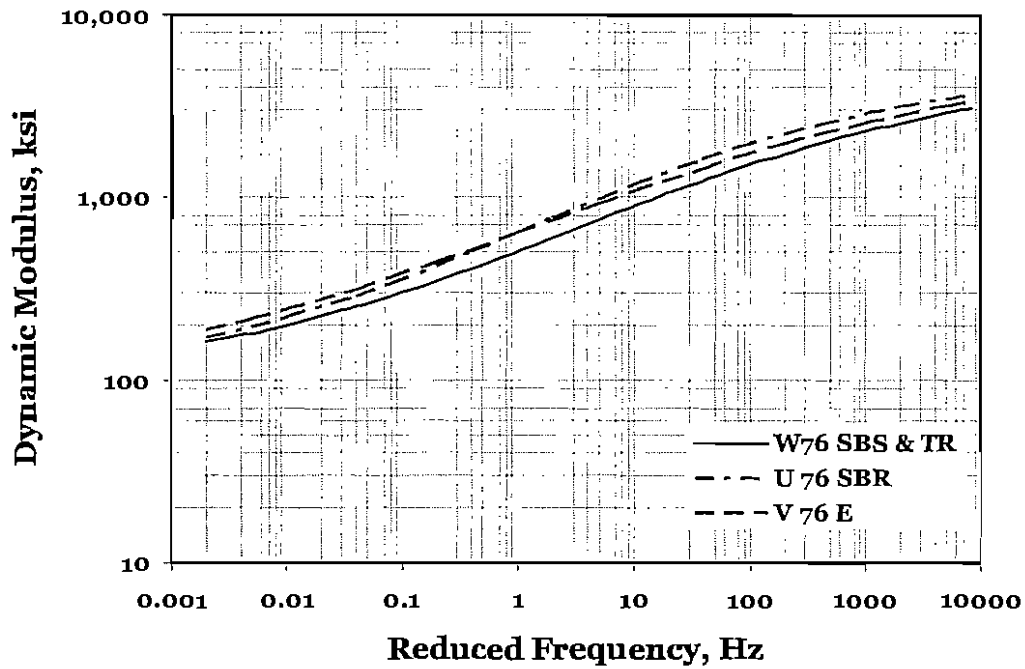


Figure 4.10 Comparison Between PG 76 Grade Asphalt Binder and Type D Mixes

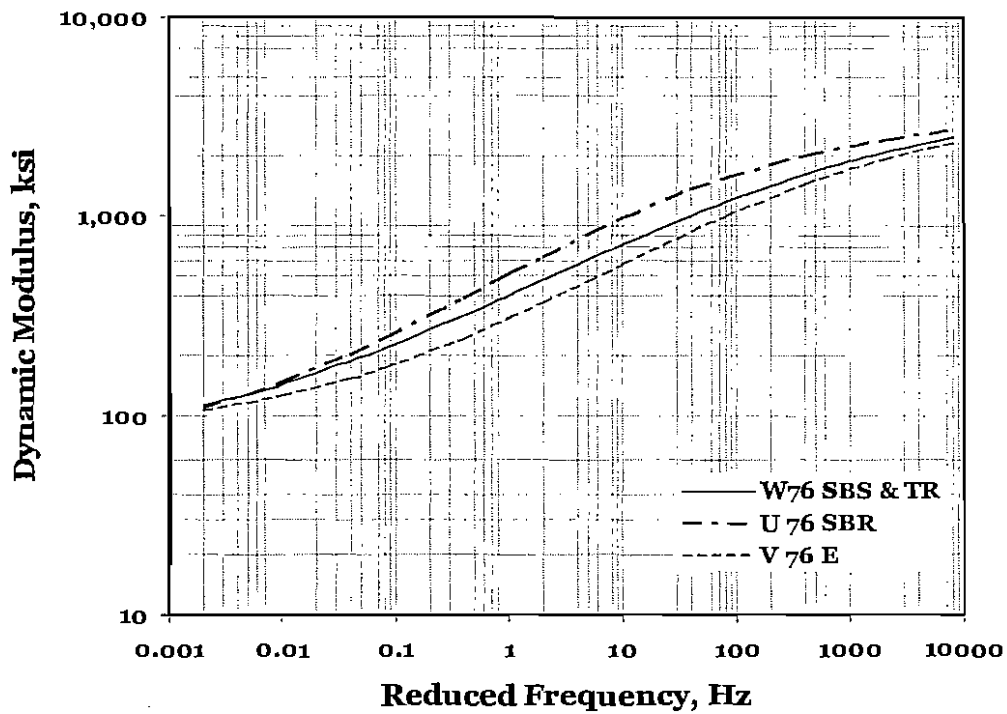


Figure 4.11 Comparison Between PG 76 Grade Asphalt Binder and CMHB-C Mixes

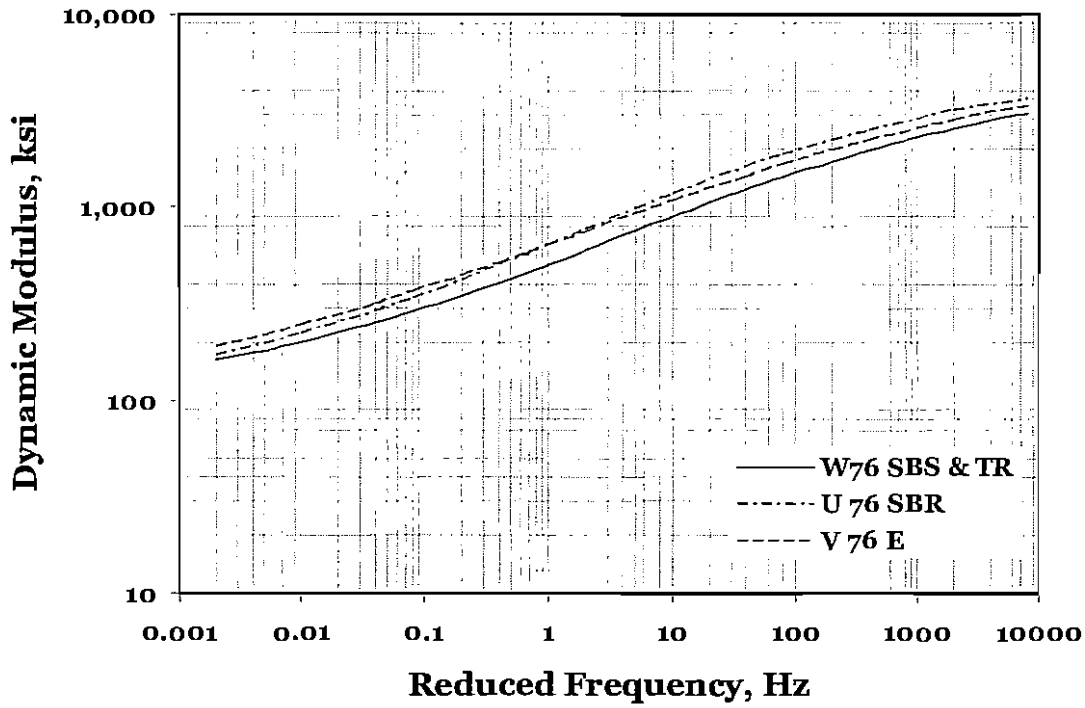


Figure 4.12 Comparison Between PG 64 Grade Asphalt Binder and Type D Mixes

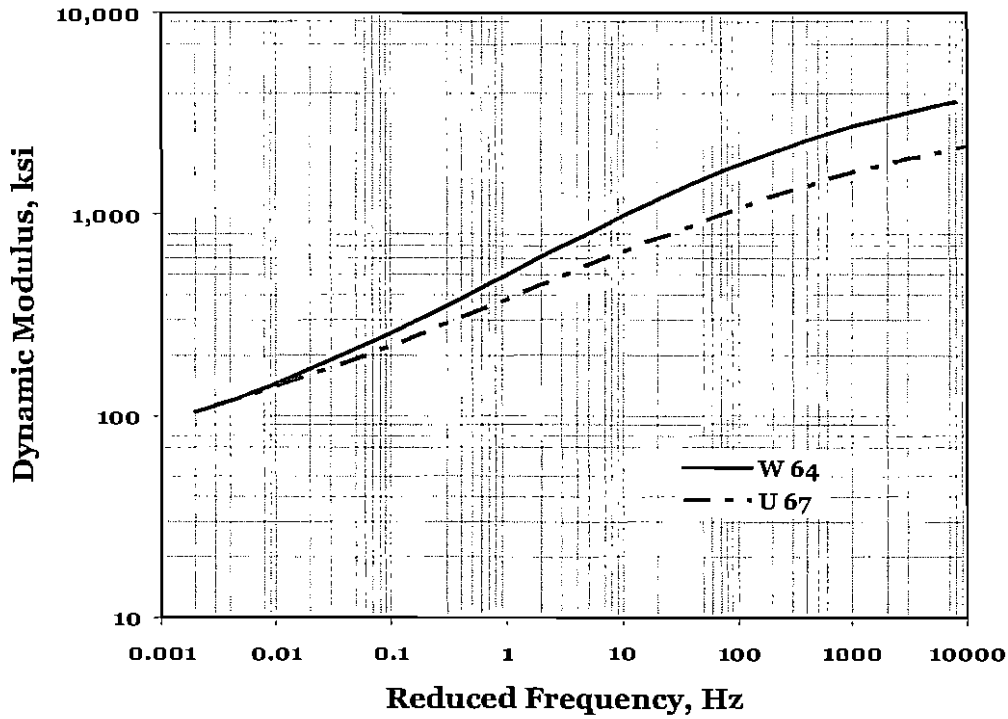


Figure 4.13 Comparison Between PG 64 Grade Asphalt Binder and CMHB-C Mixes

Data taken for all the binder types with two mix types is summarized in Figures 4.14 and 4.15. Just considering the band width, the dynamic modulus at lower frequencies varied 100 to 175 ksi while it varied from 2,000 to 3,000 ksi at higher frequencies. The Ultrapave binder seems to perform better with Type D mix, but this does not hold true for CMHB-C mix types. The data also indicate that the tests performed at 10 Hz frequency show differences between the various binder types, but that is not the case with Type D mixes. The data is not showing a clear trend in terms of which asphalt binder is better and whether or not a modifier is present.

Since PFC tests were only performed on Wright Asphalt, the data for PFC mixes are summarized in Figure 4.16. The data suggests that the PG 76 and PG 70 grade binders are better than the PG 64 grade. Since the PFC is of lower stiffness, the influence of asphalt binder grade is significant as is seen with Type D and CMHB-C mixes. In addition, the dynamic modulus of PG 64 grade asphalt is significantly lower at lower frequency ranges, which was not identified with other mix types.

Overall, the test results indicate that the influence of an asphalt binder is more pronounced in a weaker aggregate skeleton than in a stronger aggregate skeleton. In addition, the influence of asphalt binders is more pronounced in the frequency range of 0.1 to 10 Hz range and should be used for comparison purposes. However, the dynamic modulus test system does not consistently identify the presence of modifier.

4.2.2 Prediction of Master Curve Using Models

Since dynamic modulus tests require a significant amount of time and money, the new Mechanistic Pavement Design Guide proposes to generate Master curves using mix design information. To construct master curves, the data presented in Table 3.1 along with binder viscosity are needed. The binder viscosities can be found using the relationship proposed in Equation 4.1. The master curve was generated from the results obtained in the lab and the Witczak models were generated using equations (2.4) and (2.5). To construct the graphs, in addition to the data shown in tables 3.1 and 3.2, the viscosities were found using the following formula:

$$\log \log \eta = A + VTS \cdot \log T_R \quad (4.1)$$

Where:

- η = bitumen viscosity, cP
- T_R = temperature, Rankine ($T_R = T_F + 460$, T_F = temperature Fahrenheit)
- A = regression intercept
- VTS = regression slope of viscosity temperature susceptibility

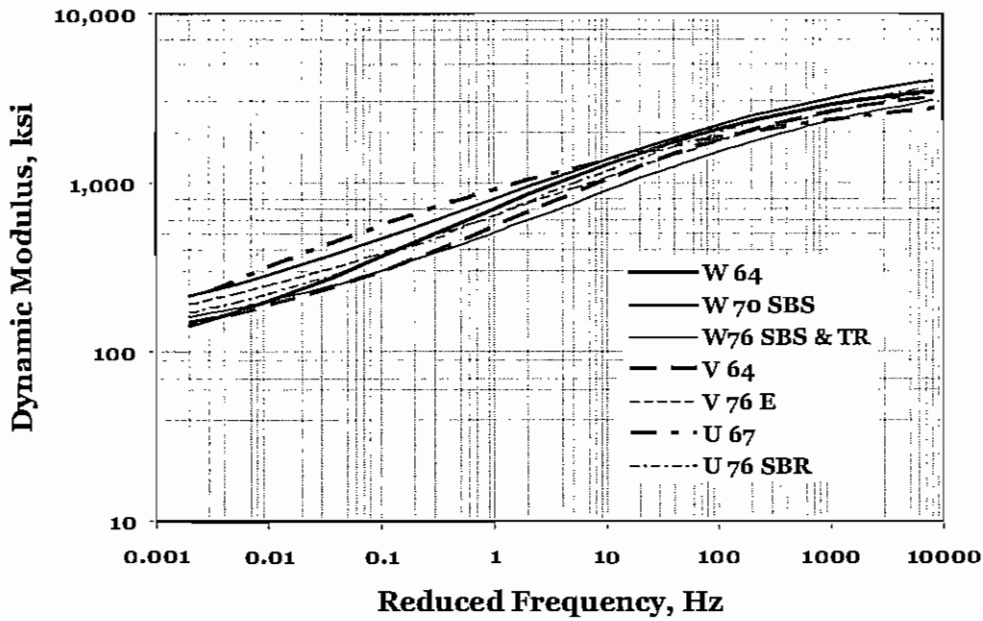


Figure 4.14 Comparison Between all Asphalt Binders and Type D Mixes

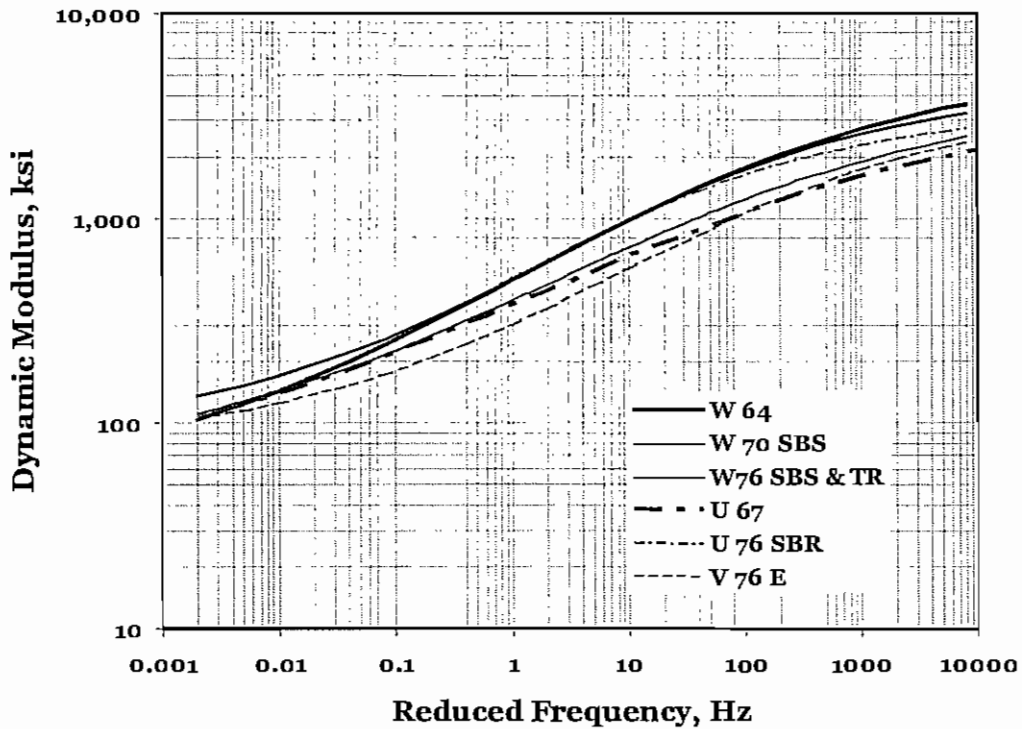


Figure 4.15 Comparison Between all Asphalt Binders and CMHB-C Mixes

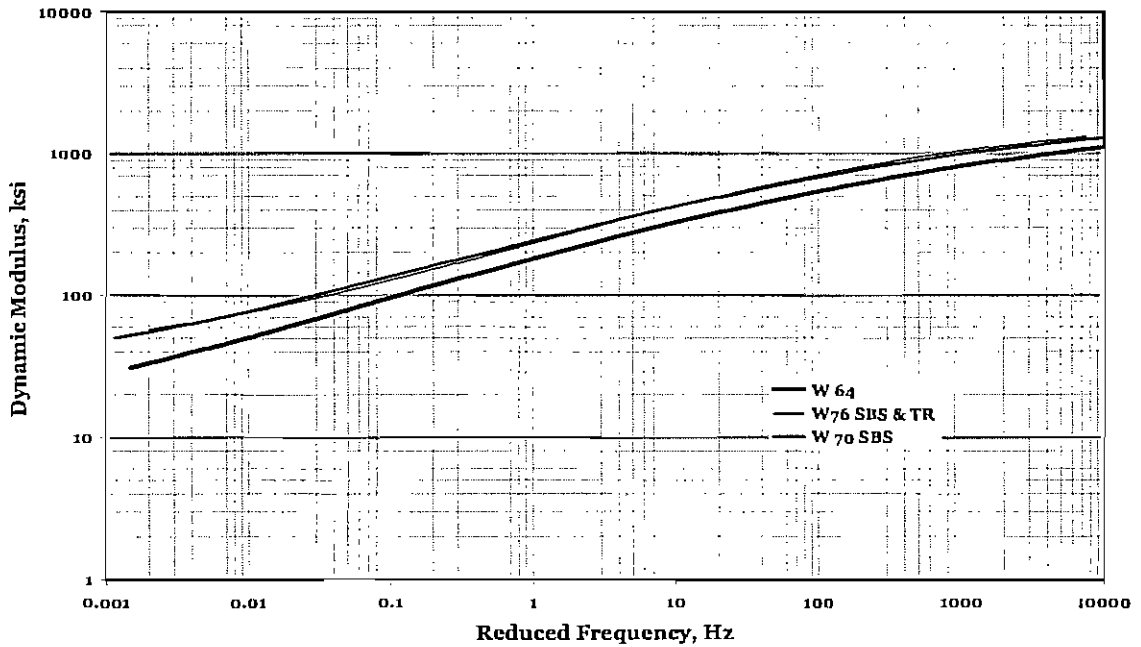


Figure 4.16 Comparison Between all Asphalt Binders and PFC Mixes

The *A* and *VTS* parameters are a function of binder type and thus are mixture characteristics. The *A* and *VTS* parameters were available in the Mechanistic-Empirical Pavement Design Guide developed by NCHRP. Table 4.6 shows the *A* and *VTS* parameter for the binders used.

Table 4.6 A and VTS Parameters for Dynamic Modulus Prediction

Binder Type	PG Grade	A	VTS
W 64	64-22	10.980	-3.680
W 70 SBS	70-22	10.299	-3.426
W 76 SBS & TR	76-22	9.715	-3.208
U 67	67-22	10.980	-3.680
U 76 SBR	76-22	9.715	-3.426
V 64	64-22	10.980	-3.680
V 76 E	76-22	9.715	-3.426

A typical graph generated using Equations 2.4 and 2.5 for CMHB-C mix consisting of W 76 SBS & TR is presented in Figure 4.17. The Witczak 1995 model is based on Equation 2.4, while the Witczak 2000 model is based on Equation 2.5. The master curve obtained using Equation 2.8 is also shown in the figure. The data shows that the dynamic modulus predicted using Witczak Model 1995 is closer to the dynamic modulus obtained from the laboratory study. However, the shape of the Witczak 2000 model is similar to that of measured

dynamic modulus, but the predicted modulus values are 5 to 7 times higher than the measured values. The data for Type D mix for the same binder type is presented in Figure 4.18, which shows similar trends. Similar trends were observed for the other mix types as well. Thus, prediction of the dynamic modulus using two models was not evaluated further.

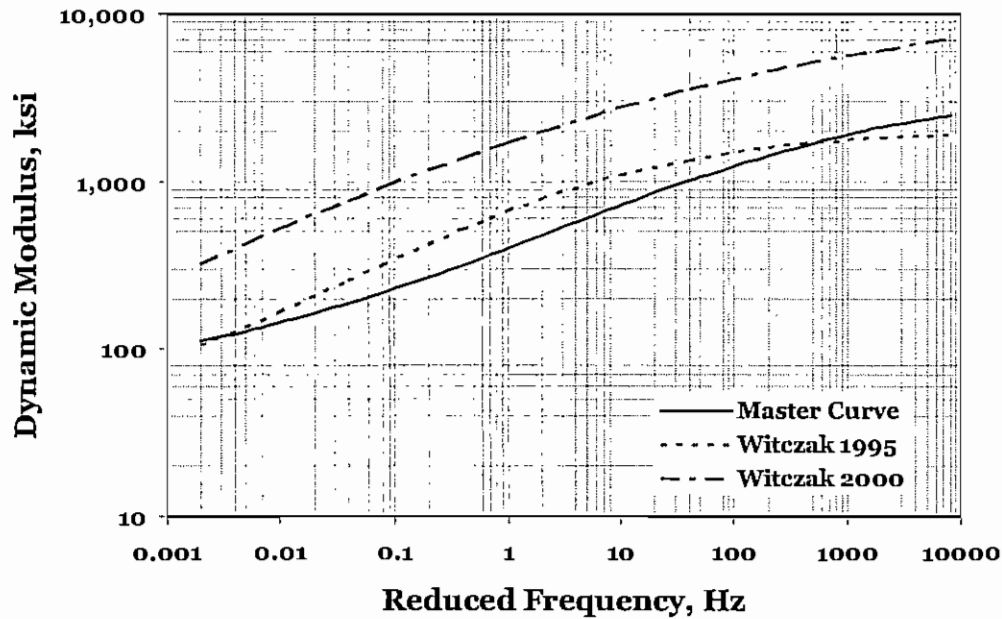


Figure 4.17 Dynamic Modulus Comparisons for CMHB-C Consisting of W 76 SBS & TR

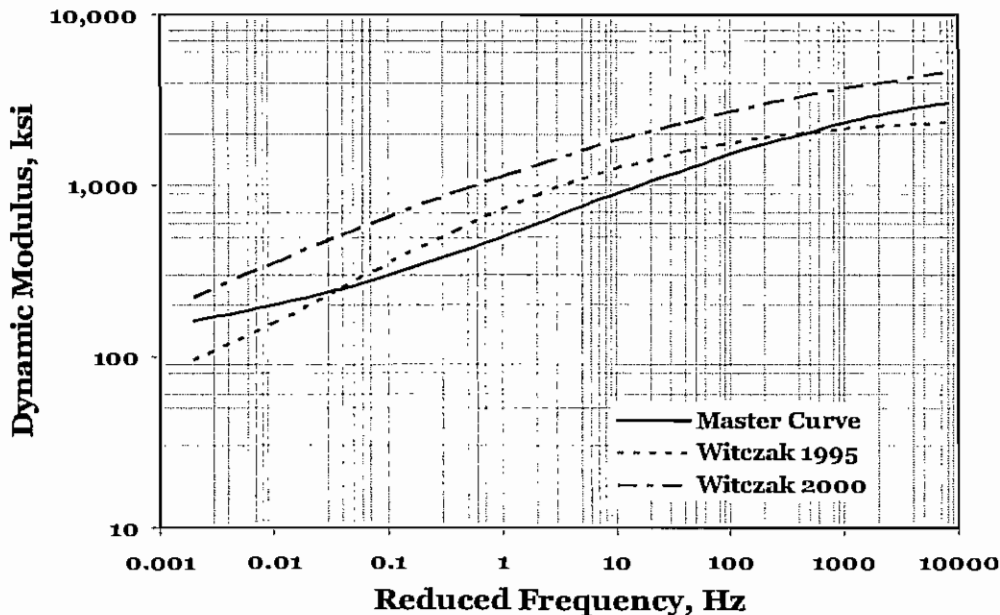


Figure 4.18 Dynamic Modulus Comparisons for Type D Consisting of W 76 SBS & TR

4.3 Flow Number and Flow Time Test Results

Three replicates of each mix were tested at a temperature of 140°F (54°C) and a stress level of 30 psi (210 kPa), testing as per flow time as well as flow number test. The CMHB-C and Type D mixes were tested under no confinement while the PFC mixes were tested under confinement (by applying a vacuum of 10 in. of Hg and enclosing the specimen in a membrane).

Although specimens are loaded differently for two tests, the results are analyzed in a similar fashion, i.e., the magnitude of accumulated strains with increase in time. The flow number test procedure suggests performing tests by application of repeated loads, and the accumulation of strain with the number of repeated loads is plotted to identify when the flow occurs or identify the accumulated strain at the end of the test. The test results for Type D and CMHB-C mixes for three binder types are shown in Figures 4.19 through 4.21. The test results show that the mixes with unmodified binder exhibited tertiary flow before reaching 10,000 cycles, while mixes with modified binder did not exhibit tertiary flow.

The data shown in Figure 4.19 suggests that the Valero Asphalt's rutting potential significantly decreased with the addition of modifier (V 76 Elvaloy). Both mixes (consisting of V64 binder) flowed before the number of load cycles reached 3,000, indicating that the mixes will fail prematurely in the field. However, the mixes experienced minimal damage when modified asphalt binder is used. Similar trends were observed with other binder types, as shown in Figures 4.20 and 4.21. The test results presented in the figures also show that the CMHB-C mixes exhibited better performance in comparison to Type D mixes when considering the number of cycles to reach failure before the end of the tests. For instance, the Type D mixes with Wright Asphalt (W 64) failed before 2,000 cycles while CMHB-C mixes failed after 4,000 cycles. Similar trends were observed for other binder types indicating that the CMHB-C mixes are more stable than Type D mixes, especially when the binder quality is poor.

Similar trends were observed with flow time tests where the load is applied and maintained till the end of 10,000 seconds. A typical test result for Wright Asphalt is shown in Figure 4.22. The test results suggest that CMHB-C performs better in comparison to Type D in the presence of lower binder quality, and mixes do not fail in the presence of modified binders.

Flow number and flow time test results are summarized in Table 4.7, which indicate that the test results are less repeatable because the COV varied from 5% to 30% depending on the mix types. However, the Type D test results showed lower COV for flow time in comparison to the CMHB-C mixes.

In terms of flow number test results, the data suggests that the permanent strain of less than 1% is an indicator of the presence of a modifier for mix types CMHB-C and Type D mixes. The same cannot be said about PFC mixes because test conditions were changed and only one asphalt type was used. In terms of flow time test results, the data suggests that the total axial strain less than 7,000 μ

in./in. is an indicator of the presence of a modifier for CMHB-C and Type D mixes.

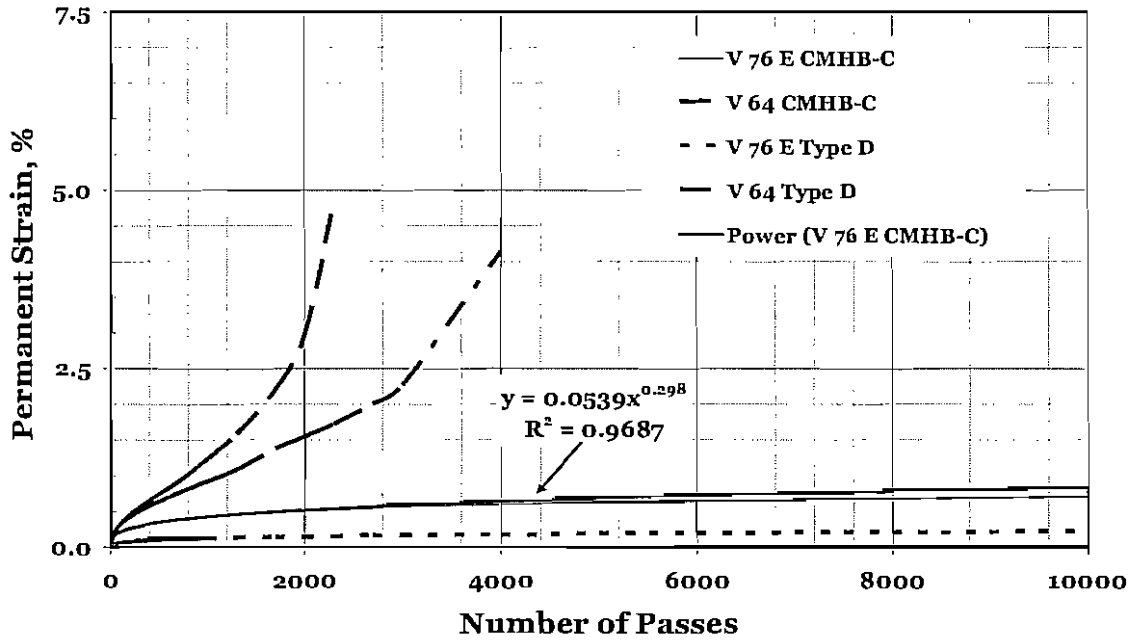


Figure 4.19 Flow Number Test Results for Mixes Consisting of Valero Asphalt

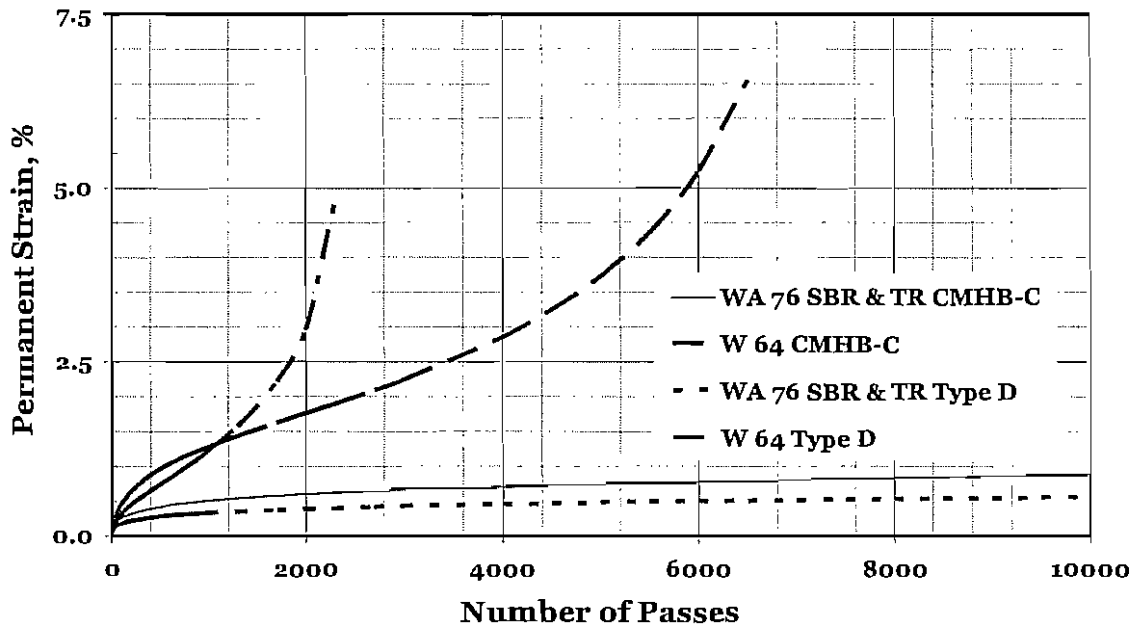


Figure 4.20 Flow Number Test Results for Mixes Consisting of Wright Asphalt

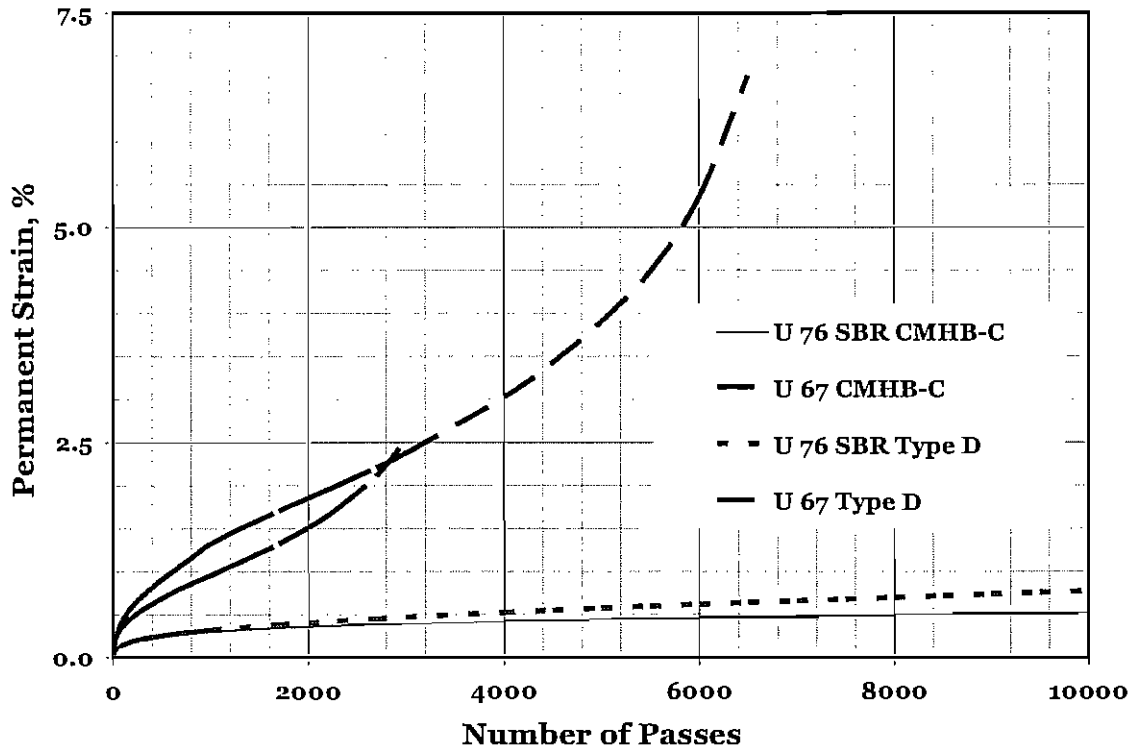


Figure 4.21 Flow Number Test Results for Mixes Consisting of Ultrapave Asphalt

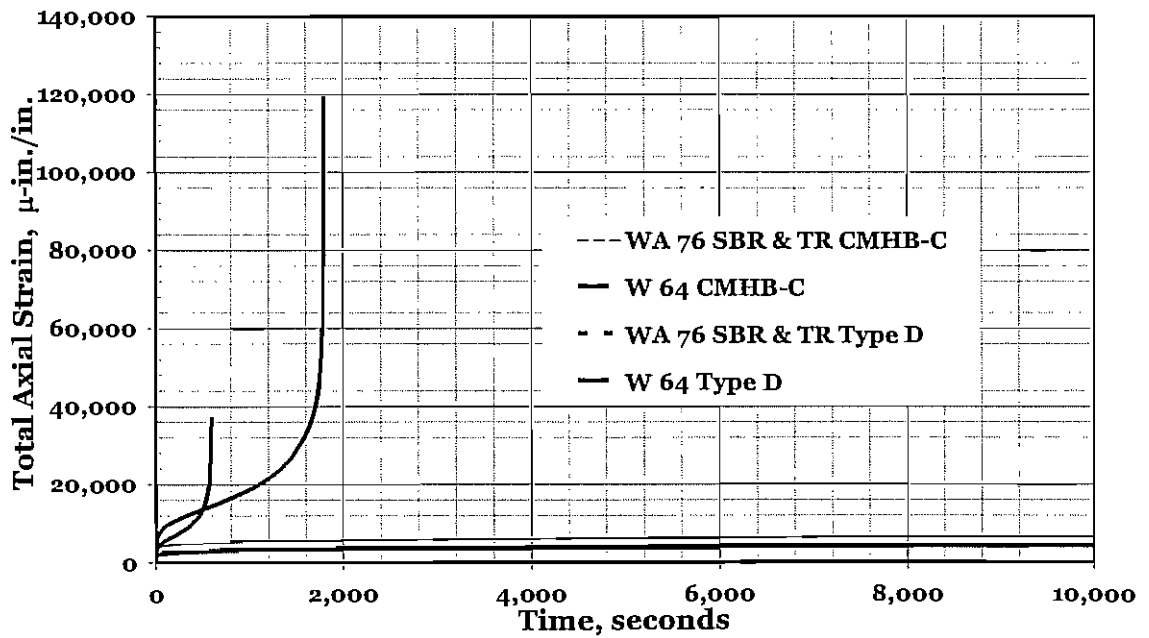


Figure 4.22 Flow Time Test Results for Mixes Consisting of Wright Asphalt

Table 4.7 Flow Number and Flow Time Test Results

a) CMHB-C

Asphalt Type	Flow Number (Total Permanent Strain, %)			Flow Time (Total Axial Strain, μ in./in.)		
	Average, %	SD, %	COV, %	Average, μ in./in.	SD, μ in./in.	COV, %
W 64	4.37	1.00	26.34	30,913	9,222	29.83
	Flowed after 5,800 cycles			Flowed after 1,750 seconds		
W 70 SBS	0.64	0.08	11.67	4,984	397	7.97
	No Flow			No Flow		
W76 SBS & TR	0.87	0.16	17.95	6,511	163	2.50
	No Flow			No Flow		
U 67	3.83	0.00	7.97	26,232	3,818	14.56
	Flowed after 5,000 cycles			Flowed after 2,400 seconds		
U 76 SBR	0.53	0.01	1.10	5,224	288	5.51
	No Flow			No Flow		
V 64	4.37	1.00	26.34	30,913	9,222	19.79
	Flowed after 5,500 cycles			Flowed after 1,900 seconds		
V 76 E	0.70	0.06	9.12	5,666	1,121	29.83
	No Flow			No Flow		

b) Type D

Asphalt Type	Flow Number (Total Permanent Strain, %)			Flow Time (Total Axial Strain, μ in./in.)		
	Average, %	SD, %	COV, %	Average, μ in./in.	SD, μ in./in.	COV, %
W 64	2.00	0.20	10.00	17,204	2,963	17.41
	Flowed after 1,800 cycles			Flowed after 640 seconds		
W 70 SBS	0.39	0.05	11.75	4,953	749	15.11
	No Flow			No Flow		
W76 SBS & TR	0.56	0.07	11.89	3,937	145	3.68
	No Flow			No Flow		
U 67	2.27	0.40	17.83	19,832	3,332	16.80
	Flowed after 2,700 cycles			Flowed after 1,450 seconds		
U 76 SBR	0.78	0.15	19.33	5,504	118	2.14
	No Flow			No Flow		
V 64	1.80	0.44	24.22	13,253	720	5.44
	Flowed after 5,800 cycles			Flowed after 1,250 seconds		
V 76 E	0.28	0.07	26.29	5,503	462	8.40
	No Flow			No Flow		

c) PFC

Asphalt Type	Flow Number (Total Permanent Strain, %)			Flow Time (Total Axial Strain, μ in./in.)		
	Average, %	SD, %	COV, %	Average, μ in./in.	SD, μ in./in.	COV, %
W 64	3.830	0.99	25.75	27,000	859	3.17
	Flowed after 640 cycles			Flowed after 2,500 seconds		
W 70 SBS	0.56	0.05	9.71	7,362	1,385	18.81
	No Flow			No Flow		
W76 SBS & TR	1.24	0.30	23.94	9,284	597	6.43
	No Flow			No Flow		

To estimate the flow time and flow number curve, the test procedure suggests that a power law curve needs to be fitted to the data. The fit parameters for different mix types are shown in Tables 4.8 and 4.9 for flow time and flow number tests, respectively. The curve fits were generated using Table Curve Software. Two curve types were fitted to the data as shown in the table. The data indicates that both of the models fit the data reasonably well.

To compare the flow number and flow time test results for CMHB-C and Type D mixes, the data from all of the binder tests is summarized in Figures 4.23 and 4.24, respectively. The data exhibits strong correlations between the two mixes. Overall, the CMHB-C exhibited permanent strains around two times higher than Type D mixes for flow number tests.

4.4 Indirect Tensile Strength Test Results

The IDT tests were performed according to Tex-26-F "Indirect Tensile Strength Test." Three replicates of each mix were prepared, with the exception that specimens were not prepared and tested for Type D Valero Asphalt (V 64) and for CMHB-C V64 and V76 E due to a shortage of the asphalt binder. In addition, the tests were not performed on PFC mixes. The IDT tests were performed at a temperature of 40°F rather than 77°F to assess the cracking potential of the mixes. To ensure that the specimens achieved the desired test temperatures, they were placed in a temperature-controlled chamber maintained at 40°F overnight prior to the start of the test. The analysis of the mixes can be performed in three different ways: tensile strength at peak load, energy until failure, and fracture energy. Energy until failure is the area under the curve till peak load, while fracture energy considers the whole area under the curve.

The test results for CMHB-C and Type D mixes are summarized in Tables 4.10 and 4.11, respectively. The test results suggest that the test setup is repeatable because COV of less than 20% was observed most of the time with few exceptions. However, the test results are not able to differentiate between different binder types.

Tensile strength varied from 323 to 404 ksi for CMHB-C mixes, indicating that W 64 and W 70 SBS binders performed better. However, the differences between the binder types diminished significantly for Type D mixes because the tensile strength varied between 336 and 365, which is within the COV of the test procedure. In terms of fracture energy and energy until failure, the test results show similar trends of not being able to identify the presence of modifiers because the estimated energies did not identify the differences. In addition, in a number of instances the measured values are very close, making it difficult to determine the influence of binder types.

Table 4.8 Flow Number Model Data

Mix Type	Binder Type	Model Fitted										
		y=c+aN ^b						y=aN ^b				
		c	a	b	R ²	Std. Error	rank	a	b	R ²	Std. Error	rank
Type D	W 64	0.801588	0.109254	0.00475	0.980412	0.045998	7	0.019725	0.606067	0.971092	0.055645	11
	W 70 SBS	0.139977	-0.18697	0.16089	0.99922	0.002708	1	0.030605	0.284276	0.979131	0.013956	5
	W76 SBS & TR	0.158465	-0.17196	0.168555	0.999696	0.002244	1	0.050779	0.263853	0.989688	0.013019	7
	U 67	0.806668	0.139942	0.003238	0.979486	0.0533	6	0.020803	0.570316	0.960864	0.073319	13
	U 76 SBR	0.344346	-0.01492	0.031923	0.997704	0.008432	2	0.026125	0.364824	0.997439	0.008872	3
	V 64	0.843305	0.158108	0.002724	0.969969	0.056629	7	0.025277	0.549144	0.946635	0.075175	16
	V 76 E	0.178096	-0.06826	0.056018	0.999853	0.000658	1	0.013624	0.307778	0.984993	0.00662	6
CMHB-C	W 64	0.977755	0.266036	0.00083	0.955347	0.157826	6	0.018627	0.612791	0.921346	0.208648	22
	W 70 SBS	0.159395	0.197984	-0.20976	0.999738	0.002475	2	0.055961	0.270894	0.988082	0.01663	6
	W76 SBS & TR	0.1825	-0.21216	0.20199	0.999916	0.00189	1	0.067255	0.282506	0.991004	0.019463	6
	U 67	0.750142	0.168994	0.005857	0.978877	0.081527	4	0.026599	0.566525	0.96508	0.104403	9
	U 76 SBR	0.184538	-0.13937	0.121035	0.999612	0.00249	3	0.034855	0.298836	0.987878	0.013866	6
	V 64	0.849525	0.198862	0.002644	0.970387	0.097612	6	0.021811	0.592285	0.947027	0.130031	16
	V 76 E	0.158791	0.219326	0.215856	0.999775	0.002479	1	0.065755	0.263113	0.989599	0.016811	7
PFC	W 64	0.079586	-4.58024	4.122555	0.973812	0.116779	5	0.325045	0.295687	0.922941	0.199509	12
	W 70 SBS	0.074754	0.572024	-0.58567	0.999622	0.002432	1	0.07565	0.222122	0.977011	0.018896	7
	W76 SBS & TR	0.126696	-0.63777	0.582888	0.999435	0.006973	1	0.115071	0.263375	0.981306	0.039977	6

Table 4.9 Flow Number Model Data

Mix Type	Binder Type	Model Fitted										
		y=c+at ^m						y=at ^m				
		c	a	m	R ²	Std. Error	rank	a	m	R ²	Std. Error	rank
Type D	W 64	1.849164	4547.112	0.105389785	0.902222	1124.745	20	253.080324	0.637498	0.781735	1680.051	35
	W 70 SBS	0.030518	12166.28	-11273.9616	0.645426	347.263	1	1724.53973	0.112318	0.629696	354.8784	2
	W76 SBS & TR	0.01798	-12702.9	14071.48735	0.369531	381.7315	1	1851.05915	0.080987	0.352885	386.7339	3
	U 67	1.4216	4684.404	0.39997699	0.906322	913.4273	20	424.844597	0.478325	0.78627	1379.569	32
	U 76 SBR	0.082017	-3804.74	4276.893302	0.776608	348.1669	1	1277.08142	0.154885	0.77222	351.5657	2
	V 64	1.364516	4739.081	0.581425335	0.965755	448.7445	7	657.054721	0.408143	0.878315	845.804	29
	V 76 E	0.070956	-3066.27	4497.371339	0.802931	267.4732	1	1890.22472	0.117843	0.800719	268.9674	2
CMHB-C	W 64	1.51751	8232.143	0.268285428	0.939035	1206.119	12	702.036029	0.470462	0.831684	2003.884	32
	W 70 SBS	0.077908	-170.523	2482.967977	0.987229	38.90042	1	2332.30745	0.081024	0.987209	38.93011	2
	W76 SBS & TR	0.150342	2076.51	1128.347129	0.996729	29.57689	2	2754.79286	0.094171	0.994904	36.91662	3
	U 67	2.23358	6663.073	1.13E-03	0.798285	2417.731	16	1.63E+02	0.643699	0.602111	3395.362	31
	U 76 SBR	0.117501	-74.3527	1883.02613	0.996662	30.45586	1	1825.00405	0.119453	0.996659	30.46819	2
	V 64	3.501608	8084.845	2.32E-08	0.84667	2816.935	10	27.1241605	0.85865	0.597287	4565.004	30
	V 76 E	0.089626	-2419.13	3507.8209	0.835797	272.6353	1	1586.2964	0.137036	0.833889	274.2113	2
PFC	W 64	0.912128	12525.18	12.33907976	0.765961	1772.997	35	5017.00802	0.198269	0.643887	2186.892	53
	W 70 SBS	0.011749	-9538.03	15356.17425	0.833349	89.3952	1	5905.98222	0.027046	0.820687	92.72778	3
	W76 SBS & TR	0.011847	-27762.6	33516.6596	0.895815	149.4681	1	6165.52671	0.048371	0.875594	163.3282	2

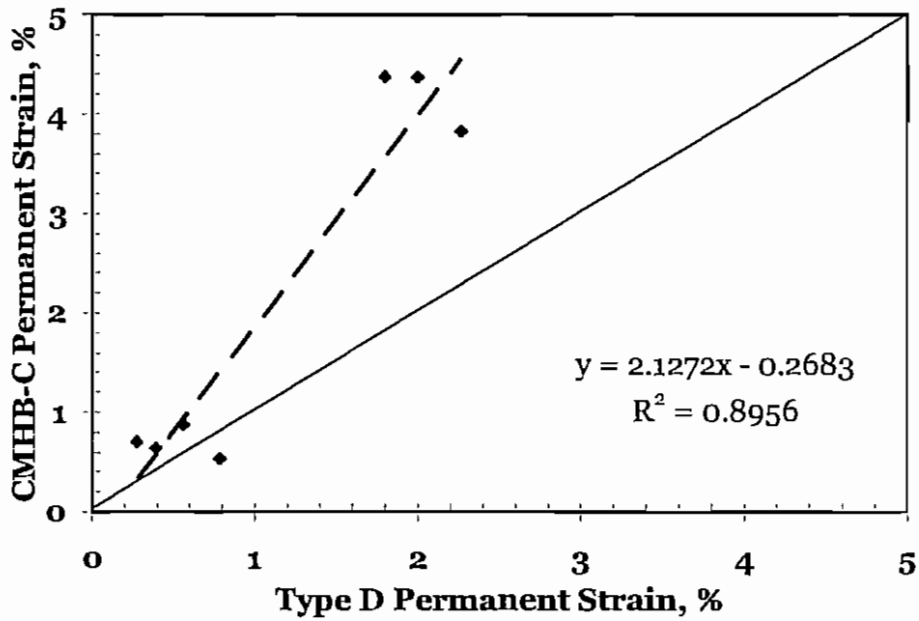


Figure 4.23 Flow Number Test Results for Two Mix Types

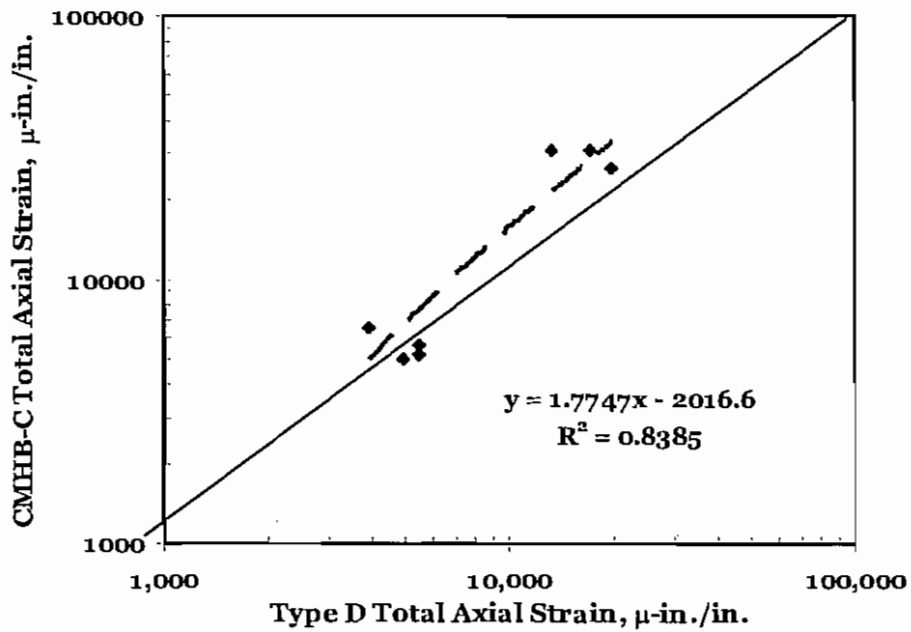


Figure 4.24 Flow Time Test Results for Two Mix Types

Table 4.10 Indirect Tensile Strength Test Results for CMHB-C

Asphalt Type	Load at Failure			Tensile Strength			Fracture Energy			Energy Until Failure		
	Average,	SD,	COV,	Average,	SD,	COV,	Average,	SD,	COV,	Average,	SD,	COV,
	lbs	lbs	%	psi	psi	%	lbs-in.	lbs-in.	%	lbs-in.	lbs-in.	%
W 64	4664	137.9	3.0	371	11.0	3.0	218	12.1	5.6	208	1.3	0.6
W 70 SBS	5083	210.0	4.1	404	16.7	4.1	181	61.0	33.8	208	22.8	11.0
W76 SBS & TR	4102	221.3	5.4	326	17.6	5.4	195	5.8	3.0	158	15.3	9.7
U 67	4063	166.9	4.1	323	13.3	4.1	197	13.6	6.9	185	31.7	17.2
U 76 SBR	4219	903.7	21.4	336	71.9	21.4	207	39.9	19.3	166	46.3	27.9
V 64	N/T			N/T			N/T			N/T		
V 76 E	N/T			N/T			N/T			N/T		

Table 4.11 Indirect Tensile Strength Test Results for Type D

Asphalt Type	Load at Failure			Tensile Strength			Fracture Energy			Energy Until Failure		
	Average,	SD,	COV,	Average,	SD,	COV,	Average,	SD,	COV,	Average,	SD,	COV,
	lbs	lbs	%	psi	psi	%	lbs-in.	lbs-in.	%	lbs-in.	lbs-in.	%
W 64	4463	340.8	7.6	355	27.1	7.6	215	10.1	4.7	208	20.7	9.9
W 70 SBS	4350	630.7	14.5	346	50.2	14.5	205	4.3	2.1	199	12.5	6.3
W76 SBS & TR	4593	202.9	4.4	365	16.1	4.4	264	2.5	0.9	183	11.2	6.1
U 67	4553	784.2	17.2	362	62.4	17.2	194	18.2	9.4	190	12.3	6.5
U 76 SBR	4228	527.5	12.5	336	42.0	12.5	220	42.8	19.4	148	31.0	21.0
V 64	N/T			N/T			N/T			N/T		
V 76 E	4485	540.9	12.1	357	43.0	12.1	239	5.3	2.2	138	90.1	65.1

The test results were also compared in terms of mix types, and the results are summarized in Figures 4.25 through 4.27. Results of the energy till failure test (Figure 4.25) suggest that there is an influence of mix type as the data is close to unity. In terms of tensile strength, Type D (Figure 4.26) exhibited similar strengths regardless of the binder type, while in terms of fracture energy the CMHB-C mixes (Figure 4.27) exhibited similar energy levels regardless of the binder types.

Overall, the test results suggest that the IDT tests are not able to identify the presence of modifiers. Swami et al. (2006) showed that IDT can discriminate between different mix types. However, the testing was performed at 14°F rather than 40°F, which may be why results of testing conducted for this study did not identify the differences.

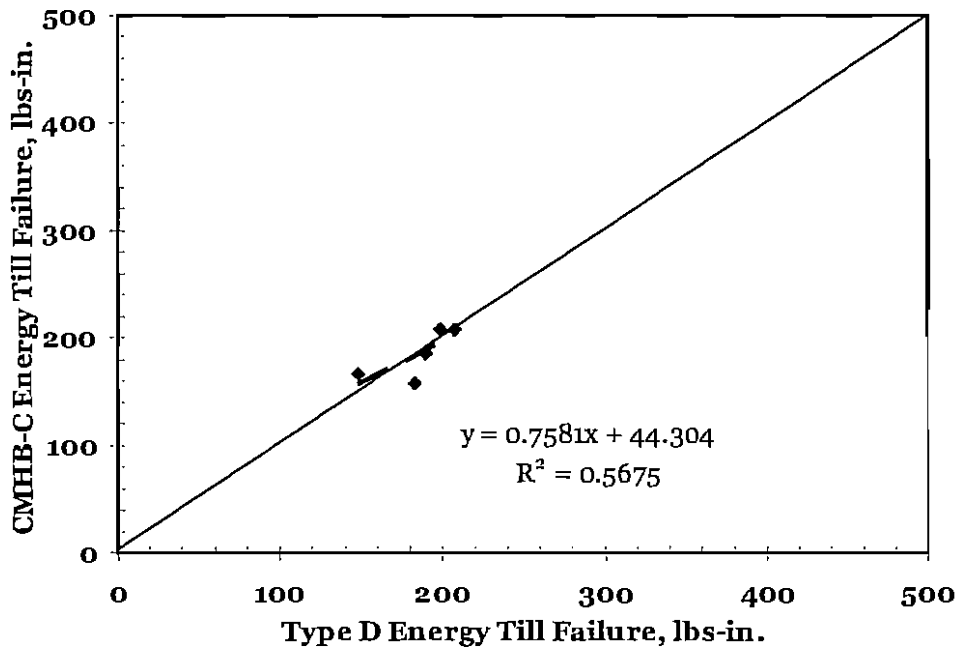


Figure 4.25 Energy till Failure Test Results for Type D and CMHB-C Mixes

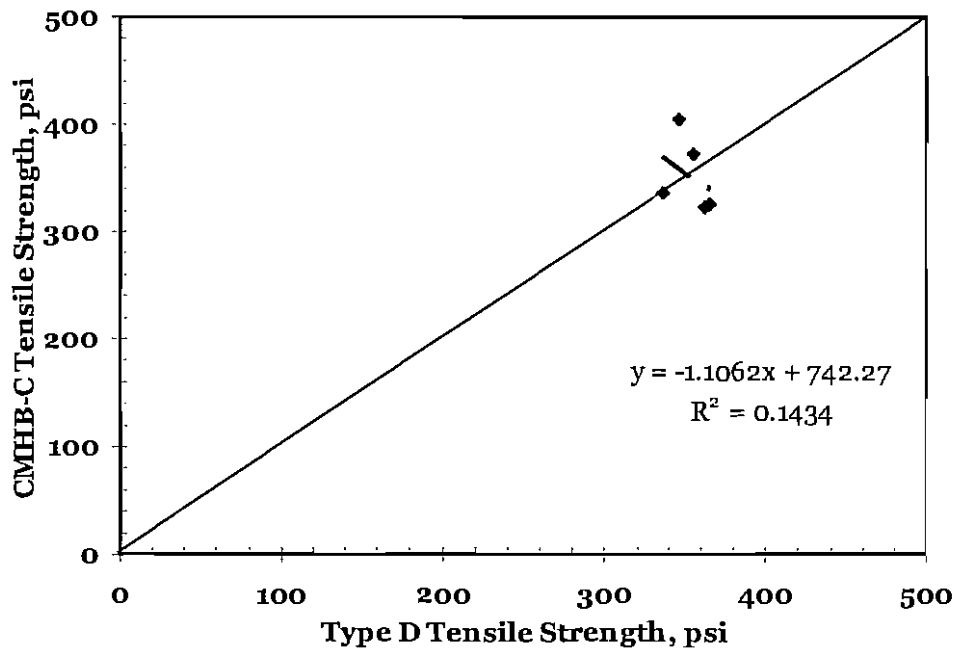


Figure 4.26 Tensile Strength Test Results for Type D and CMHB-C Mixes

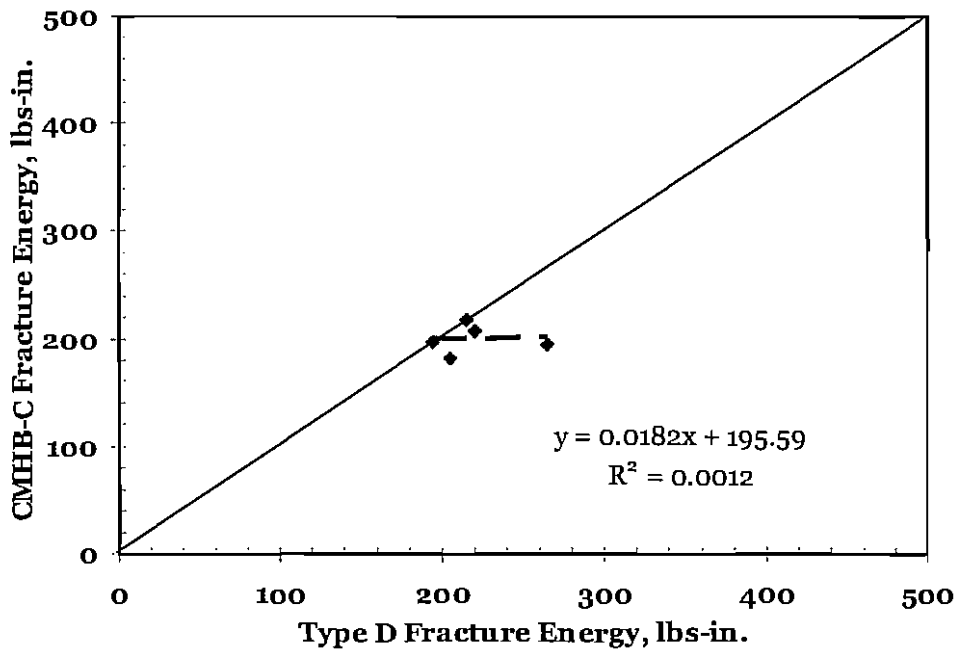


Figure 4.27 Fracture Energy Test Results for Type D and CMHB-C Mixes

4.5 Static Creep Test Results

Duplicate specimens of each mix were prepared according to Tex-231-F, the exception being that specimens were not prepared and tested for the Valero Asphalt (V 64) due to a shortage of the binder. In addition, the tests were not performed on PFC mixes. The specimens were prepared according to Tex-231-F. A typical test result is shown in Figure 4.28 for Type D mix consisting of Wright Asphalt (W 64). The test results show that some of the deformation is recovered after the removal of load; however, some of the deformation is not recovered and is thus termed as permanent deformation. Typically, the static creep test results are presented in terms of total strain, creep stiffness, and permanent strain. To obtain these parameters, the observed deformations are converted into strain and the results are summarized in Tables 4.12 and 4.13.

A total strain of more than 4.7 was observed for CMHB-C mix consisting of Ultrapave asphalt (U 67), while a minimum strain of 1.76 was observed for Type D mix consisting of Wright Asphalt (W 70 SBS). In general, the total strain ranged from 2% to 3%. However, the acceptance criterion is less than 2%, indicating that only Type D mix consisting of W 70 SBS asphalt meets the criterion.

The test results can also be interpreted in terms of the permanent strain. The results presented in Tables 4.12 and 4.13 suggest that the Type D mix consisting of W 76 SBS & TR exhibited the lowest permanent strain (1.03) while CMHB-C mix consisting of W 64 exhibited the highest strain (3.48). However, none met the criterion of 0.6 maximum.

In terms of creep stiffness, the maximum creep stiffness of 5,800 psi was observed for Type D mix consisting of W 70 SBS asphalt while minimum creep stiffness of 2,200 psi was observed for CMHB-C mix consisting of U 67 asphalt. Since TxDOT specifications call for a minimum stiffness of 4,000 psi, the Type D mixes consisting of modified asphalts met the criterion with the exception of V 76 E, while CMHB-C mixes consisting of modified asphalt met the criterion with the exception of W 70 SBS.

COVs varied between 6% and 60% depending on the parameters evaluated, indicating that test repeatability is poor and the results may not be reliable. More than 3 specimens need to be tested to obtain statistically reliable results.

Overall, the only parameter that met the TxDOT criterion was creep stiffness, which can also identify the presence of modifiers. The other two criteria were not met, but they do identify the presence of modifiers. For example, the permanent strain of less than 2.0% indicates the presence of a modifier.

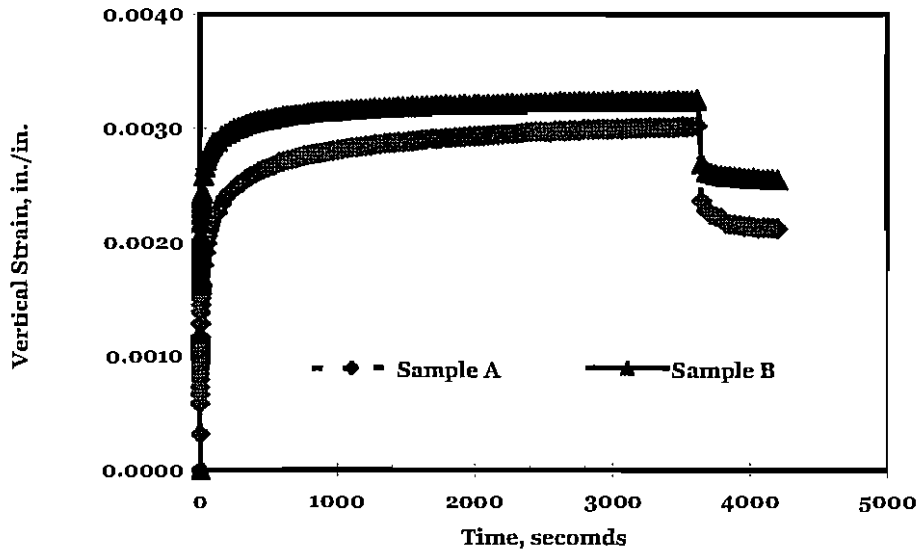


Figure 4.28 Static Creep Test Results for Type D Mix Consisting of W 64 Asphalt Type

Table 4.12 Static Creep Test Results for CMHB-C

Binder Type	Parameter	Total Strain (in/in) $\times 10E3$	Creep Stiffness (lbs/in ²)	Permanent Strain (in/in) $\times 10E3$
W 64	Average	4.41	2262.02	3.48
	SD	0.43	201.33	0.22
	COV,%	9.84	8.90	6.30
W 70 SBS	Average	2.83	3505.95	2.02
	SD	0.06	67.72	0.07
	COV,%	2.27	1.93	3.47
W76 SBS & TR	Average	2.59	3996.83	1.18
	SD	0.53	690.52	0.08
	COV,%	20.46	17.28	7.20
U 67	Average	4.72	2215.80	3.63
	SD	0.30	164.71	0.48
	COV,%	6.28	7.43	13.16
U 76 SBR	Average	2.25	4636.37	1.40
	SD	0.79	1678.55	0.84
	COV,%	35.15	36.20	59.81
V 64	Average	N/T	N/T	N/T
	SD			
	COV,%			
V 76 E	Average	2.49	4150.15	1.15
	SD	0.44	822.58	0.16
	COV,%	17.74	19.82	13.72

Table 4.13 Static Creep Test Results for Type D

Binder Type	Parameter	Total Strain (in/in)x10E3	Creep Stiffness (lbs/in²)	Permanent Strain (in/in)x10E3
W 64	Average	3.13	3239.03	2.34
	SD	0.16	160.41	0.30
	COV,%	5.11	4.95	12.93
W 70 SBS	Average	1.76	5830.43	1.08
	SD	0.21	682.77	0.41
	COV,%	12.08	11.71	38.35
W76 SBS & TR	Average	2.04	4917.43	1.03
	SD	0.34	989.88	0.06
	COV,%	16.42	20.13	5.80
U 67	Average	4.01	2514.84	2.79
	SD	0.47	243.43	0.30
	COV,%	11.81	9.68	10.80
U 76 SBR	Average	2.88	4381.41	1.82
	SD	1.80	2774.98	1.38
	COV,%	62.60	63.34	75.79
V 64	Average	N/T	N/T	N/T
	SD			
	COV,%			
V 76 E	Average	3.06	3390.80	1.82
	SD	0.86	995.37	1.07
	COV,%	28.25	29.35	58.63

To compare the influence of parameters on the mix types, the three parameters for the two mix types are summarized in Figures 4.29 through 4.31. The results suggest that the creep stiffness of Type D mixes (Figure 4.31) is higher in comparison to CMHB-C mixes. No other clear trend could be observed from the other parameters.

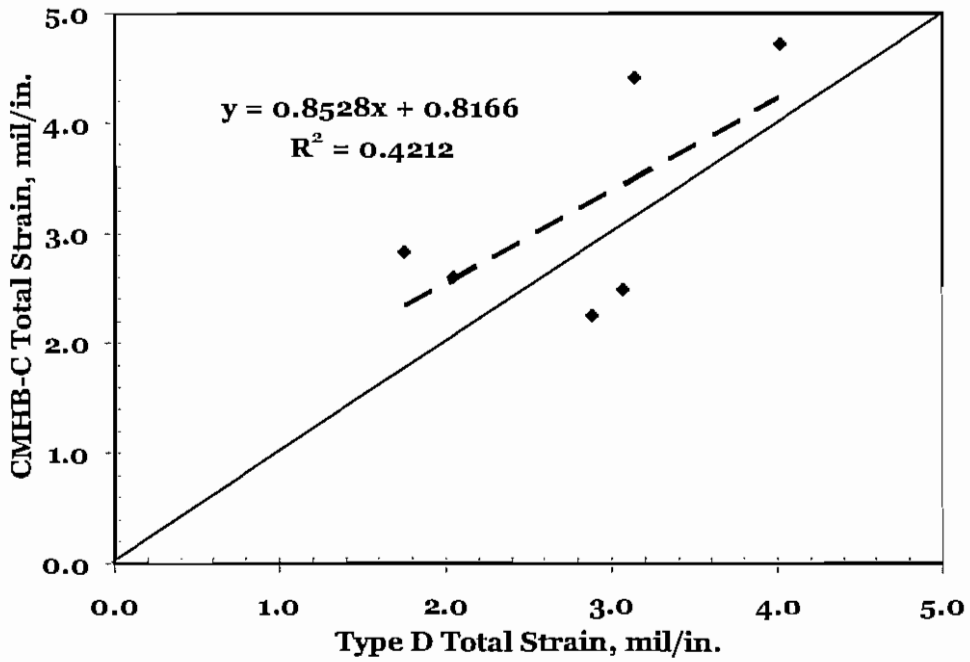


Figure 4.29 Total Strain Comparison for Type D and CMHB-C Mixes

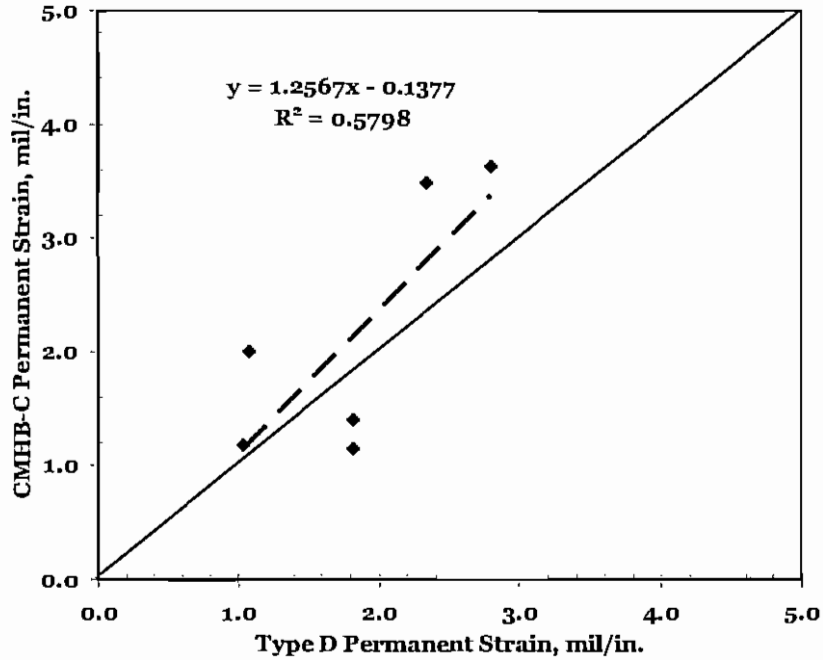


Figure 4.30 Permanent Strain Comparison for Type D and CMHB-C Mixes

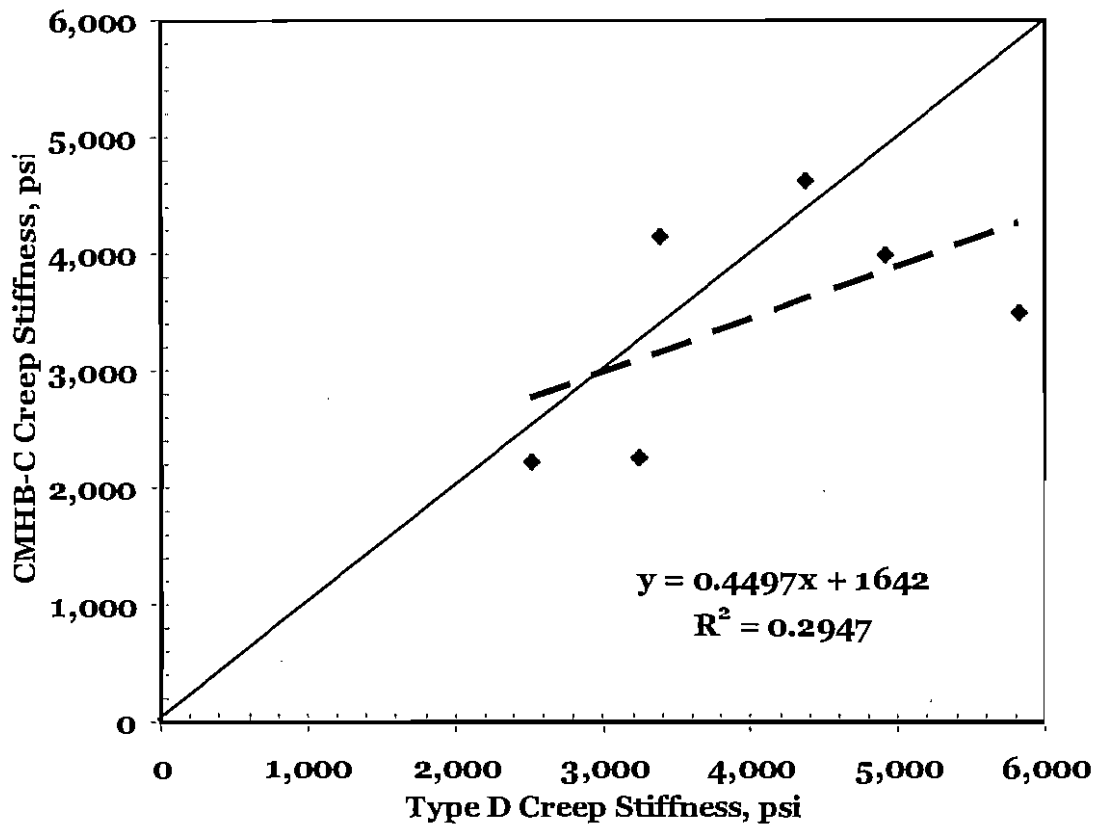


Figure 4.31 Creep Stiffness Comparison for Type D and CMHB-C Mixes

4.6 Seismic Modulus

The specimens prepared for flow number and flow time tests were also subjected to seismic modulus testing. Since seismic modulus tests are nondestructive, the flow number and flow time tests can be performed without fear of damage to the specimen. The seismic tests were performed at three different specimen stages and at two temperatures. The flow number and flow time test procedures suggest that the specimens should be prepared to a size of 6 in. by 7 in., and then specimens of 4 in. by 6 in. should be cored from the bigger specimens. Therefore, seismic modulus tests were performed before coring and after coring at 73°F, and just before the specimens were tested for flow time and flow number, i.e., at 130°F. The tests were performed on all three mix types and the results are summarized in Table 4.14.

Table 4.14 Seismic Modulus Test Results

a) Type D

Asphalt Type	Seismic Modulus, ksi Of 6 by 7 in. Specimen at 73 °F			Seismic Modulus, ksi Of 4 by 6 in. Specimen at 73 °F			Seismic Modulus, ksi Of 4 by 6 in. Specimen at 130 °F		
	Avg.,	SD,	COV,	Avg.,	SD,	COV,	Avg.,	SD,	COV,
	ksi	ksi	%	ksi	ksi	%	Ksi	ksi	%
W 64	2,590	64.7	2.50	Not Tested			1,881	57.0	3.03
W 70 SBS	3,010	188.4	6.26				2,240	183.3	8.18
W76 SBS & TR	2,843	67.7	2.38				1,800	68.6	3.81
U 67	2,904	91.9	3.16				2,048	86.2	4.21
U 76 SBR	2,851	40.2	1.41				1,927	40.4	2.10
V 64	2,633	63.3	2.40				1,808	80.9	4.47
V 76 E	2,697	125.1	4.64				1,750	72.3	4.13

b) CMHB-C

Asphalt Type	Seismic Modulus, ksi Of 6 by 7 in. Specimen at 73 °F			Seismic Modulus, ksi Of 4 by 6 in. Specimen at 73 °F			Seismic Modulus, ksi Of 4 by 6 in. Specimen at 130 °F		
	Avg.,	SD,	COV,	Avg.,	SD,	COV,	Avg.,	SD,	COV,
	ksi	ksi	%	ksi	ksi	%	Ksi	ksi	%
W 64	2,511	71.4	2.85	2,703	105.6	3.91	2,039	71.9	3.53
W 70 SBS	2,482	31.8	1.28	2,857	52.7	1.84	1,983	51.5	2.60
W76 SBS & TR	2,517	77.3	3.07	2,684	47.1	1.75	1,844	48.3	2.62
U 67	2,521	32.3	1.28	2,833	142.1	5.01	1,823	27.9	1.53
U 76 SBR	2,501	62.1	2.48	2,945	19.1	0.65	2,077	69.8	3.36
V 64	2,523	40.1	1.59	2,917	44.4	1.52	1,830	40.9	2.24
V 76 E	2,231	112.8	5.06	2,612	120.8	4.63	1,678	100.2	5.97

c) PFC

Asphalt Type	Seismic Modulus, ksi Of 6 by 7 in. Specimen at 73 °F			Seismic Modulus, ksi Of 4 by 6 in. Specimen at 73 °F			Seismic Modulus, ksi Of 4 by 6 in. Specimen at 130 °F		
	Avg.,	SD,	COV,	Avg.,	SD,	COV,	Avg.,	SD,	COV,
	ksi	ksi	%	ksi	ksi	%	ksi	ksi	%
W 64	1,182	45.9	3.88	1,371	158.1	11.53	845	73.3	8.68
W 70 SBS	1,251	95.5	7.63	1,716	59.6	3.47	1,015	63.9	6.29
W76 SBS & TR	1,195	35.1	2.94	1,491	64.9	4.36	834	42.8	5.13

The seismic modulus test results suggest that the tests are repeatable because COV was around 5%, increasing to 10% on only a few occasions. Overall, the measured modulus decreased with the increase in temperature and increased when the specimen was cored out (Figure 4.32). The test results indicate that the outer shell is weaker. In addition, the test results were not able to identify the presence of modifiers.

Comparison of data from Type D and CMHB-C mixes showed that the tests performed at 130°F suggested that the Type D mixes exhibited higher modulus values to those of the CMHB-C mixes (Figure 4.33) but no other clear trend could be observed.

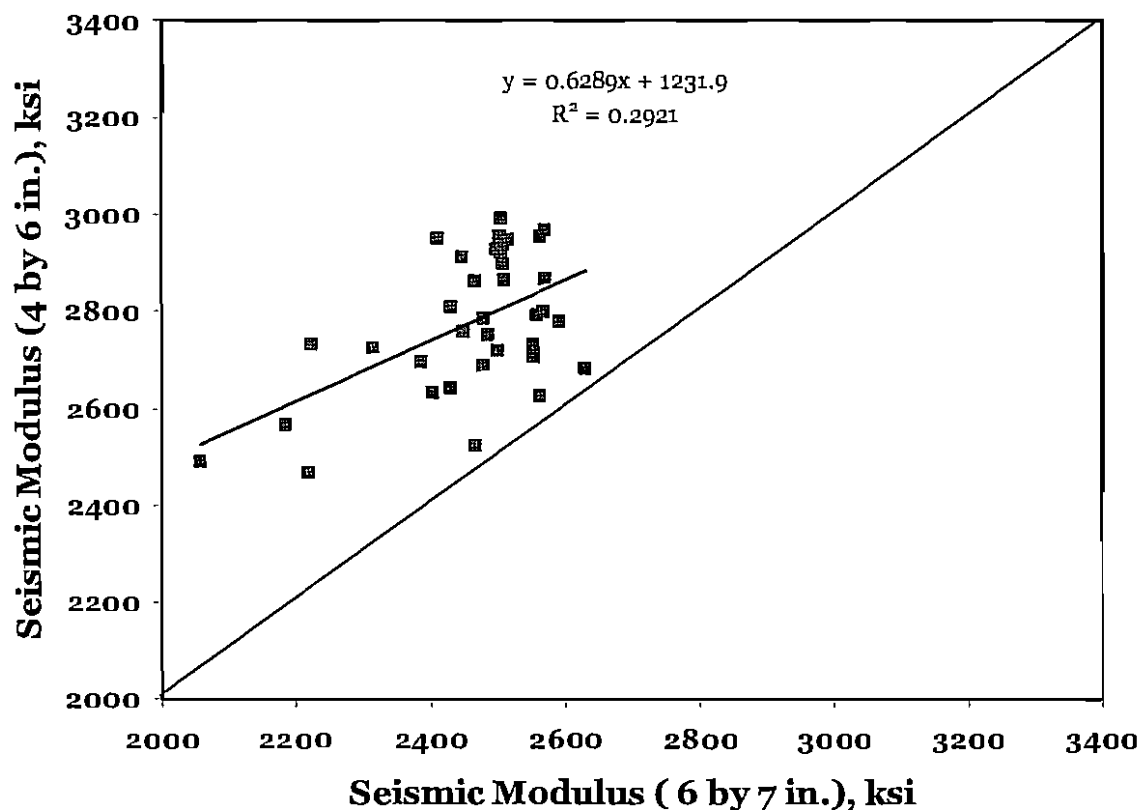


Figure 4.32 Influence of Coring on Seismic Modulus

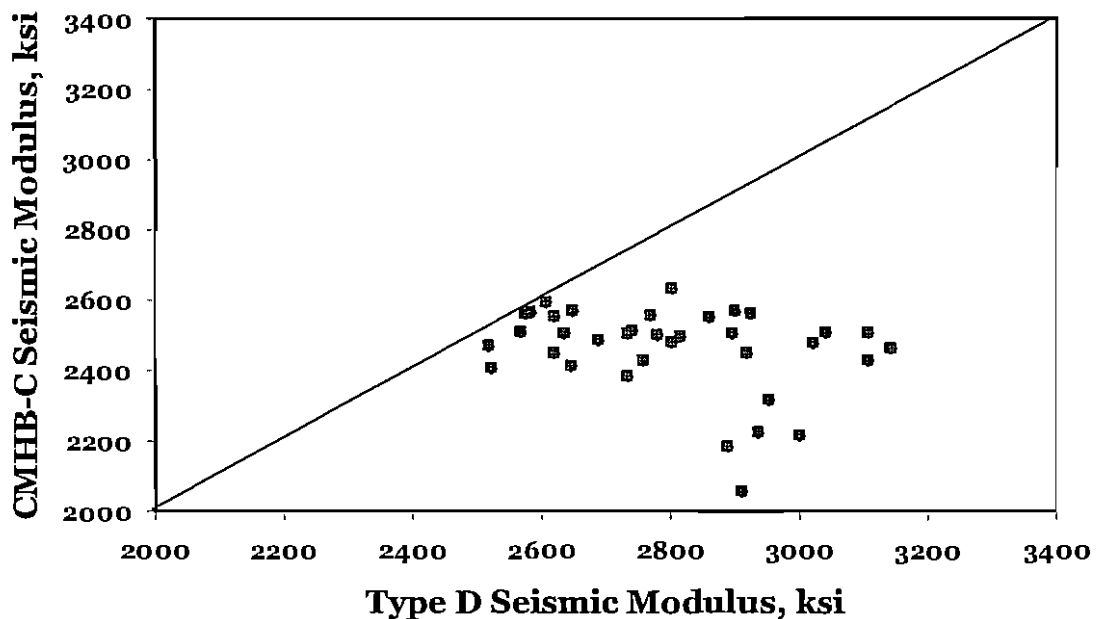


Figure 4.33 Seismic Modulus Comparison between Type D and CMHB-C Mixes

4.7 Flexural Fatigue Beam Test Results

During the third-point flexural fatigue beam test, the asphalt beam is subjected to a sinusoidal load. The load is monitored and adjusted accordingly such that the maximum tensile strain at the bottom of the beam remains constant. This is often referred to as the constant strain test mode. As damage to the asphalt beam progresses, the calculated flexural stiffness of the beam decreases. Figure 4.34 illustrates a typical change in the flexural stiffness with number of load during one of the experiments. As per current specifications, fatigue life (fatigue failure) is considered when the calculated stiffness reaches 50 percent of its initial value. At that point, the test is stopped. Figure 4.34 shows a “dip” in the curve, which occurs after the 50 percent stiffness drop point. It is the authors’ opinion that this “dip” is important to capture as it leads to a significant loss of strength with only a few repetitions and it is a less subjective definition of failure. The current termination criterion (50 percent of the initial stiffness) does not always capture this “dip”. Hence, it is recommended that the duration of the fatigue tests be extended until 15-20 percent of the initial stiffness is reached. Continuing the test to these levels implies an increased testing time and cost, therefore this is not recommended on a routine basis but only for research purposes until a more laboratory failure criterion is agreed upon.

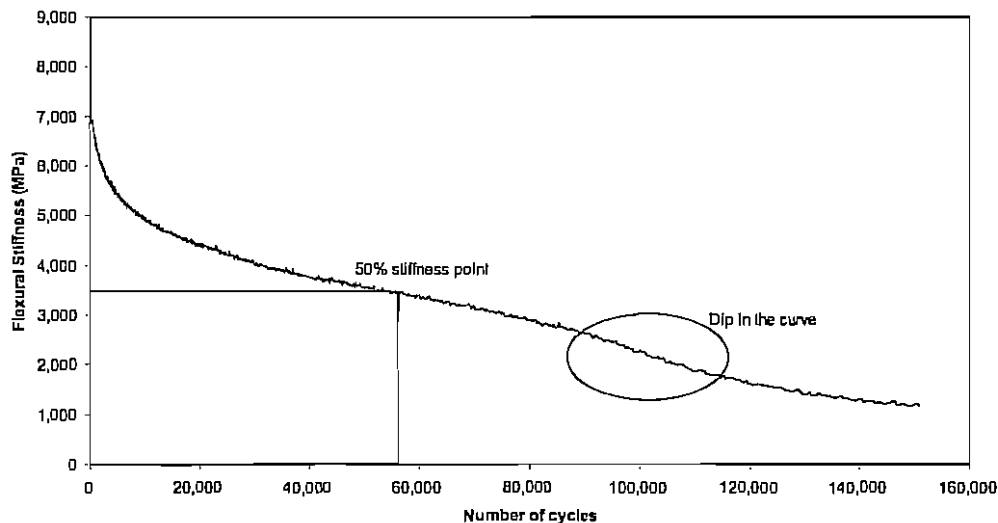


Figure 4.34 A Typical Flexural Stiffness-Cycle Curve Obtained from Fatigue Test

Tables 4.15 and 4.16 depict all the beams tested for the Type D and CMHB-C mixture, respectively. It should be noted that the results have been obtained using the current failure criterion as per AASHTO specifications.

The Type D mix test results suggest that the fatigue life of mixes increased significantly with the presence of modifier. For instance, the fatigue life of specimens prepared with Ultrapave base binder is 252,745 cycles while the modified binder had a fatigue life of 2,740,495 for tensile strain of $500 \mu\epsilon$, which is more than ten times of base binder. The fatigue life of specimens prepared with PG70-22 (Wright asphalt) also increased significantly in comparison to base binder (PG64-22 of Wright asphalt). The test results also suggest that there is influence of binder type on fatigue life. For instance, Wright asphalt base binder had a fatigue life of 132,905 while Velero Armor had a fatigue life of 470,555 at the tensile strain of $500 \mu\epsilon$. The test results also suggest that the fatigue life decreased with increase in strain levels. An increase in strain level by 40% decreased the fatigue life by almost 80% for all binder types.

The CMHB-C mixes exhibited trends similar to Type D mixes except that the fatigue lives were significantly lower (almost half) for all binder types. For instance, a fatigue life of 119,510 was observed with CMHB-C mix while 252,745 was observed with Type D mixes at the tensile strain of $500 \mu\epsilon$. Overall, the test results suggest that the Type D has a higher resistance to fracture and fatigue.

Table 4.15 Results of the Fatigue Test for Type D Mixes

Manufacturer	PG Grade	Modifier Type	Strain, $\mu\epsilon$	No. of Cycles	Avg. No. of Cycles
Wright Asphalt	PG64-22	Unmodified	300	2,892,130	2,165,095
			300	1,438,060	
			500	190,570	132,905
			500	75,240	
Wright Asphalt	70-22	3.5% SBS	400	2,654,890	653,940
			500	569,350	
			500	738,530	
			600	186,240	
Wright Asphalt	76-22	SBS+TR	500	789,650	937,340
			500	1,085,030	
			700	232,620	195,645
			700	158,670	
Ultrapave	67-22	Unmodified	300	2,694,580	3,729,045
			300	4,763,510	
			500	325,860	252,745
			500	179,630	
Ultrapave	76-22	3.5% SBR	500	3,584,190	2,740,495
			500	1,896,800	
			700	75,820	98,600
			700	121,380	
Valero Asphalt	64-22	Unmodified	500	155,800	470,555
			500	785,310	
			700	38,470	35,585
			700	32,700	
Valero Asphalt	76-22	3.5% Elvaloy	500	3,582,710	2,423,715
			500	1,264,720	
			750	35,370	73,055
			750	110,740	

Table 4.16 Results of the Fatigue Test for CMHB-C Mixes

Manufacturer	PG Grade	Modifier Type	Strain, $\mu\epsilon$	No. of Cycles	Avg. No. of Cycles
Wright Asphalt	PG64-22	Unmodified	300	1,847,700	1,486,310
			300	1,124,920	
			500	56,550	49,395
			500	42,240	
Wright Asphalt	70-22	3.5% SBS	400	1,319,950	230,585
			500	206,220	
			500	254,950	
			600	70,046	
Wright Asphalt	76-22	SBS+TR	500	327,450	401,210
			500	474,970	
			700	73,000	68,870
			700	64,740	
Ultrapave	67-22	Unmodified	300	1,639,380	1,920,305
			300	2,201,230	
			500	98,410	119,510
			500	140,610	
Ultrapave	76-22	3.5% SBR	500	1,385,740	1,185,550
			500	985,360	
			700	69,970	48,300
			700	26,630	
Valero Asphalt	64-22	Unmodified	300	8,514,010	6,279,570
			300	4,045,130	
			500	127,250	136,240
			500	145,230	
Valero Asphalt	76-22	3.5% Elvaloy	500	1,427,940	1,145,505
			500	863,070	
			700	104,540	78,395
			700	52,250	

The Type D and CMHB-C mix test results are also shown graphically in Figures 4.35 and 4.36, respectively. The data presented in the two figures is the data for each specimen rather than the averages shown in the Tables 4.15 and 4.16. The data suggests that increase in tensile strain reduces the fatigue life as well as the fatigue life is higher in the presence of modifier. If a value needs to be identified to determine the presence of modifier, the Type D mixes fatigue life should be more than 500,000 cycles while CMHB-C fatigue life should be more than 200,000 cycles. However, more testing needs to be done before this can be specified.

To identify influence of binder, an exponential curve was fit to the data obtained from the two mix types and the developed relationship is shown in Figure 4.37a. The data suggests that the correlation for both mix types is weak (R^2 values less than 0.7). However, the correlation increased significantly when the data is separated according to the binder grade type. The data for only base binders is plotted in Figure 4.37b and the R^2 value increased to more than 0.9 for both mix types suggesting that the base binder and modified binders provide significantly different fatigue lives. The data for modified binders is included in Figure 4.37c and again the R^2 value is more than 0.9 for both mix types.

Since the tests were performed on each mix type and binder type at 500 $\mu\epsilon$, it was decided to identify the relationship between the two mix types. The data is plotted in Figure 4.38 and it suggests that there is a strong correlation between the two mix types and CMHB-C mixes have 55% less fatigue life in comparison to Type D mixes regardless of binder type or grade. This suggests that influence of binder grade or type is dependent on the strain levels and is minimal at 500 $\mu\epsilon$. A statistical analysis of the fatigue was performed and is included in the next chapter.

4.7.1 Input in the Mechanistic-Empirical Pavement Design Guide

In addition to the above analyses, a series of 16 supplementary regression equations were developed to facilitate the implementation of the results of this research study into the recently developed Mechanistic-Empirical Pavement Design Guide (MEPDG). The MEPDG makes use of the most popular equation form to predict fatigue life as a function of its dynamic modulus and the expected strain level:

$$N_f = k_1 \left(\frac{1}{E^*} \right)^{k_2} \left(\frac{1}{\epsilon} \right)^{k_3} \quad (4.2)$$

Where:

- N_f = expected fatigue life of the mix in the laboratory
- E^* = dynamic modulus of the asphalt mix,
- E = peak applied tensile stain, and
- k_i = positive regression parameters determined in the laboratory.

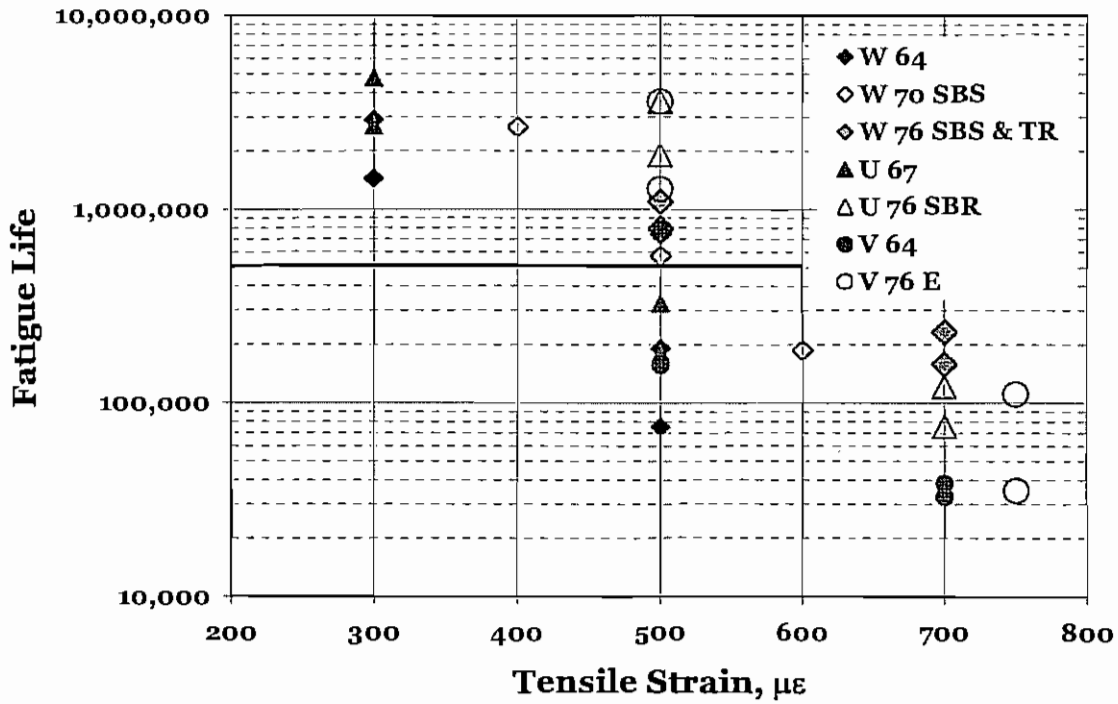


Figure 4.35 Results of the Fatigue Test for the Type D Mixes

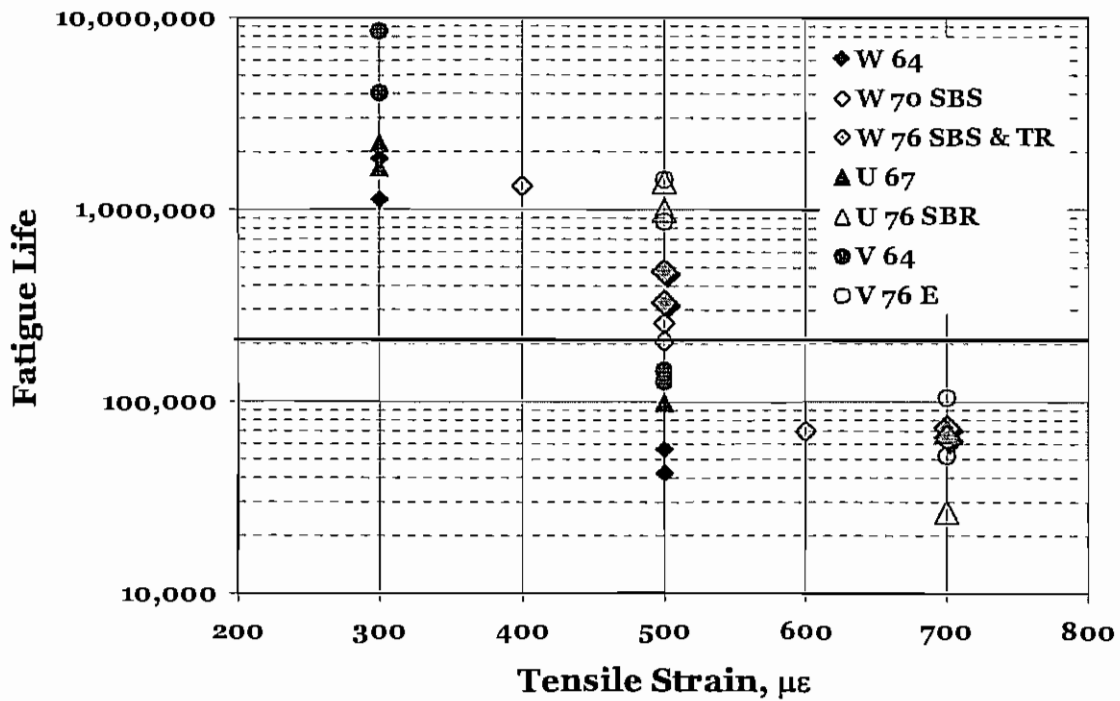


Figure 4.36 Results of the Fatigue Test for the CMHB-C Mixes

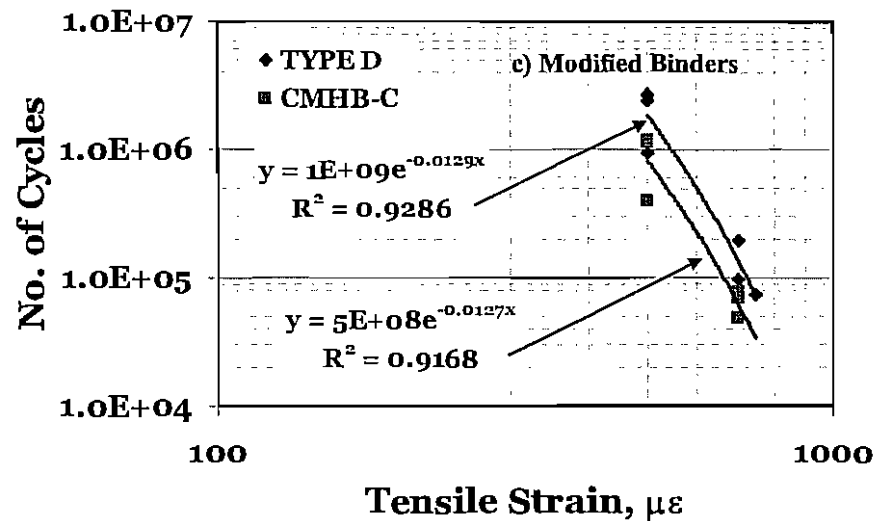
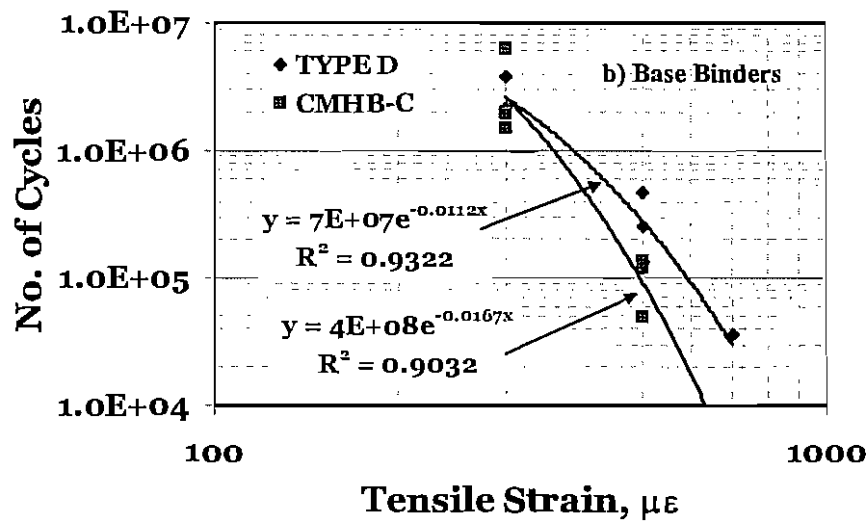
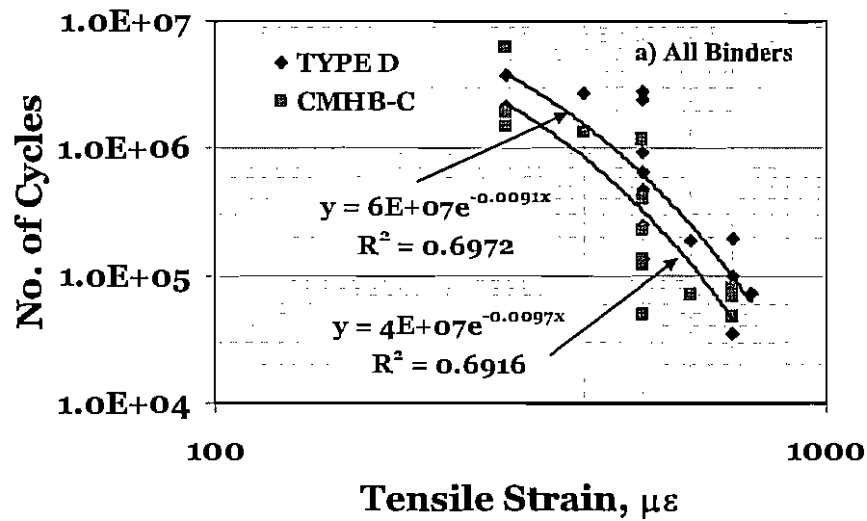


Figure 4.37 Influence of Binder Type on Fatigue Resistance

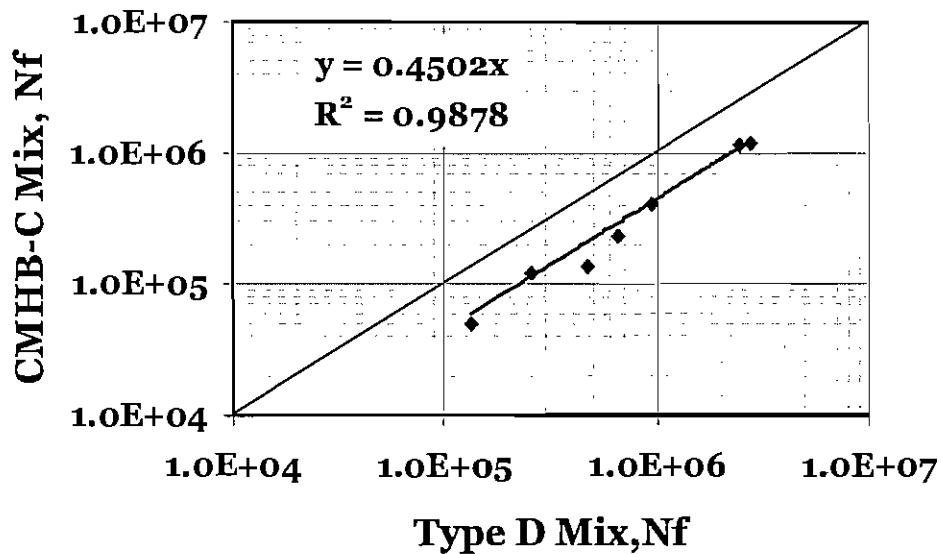


Figure 4.38 Influence of Mix Type on Fatigue Resistance

The estimated parameters are provided in Tables 4.17 and 4.18 for the CMHB-C and the Type D mixes, respectively. It should be noted that, for the purpose of this study, the term E^{*-k_2} has been incorporated into the intercept term k_1 resulting in k_1^* in Tables 4.17 and 4.18. As discussed earlier, this approach is preferred because it has been demonstrated that the dynamic modulus, E^* , is not a good predictor of fatigue performance. These parameters can be used in MEPDG program for the analyses.

Table 4.17 Fatigue Parameters for CMHB-C Mixes

Manufacturer	PG Grade	Modifier Type	Parameter	
Wright Asphalt	PG64-22	Unmodified	k ₁ [*]	3.72 10 ²²
			k ₃	-6.6
Wright Asphalt	70-22	3.5% SBS	k ₁ [*]	1.06 10 ²⁵
			k ₃	-7.3
Wright Asphalt	76-22	SBS+TR	k ₁ [*]	4.06 10 ¹⁹
			k ₃	-5.2
Ultrapave	67-22	Unmodified	k ₁ [*]	5.89 10 ¹⁹
			k ₃	-5.4
Ultrapave	76-22	3.5% SBR	k ₁ [*]	3.36 10 ³²
			k ₃	-9.8
Valero Asphalt	64-22	Unmodified	k ₁ [*]	1.06 10 ²⁵
			k ₃	-7.4
Valero Asphalt	70-22	2.0% Elvaloy	k ₁ [*]	1.01 10 ²⁶
			k ₃	-7.6
Valero Asphalt	76-22	3.5% Elvaloy	k ₁ [*]	6.01 10 ²⁷
			k ₃	-8.1

Table 4.18 Fatigue Parameters for Type D Mixes

Manufacturer	PG Grade	Modifier Type	Parameters	
Wright Asphalt	PG64-22	Unmodified	k_1^*	$1.14 \cdot 10^{20}$
			k_3	-5.5
Wright Asphalt	70-22	3.5% SBS	k_1^*	$2.83 \cdot 10^{23}$
			k_3	-6.5
Wright Asphalt	76-22	SBS+TR	k_1^*	$3.79 \cdot 10^{18}$
			k_3	-4.7
Ultrapave	67-22	Unmodified	k_1^*	$4.21 \cdot 10^{19}$
			k_3	-5.3
Ultrapave	76-22	3.5% SBR	k_1^*	$8.06 \cdot 10^{32}$
			k_3	-9.8
Valero Asphalt	64-22	Unmodified	k_1^*	$7.99 \cdot 10^{23}$
			k_3	-6.8
Valero Asphalt	70-22	2.0% Elvaloy	k_1^*	$7.10 \cdot 10^{27}$
			k_3	-7.0
Valero Asphalt	76-22	3.5% Elvaloy	k_1^*	$6.36 \cdot 10^{29}$
			k_3	-8.7

This page replaces an intentionally blank page in the original.

-- CTR Library Digitization Team

CHAPTER 5 STATISTICAL ANALYSES AND COMPARISON OF PERFORMANCE TEST RESULTS

5.1 Statistical Analyses

To statistically evaluate the influence of mix parameters on measured performance, an analysis of variance (ANOVA) was performed using MINITAB® 14.11. The purpose of this ANOVA was to determine if the performance test can successfully identify the impact of changes in the mix parameters. In this study, the measured performance was considered to be the dependent parameter while mix type, binder type, etc. were considered to be independent parameters. Since the tested number of mix types varied along with independent parameters, it was decided to perform two or four factor ANOVA depending on the performance test and mix types evaluated. Since ANOVA of Fatigue test is already discussed in the previous section, the ANOVA evaluation of flow number, flow time, dynamic modulus, and seismic modulus tests is presented in this section. In addition, ANOVA of HWTD, static creep, and IDT tests was not performed because these tests have been extensively used in the past and their reliability is well documented.

The null hypothesis selected for the ANOVA was that the measured performance is independent of the mix parameters. If the null hypothesis is rejected, it can be concluded that the measured performance relies on the independent mix parameters. A confidence level of 95% was assumed for the analysis. The probability factor of falsely rejecting the null hypothesis (p-value) should be less than 0.05 in order to conclude that a difference is significant, since a 95% confidence level was chosen. The null hypothesis was rejected when the p-value was less than 0.05 and was accepted when the p-value was greater than 0.05.

The results of the ANOVA analysis for the flow number tests are shown in Table 5.1. The first column shows evaluated factors and their interactions. The second column shows degree of freedom and the third column shows Sequential Sum of Squares. The fourth column shows F-statistics and the fifth column shows p-value obtained. The sixth column shows the conclusion of the ANOVA analysis. The Y in the sixth column indicates that the device is able to identify the effect of parameter changes while N in the sixth column indicates that the effect of the parameter is insignificant. Since not all of the binder types were used in all of the mix types, the evaluation was performed two ways. In the first evaluation, the ANOVA was performed by comparing Type D and CMHB-C mix test results. In the second evaluation, the ANOVA was performed for Wright Asphalt only and the measured data was compared for all three mix types (Type D, CMHB-C, and PFC). The ANOVA evaluation suggests that the measured permanent strain is statistically different for different mix types and binder types, indicating that the test setup can identify the influence of binder type as well as mix type.

Similar observations can be made for the flow time test results (Table 5.2), the only difference being that the standard error is significantly higher. However, the error is dependent on the measurements. The flow time total axial strain is in $\mu\epsilon$, which is higher than the total strain measured using flow number tests.

Table 5.1 Flow Number ANOVA

Source	Degree of Freedom	Sequential SS	F Static	P Value	Statistically Significant (Y/N)
Comparison Between CHHB-C and Type D Mixes					
Mix Type	1	5.6565	19.52	<0.001	Y
Binder Type	5	54.1722	37.39	<0.001	Y
Mix Type*Binder Type	5	7.119	4.91	0.003	Y
Error	24	6.954			
Total	35	73.9018			
Comparison Between All Mix Types for Wright Asphalt					
Mix Type	2	2.1237	8.36	0.003	Y
Binder Type	2	23.0966	90.9	<0.001	Y
Mix Type*Binder Type	4	3.456	3.4	0.031	Y
Error	18	4.5736			
Total	26	58.4702			

Table 5.2 Flow Time ANOVA

Source	Degree of Freedom	Sequential SS	F Static	P Value	Statistically Significant (Y/N)
Comparison Between CHHB-C and Type D Mixes					
Mix Type	1	2.81E+08	7.07	0.01	Y
Binder Type	5	1.23E+09	30.93	<0.001	Y
Mix Type*Binder Type	5	7.44E+08	3.75	0.005	Y
Error	59	2.34E+09			
Total	70	9.53E+09			
Comparison Between All Mix Types for Wright Asphalt					
Mix Type	2	1.86E+08	14.68	<0.001	Y
Binder Type	2	9.19E+08	72.59	<0.001	Y
Mix Type*Binder Type	4	1.99E+08	3.93	0.018	Y
Error	18	2.28E+08			
Total	26	2.64E+09			

The dynamic modulus tests were performed at various temperatures as well as frequencies; therefore, a four factor ANOVA was performed. The test results for two mix types are presented in Table 5.3, while three mix types for Wright Asphalt are presented in Table 5.4. The data suggests that the measured modulus is dependent on the mix type, binder type, frequency, and temperature. However, the dynamic modulus measurements were not able to differentiate between binder type and frequency when two-way interaction was evaluated. This phenomenon was also true when three-way interaction (mix type, frequency and binder type or temperature) was evaluated. The ANOVA results also suggest that the dynamic modulus measurements were not able to differentiate between mix parameters in the presence of four-way interaction. Similar trends were observed when three mix types for Wright Asphalt were compared (Table 5.4).

The ANOVA of seismic modulus measurements suggests that the test is able to distinguish between different binder types and mix types at both specimen sizes (Table 5.5).

To statistically evaluate the variables that significantly affected the fatigue performance, several models were developed and evaluated using ANOVA. The models represented in Equations 5.1 and 5.2 were deemed to be best because they capture the effects of the most important variables tested. The statistics of the regression analyses are presented in Figures 5.1 and 5.2 for the CMHB-C and Type D mixes, respectively. Notice that in both cases the base case was selected as those mixes prepared with a PG64 Wright Asphalt. For these reason a number of dummy variables were incorporated to assess the effects of changing binder grade and binder source.

$$\ln N_{JC} = 52.8 - .224 UL + .606 VA + .871 PG70 + 2.22 PG76 - 6.71 \ln \epsilon \quad (5.1)$$

$$\ln N_{JD} = 48.2 - .311 UL + .349 VA + 1.05 PG70 + 2.06 PG76 - 5.84 \ln \epsilon \quad (5.2)$$

Where:

- N_{JC} = fatigue life of the CMHB-C mixes,
- N_{JD} = fatigue life of the Type D mixes,
- UL = dummy variable to capture the effect of using Ultrapave binders,
- VA = dummy variable to capture the effect of using Valero binder,
- $PG70$ = dummy variable to capture the effect of using PG70 binder, and
- $PG76$ = dummy variable to capture the effect of using PG76 binder.

The most important result of the regression analyses is quantification that Type D mixes tend to over perform CMHB-C mixes in terms of fatigue performance. This finding was generally expected due to the denser nature of the Type D mixes as compared with the more open CMHB Type C mixes.

Table 5.3 Dynamic Modulus ANOVA for Type D and CMHB-C Mixes

Source	Degree of Freedom	Sequential SS	F Static	P Value	Statistically Significant
Mix Type (M)	1	15417459	1051.15	<0.001	Y
Binder Type (B)	6	14651099	166.48	<0.001	Y
Test Frequency (F)	3	28971401	658.42	<0.001	Y
Test Temperate (T)	3	5E+08	1.10E+04	<0.001	Y
M*B	6	4584162	52.09	<0.001	Y
M*F	3	316284	7.19	<0.001	Y
M*T	3	2761128	62.75	<0.001	Y
B*F	18	183578	0.7	0.817	N
B*F	18	5770021	21.86	<0.001	Y
F*T	9	6556341	49.67	<0.001	Y
M*B*F	18	154489	0.59	0.911	N
M*B*T	18	1142646	4.33	<0.001	Y
B*F*T	54	286897	0.36	<0.001	Y
M*F*T	9	112473	0.85	0.568	N
M*B*F*T	54	249958	0.32	1.00	N
Error	448	6570909			
Total	671	5.87E+08			

Table 5.4 Dynamic Modulus ANOVA for Three Mix Types

Source	Degree of Freedom	Sequential SS	F Static	P Value	Statistically Significant
Mix Type (M)	2	78087773	4560.46	<0.001	Y
Binder Type (B)	2	4124307	240.87	<0.001	Y
Test Frequency (F)	3	12867531	500.99	<0.001	Y
Test Temperate (T)	3	2.29E+08	8923.41	<0.001	Y
M*B	4	3991987	116.57	<0.001	Y
M*F	6	1556881	30.31	<0.001	Y
M*T	6	31804927	619.15	<0.001	Y
B*F	6	61160	1.19	0.311	N
B*F	6	1344896	26.18	<0.001	Y
F*T	9	2968935	38.53	<0.001	Y
M*B*F	12	78010	0.76	0.692	N
M*B*T	18	293636	1.91	0.015	Y
B*F*T	12	1383461	13.47	<0.001	Y
M*F*T	18	11688	0.08	1.000	N
M*B*F*T	36	70226	0.23	1.000	N
Error	288	2465683			
Total	431	3.7E+08			

Table 5.5 Seismic Modulus ANOVA

Source	Degree of Freedom	Sequential SS	F Static	P Value	Statistically Significant (Y/N)
Tested at 130 °F (54 °C) on 4by 6 Specimens					
Mix Type	2	6674128	1093.46	<0.001	Y
Binder Type	2	311112	50.97	<0.001	Y
Mix Type*Binder Type	4	347782	14.24	<0.001	Y
Error	44	268563			
Total	52	14549104			
Tested at 73 °F (23 °C) on 6by 7 Specimens					
Mix Type	2	12431356	1616.01	<0.001	Y
Binder Type	2	97053	12.62	<0.001	Y
Mix Type*Binder Type	4	347022	11.28	<0.001	Y
Error	44	338476			
Total	52	25837698			

<i>Regression Statistics</i>	
Multiple R	0.95
R Square	0.90
Adjusted R Square	0.88
Standard Error	0.55
Observations	32

ANOVA				
	<i>df</i>	<i>SS</i>	<i>MS</i>	<i>F</i>
Regression	5	73.89	14.78	48.57
Residual	26	7.91	0.30	
Total	31	81.81		

	<i>Coefficients</i>	<i>Std. Error</i>	<i>t Stat</i>	<i>P-value</i>
Intercept	52.76	2.67	19.75	0.00
UL	-0.22	0.27	-0.83	0.42
VA	0.61	0.23	2.67	0.01
PG70	0.87	0.29	2.98	0.01
PG76	2.22	0.34	6.52	0.00
ST	-6.71	0.45	-14.94	0.00

Figure 5.1 Statistics of the Regression Analysis for CMHB-C Mixes

Regression Statistics					
Multiple R					0.90
R Square					0.81
Adjusted R Square					0.78
Standard Error					0.75
Observations					32

ANOVA					
	<i>df</i>	<i>SS</i>	<i>MS</i>	<i>F</i>	
Regression	5	63.81	12.76	22.71	
Residual	26	14.61	0.56		
Total	31	78.42			

	<i>Coefficients</i>	<i>Std. Error</i>	<i>t Stat</i>	<i>P-value</i>	
Intercept	48.20	3.63	13.27	0.00	
UL	-0.31	0.36	-0.86	0.40	
VA	0.35	0.33	1.05	0.31	
PG70	1.05	0.36	2.89	0.01	
PG76	2.06	0.40	5.19	0.00	
ST	-5.84	0.60	-9.77	0.00	

Figure 5.2 Statistics of the Regression Analysis for Type D Mixes

While the effect of binder modification was expected to be significant, that is mixes prepared with PG70 and PG76 were expected to have different lives than those prepared with unmodified PG64 binders, these lives were not necessarily expected to be longer. As a matter of fact, for both mixes and for all binders, mixes prepared with PG76 have significant longer fatigue lives than mixes prepared with PG70. In turn, the latter ones have significant longer lives than those base mixes prepared with PG64. This is a very interesting because it contradicts the notion that mixes with higher stiffness will have shorter fatigue lives. While this concept may apply (to some extent) to traditional unmodified dense mixes, these results show that generalization of the concept is dangerous and testing mixes to fatigue failure in the laboratory should not be replaced but equations that estimate performance based on strain level and dynamic modulus.

Another interesting result of the regression analyses is that, everything else being equal, the origin of the binder has a significant effect on the fatigue life of the mixes. In this particular study, mixes prepared with Ultrapave binders showed shorter average lives. The differences, however, were not significant at a 95 percent confidence level. On the other hand, mixes prepared with Valero binders tended to over perform the other mixes. Although the difference was significant (at 95 percent confidence level) for the CMHB-C mixes, it was not for Type D mixes.

It is very important to emphasize that the reason for these difference it is believed to lie in the actual binder origin (the origin of the petroleum source) and not on

the specific brand of binder tested. In addition, these differences are believed to be variable as the petroleum sources are.

Overall, the test results suggest that the flow time, flow number, seismic modulus, and flexural fatigue beam test setups are able to identify the influence of the evaluated mix types and binder types but the dynamic modulus measurements are not able to identify the influence due to temperature and frequency interactions.

5.2 Comparison of Performance Test Results

Although various tests were performed and the test results were analyzed individually, it is essential that the performance test results be compared to identify a suitable test. One way to make this comparison is by ranking the mixes for individual performance tests and comparing them to the perceived field performance. One of the disadvantages of this approach is that not all of the tests characterize the same mix properties. For example, the static creep test evaluates the stiffness as well as rutting potential of the mix while HWTD evaluates rutting potential of the mix. Therefore, it is appropriate to compare the tests that evaluate similar mix characteristics. The test results obtained from the HWTD tests and permanent deformation from the static creep tests can be compared to assess the rutting potential of mixes. Thus, the comparison is performed in two different modes, rutting and stiffness, and is discussed in the following sections

5.2.1 Rutting Potential of HMA

To compare the rankings obtained from the different permanent deformation tests, the test results from the HWTD, permanent deformation from static creep, $E^*/\sin\Phi$ from dynamic modulus, flow time, and flow number rankings were gathered and are summarized in Tables 5.6 and 5.7 for CMHB-C and Type D mixes, respectively. The test results do not clearly indicate which asphalt type is better because rankings change from one test to another. The only conclusion from the tests is that the mixes prepared with unmodified binders are ranked lower in comparison to mixes made with modified binders with the exception of dynamic modulus where Ultrapave (U 67) unmodified binder is ranked higher in comparison to Ultrapave (U76 SBR) modified binder for Type D mix. If only flow number and flow time results are compared, then the rankings are similar. The data suggest that the total permanent strain of less than 1% indicates presence of modifiers and, similarly, total permanent deformation of less than 7,000 μ in./in. indicates presence of modifier. Static creep test results suggest that the permanent deformation of less than 2% indicates presence of modifier. Thus, the evaluated performance tests, with the exception of dynamic modulus, can identify the presence of a modifier, and the presence of a modifier decreases the rutting potential.

Table 5.6 Rutting Potential Ranking of CMHB-C Mixes

Binder Type	Dynamic Modulus	HWTD	Static Creep	Flow Number	Flow Time
	E*/sinΦ, ksi @ 130 °F and 5 Hz	Maximum Permanent Deformation, in.	Permanent Deformation, mil/in.	Total Permanent Strain, %	Total Axial Strain, μ in./in.
W 64	6 (485)	5 (6.1)	5 (3.48)	6 (4.37)	6 (30,913)
W 70 SBS	1 (624)	3 (4.9)	4 (2.02)	2 (0.64)	1 (4,984)
W76 SBS & TR	3 (520)	4 (5.4)	1 (1.18)	4 (0.87)	4 (6,511)
U 67	2 (534)	6 (11.1)	6 (3.63)	5 (3.83)	5 (26,232)
U 76 SBR	5 (514)	2 (3.9)	3 (1.40)	1 (0.53)	2 (5,224)
V 64	---	7 (12.7)	---	7 (4.37)	7 (30,913)
V 76 E	4 (514)	1 (3.4)	1 (1.15)	3 (0.7)	3 (5,666)

Table 5.7 Rutting Potential Ranking of Type D Mixes

Binder Type	Dynamic Modulus	HWTD	Static Creep	Flow Number	Flow Time
	E*/sinΦ, ksi @ 130 °F and 5 Hz	Maximum Permanent Deformation, in.	Permanent Deformation, mil/in.	Total Permanent Strain, %	Total Axial Strain, μ in./in.
W 64	7 (479)	5 (4.4)	5 (2.34)	6 (2.0)	6 (17,024)
W 70 SBS	2 (631)	4 (2.8)	2 (1.08)	2 (0.39)	2 (4,953)
W76 SBS & TR	5 (546)	2 (3.0)	1 (1.03)	3 (0.56)	1 (3,937)
U 67	3 (629)	6 (14.4)	6 (2.79)	7 (2.28)	7 (19,832)
U 76 SBR	4 (548)	2 (3.2)	3 (1.82)	4 (0.780)	4 (5,504)
V 64	6 (502)	7 (17.0)	---	5 (1.8)	5 (13,023)
V 76 E	1 (657)	1 (2.3)	3 (1.82)	1 (0.28)	3 (5,503)

5.2.2 Stiffness of HMA

To compare the stiffness obtained from different modulus and strength tests, data from the dynamic modulus, seismic modulus, IDT, and fatigue tests were ranked and are summarized in Tables 5.8 and 5.9 for CMHB-C and Type D mixes, respectively. The test results do not clearly indicate which asphalt type is better because rankings change from one test to another. The IDT test results show that there is no difference between the binder types, especially for Type D mixes. The static creep test results suggest that the stiffness of less than 3 ksi suggests that no modifier is present and a stiffness of 4 ksi or higher indicate mix with PG 76 binder. However, more testing is needed before a definite conclusion can be drawn. The seismic test results are not able to differentiate between binder types regardless of mix types.

The fatigue test results exhibit completely different picture in comparison of other test types. At strain levels of 500 $\mu\epsilon$, the binder ranking came out to be exactly same for both mix types. The fatigue test results also suggest that the modified binders ranked higher in comparison to base binders. According to the ranking, the Ultrapave modified with SBR performed the best while the Wright asphalt base binder ranked the last. This is different than the rutting potential where Wright Asphalt performed the best among different base binders.

Overall, test results suggest that the modified binders increased both the fatigue and rut resistance of the HMA. However, a specific modifier that is better than other modifier could not be clearly identified.

Table 5.8 Stiffness Ranking of CMHB-C Mixes

Mix Type	Dynamic Modulus at 10 Hz, ksi @ 73 °F	Fatigue Life, No. of Cycles to Failure	Seismic Modulus, ksi	Creep Stiffness, ksi	IDT Strength Test, psi
		At 500 $\mu\epsilon$ Strain	73 °F		
W 64	3 (1,261)	7 (49,395)	4 (2,511)	5 (2.2)	2 (371)
W 70 SBS	2 (1,333)	4 (230,585)	6 (2,482)	4 (3.5)	1 (404)
W76 SBS & TR	7 (924)	3 (401,210)	1 (2,517)	3 (4.0)	4 (326)
U 67	1 (1,420)	6 (119,510)	1 (2,521)	5 (2.2)	4 (323)
U 76 SBR	4 (1,123)	1 (1,185,550)	5 (2,501)	1 (4.6)	3 (336)
V 64	6 (965)	5 (136,240)	1 (2,523)	-----	---
V76 F	5 (1,087)	2 (1,145,505)	7 (2,231)	2 (4.2)	----

Table 5.9 Stiffness Ranking of Type D Mixes

Mix Type	Dynamic Modulus at 10 Hz, ksi @ 73 °F	Fatigue Life, No. of Cycles to Failure	Seismic Modulus, ksi	Creep Stiffness, ksi	IDT Strength Test, psi
		At 500 $\mu\epsilon$ Strain	73 °F		73 °F
W 64	3 (970)	7 (132,905)	7 (2,590)	5 (3.2)	3 (355)
W 70 SBS	2 (994)	4 (653,940)	1 (3,010)	1 (5.8)	5 (346)
W76 SBS & TR	5 (728)	3 (937,340)	3 (2,843)	2 (4.9)	1 (365)
U 67	4 (750)	6 (252,745)	2 (2,904)	6 (2.5)	1 (362)
U 76 SBR	1 (1,050)	1 (2,740,495)	3 (2,851)	3 (4.4)	6 (336)
V 64	-----	5 (470,555)	6 (2,633)	-----	---
V76 F	2 (608)	2 (2,423,715)	5 (2,697)	4 (3.4)	3 (357)

CHAPTER 6 CLOSURE

6.1 SUMMARY

To achieve SHRP specified PG grades, refineries make use of modifiers to enhance the properties of neat asphalt. Even though modified binders may meet PG specifications, some perform better than others. This can be attributed to inability of the SHRP specified tests in consistently identifying the problems with the binders especially if the modifier is added to the binder. Therefore, it is necessary to identify a binder test that can capture the true performance.

The difference in performance can also be attributed to the binder aggregate interaction and compatibility. Although SHRP evaluated various performance tests, a specific test for evaluating the performance of HMA has not been recommended. The only performance test recommended was the AASHTO T-283 test to evaluate moisture sensitivity of HMA.

Witczak et al. (2002) evaluated various performance tests and proposed what is commonly known as "Simple Performance Tests (SPT)" for National Cooperative Highway Research Program (NCHRP) Project 9-19. These tests include dynamic modulus to predict the permanent deformation and fatigue cracking and axial repeated (flow number) and axial creep (flow time) tests to predict the permanent deformation. The dynamic modulus test is also recommended in the "Guide for Mechanistic-Empirical Design of New and Rehabilitated Pavement Structures." Currently, TxDOT specifies the HWTD test (Tex-242-F) or static creep test (Tex-231-F) to evaluate performance of HMA. However, the HWTD test only identifies the rut potential of HMA, and static creep tests have lower repeatability (Swami et al., 2006). Therefore, it is necessary that a HMA test be recognized that can identify the presence of modifier and quantify the benefits of modifier.

The research performed for SHRP has significantly increased the understanding of HMA mix behavior among national and international highway-related agencies, which has resulted in an increase in the number of mixes available for placement. The increase in mix types makes it difficult for designers to select the appropriate mix for a given application.

To achieve these objectives, a survey of TxDOT Districts was conducted to identify commonly placed mixes and modifiers, and identify HMA selection criterion currently being used. The survey results have been reported by Smit et al., (2004). Based on survey results, three mixes (Type D, CMHB-C, and PFC) were selected. In addition, the four modifier types: SBS, SBR, TR, and Elvaloy were selected and evaluated.

The binders were evaluated using frequency sweep, repeated creep and elastic recovery tests. The HMA were evaluated using HWTD, flexural beam fatigue test,

IDT, dynamic modulus, static creep, flow time, flow number and seismic modulus tests.

The results of binder evaluation were reported by Hrdlicka et al. (2007) and the guidelines/expert system development and workshop materials were developed by Smit et al. (2007).

6.2 CONCLUSIONS

Based on the test results and analyses, the following recommendations can be drawn:

- The elastic recovery test can identify the presence of modifier (Hrdlicka et al., 2007). The repeated creep test can identify the presence of modifier as well as correlates well the rut depth obtained from HWTD (Hrdlicka et al., 2007).
- The performance evaluation of HMA revealed the following:
 - For the mixes tested, no matter whether the mixes were modified with SBS, SBR or Elvaloy, all outperform the unmodified mixes but none of the products significantly outperform the others.
 - Although base binders have similar PG grades, their performance can be significantly different. Therefore, it is important to closely monitor the changes in crude source or binder batch. In addition, the test results obtained with the new batch of asphalt may or may not support results reported in this study.
 - In terms of rutting, all of the performance tests with the exception of dynamic modulus can identify the presence of modifier although they ranked the different binder types differently.
 - In terms of fatigue/stiffness, the only flexural beam fatigue test was able to identify the presence of modifier consistently.
 - In comparing the two mix types, the CMHB-C has better rut resistance, especially in the presence of lower grade binder, in comparison to Type D. On the other hand, Type D has significantly higher fatigue resistance in comparison to CMHB-C.
 - The HMA test results also suggest that the test setups are highly variable.

6.3 RECOMMENDATIONS

The researchers propose that the flexural beam fatigue tests and HWTD tests on other mix types and binder sources be performed to propose new asphalt acceptance criterion to compliment the existing PG specifications.

This page replaces an intentionally blank page in the original.

-- CTR Library Digitization Team

REFERENCES

1. Andrei, D., Witzczak, M.W., Mirza, W., "Development of the 2002 Guide for the Design of New and Rehabilitated Pavement Structures." University of Maryland, 1999.
2. AVC Manual: "Asphalt Vibratory Compactor User's Guide" published by Pavement Technology Inc. (PTI), Covington, Georgia, U.S.A., 2003.
3. Hrdlicka, G., Tandon, V., Prozzi, J, Smith, A., and Yildirim, Y. (2007), "Evaluation of Binder Tests for Identifying Rutting and Cracking Potential of Modified Asphalt Binders," FHWA/TX-07/O-4824-1, Center for Transportation Infrastructure Systems, El Paso, Texas.
4. King, Gayle, Helen King, R. D. Pavlovich, Amy L. Epps and Prithvi Kandhal. (1999) "Additives in Asphalt." Proceedings AAPT. Association of Asphalt Paving Technologists, Vol. 68A.
5. Izzo, R.P., and Tahmoressi, M., "Testing Repeatability of the Hamburg Wheel-Tracking Device and Replicating Wheel-Tracking Devices among Different Laboratories," Journal of The Association of Asphalt Paving Technologists, Asphalt Paving Technology, 1999, pp. 589-612,.
6. Monismith, C. L., J. A. Epps, and F. N. Finn "Improved asphalt mix design", Proceedings, Association of Asphalt Paving Technologists, vol. 54, Clearwater, Florida, U.S.A., February 1985.
7. Nazarian S., Yuan D., Tandon V. and Arellano M., "Quality Management of Flexible Pavement Layers with Seismic Methods," Research Report 1735-3, The Center for Transportation Infrastructure Systems, The University of Texas, El Paso, TX, 2003.
8. Pagen, C. A. (1963), "*An Analysis of the Thermorheological Response of Bituminous Concrete*," Master of Science Thesis, The Ohio State University, pp. 26-33
9. Pellinen, T.K., Witzczak, M.W., "Stress Dependent Master Curve Construction fro Dynamic (Complex) Modulus," Journal of Association of Asphalt Paving Technologists, Volume 71, 2002, pp. 281-309.
10. Roque, Reynaldo, B. Birgisson, C. Drakos, and G. Sholar. (December 2004) "Guidelines for Use of Modified Binders." Florida Department of Transportation (FDOT) Report Number 4910-4504-964-12.
11. Sagi, S. V. (2004) "The Impact of Acceptance Criterion on HMA Moisture Susceptibility." University of Texas at El Paso, El Paso, Texas.
12. Smit, A., Prozzi, J., and Tandon, V. (2004) "Project Survey for Usage of Hot Mix Asphalt Concrete," Technical Memorandum Project 0-4824-1, Center for Transportation Research, The University of Texas at Austin, Austin, Texas.
13. Smit, A. F., Prozzi, J., Tandon, V., and Mikhail, M. (2007), "TexSys: Guide for Selecting HMA for Texas Flexible Pavements," Center for Transportation and Infrastructure Systems, The University of Texas at El Paso, El Paso, Texas.

14. Swami, V. (2005) "Performance Testing of Crumb Rubber Modified Hot Mix Asphalt Concrete." University of Texas at El Paso, El Paso, Texas.
15. Tangella S.C.S.R., Craus J., Deacon J. A. and Monismith C. L., "Summary response of asphalt mixtures", Report TM-UCB-A-003A-89-3, Strategic Highway Research Program Project A-003-A, Washington, D.C., U.S.A., 1990
16. Tayebali A. A., Deacon J. A., Coplantz J.S., Finn F.N. and Monismith C.L. "Fatigue Response of Asphalt-Aggregate Mixes", Report No. SHRP-A-404, Contract A-003A, ISBN 0-309-05812-0 Asphalt Research Program, Institute of Transportation Studies, University of California, Berkeley, U.S.A., 1994.
17. Witzak, M.W., Kaloush, K., Pellinen, T., El-Basyouny, M., and Von Quintus, H., "Simple Performance Test for Superpave Mix Design", NCHRP Report 465, Transportation Research Board, Washington, D.C., 2002.